Regulation of the kinases LynA and LynB and function in autoimmune disease

A DISSERTATION
SUBMITTED TO THE FACULTY OF THE UNIVERSITY OF MINNESOTA BY

Ben Frank Brian IV

IN PARTIAL FULFILLMENT OF THE REQUIREMENTS FOR THE DEGREE OF
DOCTOR OF PHILOSOPHY

Advised by Tanya S. Freedman, Ph.D.

April 2021

ACKNOWLEDGEMENTS

A great majority of the work presented in this dissertation would not have been possible without the support of far too many people to list, but I will do my best to enumerate as many as I can here.

Funding for my training was provided by (among others) the PharmacoNeuroImmunology training grant, a National Institutes of Health-funded T32. Without this funding, none of my accomplishments would have been possible. But perhaps more important than the funding, was the guidance and direction provided by Yorie Smart and Thomas Molitor. Both worked extremely hard to successfully provide a holistic training environment that expanded my scholarship into areas and fields I would never have expected to encounter otherwise. In addition to direction from Yorie and Tom, Malzona Anderson, Annette Bethke, Jim Shoemaker, Jessica Carlson and Hannah Salen provided administrative support and were always happy to answer all my organizational questions and help me navigate the university's rules and regulations.

I'd like to thank every member of the Freedman lab, past and present, for helpful discussions, assistance with experiments and general comradery. Thank you all for first enduring, and then critiquing, all of my practice talks, slide-by-painful-slide. I'd especially like to highlight helpfulness of Myra Nunez, Whitney Swanson, Frankie Sjaastad, Luis Ramirez and Adrienne Jolicoeur for doing the lion's share of managing our, at times, enormous mouse colony; for ensuring the lab ran smoothly, for every time they helped me with a large experiment, and for essential contributions that ensured the acceptance of a manuscript. I miss our lab happy hours but hope for reunions at conferences in the future and look forward to reading about the amazing work Joseph Greene, Freya van't Veer, Erandika Senevirathne, Monica Sauer, Anders Lindstedt and Olivia Funk will accomplish in the future.

I was lucky to have two places I could call home during my studies: The Department of Pharmacology, and the Center for Immunology. Thanks to Collin Campbell, Jill Siegfried and Kevin Wickman for making the Department of Pharmacology such a strong community. To all of my fellow graduate students in my cohort, especially Abir Majumdar, thanks for the many great happy hours, barbecues, and trips. I can't think of a better place

for my primary training than the Center for Immunology. The leadership of Marc Jenkins, Kris Hogquist, and others has fostered a unique environment that promotes collaboration and innovation. Every lab in the Center for Immunology contributed at least a small part to the work in this dissertation, whether it was a helpful discussion or letting me borrow an antibody for pilot experiments.

I've had the privilege of working with several amazing collaborators whose expertise and hard work made many of these discoveries possible. Candace Guerrero, of the Center for Mass Spectrometry and Proteomics, provided invaluable expertise and developed an entire proteomics method to help us detect phosphorylation in LynA, contributing to two publications. Jennifer Auger and Bryce Binstadt provided key guidance and tissue sectioning for our investigation into the development of autoimmunity in novel knockout mice. Brandon Burbach of the Shimizu lab was always willing to share expertise and reagents. Furthermore, Brandon's inclusive spirit helped ensure that the Freedman lab found a welcome home at the far end of 2nd floor of WMBB. I'd also like to thank Carol Lange and Michael Farrar for serving on my committee and providing feedback, guidance, and just the right amount of tough questioning during my preliminary exam and committee meetings.

Kaylee Schwertfeger acted as a co-mentor for the majority of my studies. Initially, this project began as an investigation into the role Lyn plays in regulating macrophage activation in the tumor microenvironment. To those ends, Kaylee provided expertise, guidance and reagents, as well as a venue to present my findings and gain critical feedback on my project. Even when my project slowly started to move farther and farther away from a focus on cancer to a focus on autoimmunity, she still welcomed me to present and attend her lab meetings and was always willing to provide feedback.

Many mice paid the ultimate sacrifice for this work and their contribution should not go unacknowledged. I'd also like to thank the animal research support staff for ensuring their health and well-being, especially throughout the COVID shutdown.

Kristen Jahr saw me at intense highs and lows and somehow decided she'd stay with me through them. Thanks for always being so goofy and brightening my days. Thanks for

understanding that whatever time I'd tell you I'd be home, it would inevitably be later than I imagined. Although I can't promise there won't be more experiments that keep me in lab into the wee morning, I'm looking forward to all our future adventures. Thanks also to Don and Brenda Jahr, and Kevin and Katy Jahr for always treating me like family.

I could always count on my Mom, Dad, brother and sister for support and guidance. My mom, Gail, deserves the most credit for setting me on this journey by indulging my interest in the natural world from a young age and letting me pretend to be a dinosaur until I was far older than appropriate. Jack and Addie were always there whenever I needed anything, including a good laugh. Thanks for checking in on me and inquiring about how my cells and my proteins were doing. Thanks for the cheese bread, the beer, the laughter, the Minnesota State fair memories, and of course, being role models that helped mold me into the person I am today.

I'm indebted to one person above all for the work presented in this dissertation. My mentor, Tanya Freedman, provided the perfect amount of guidance and freedom that allowed me to improve throughout graduate school as a both a scientist and mentor. I knew when I joined the Freedman lab that at the outset, I would be joining a small lab, and could encounter the headaches that may come with being the first graduate student joining a lab. I also knew that being in a small lab, I would have the opportunity to really shape my training in a unique way. It has been quite a journey and it's amazing to look back on all the iterations the lab has gone through. I'm (almost) more excited to see what the next crop of Freedman lab graduate students does than I am with my postdoctoral work. Thanks for letting me grow as a scientist, for endlessly editing all of my writing, even when the grant deadlines fell over holiday breaks, for mercilessly critiquing my practice seminars, for letting me attend amazing conferences and helping me network, for the happy hours and parties, and for years of great discussions. I became a better scientist with your guidance and am eternally grateful.

Dedicated to my parents,
for letting me climb trees with reckless abandon.

ABSTRACT

Cell-surface receptors on immune cells direct immune-cell function by sensing and responding to signs of pathogens and tissue damage. Signaling initiated by immunoreceptors is responsible for essential aspects of the immune response, including phagocytosis by myeloid cells, and antigen sensing by B and T cells. Efficient regulation of immunoreceptor signaling ensures that inflammation arising from pathogen clearance is limited in order to prevent tissue damage. Autoimmune diseases, such as systemic lupus erythematosus, can occur when these signaling pathways are improperly regulated. The tyrosine kinase Lyn is an important regulator of immune function due to its unique ability to both initiate signaling that can generate inflammation, and also recruit and activate proteins that dampen cellular activation. Alterations to Lyn expression and signaling in both human and mice can worsen or cause autoimmune disease. Understanding how Lyn is regulated and balances these roles is necessary to develop therapies that selectively limit autoinflammation but preserve pathogen clearance. Alternative splicing of the *lyn* gene produces two proteins, LynA and LynB, that differ by the presence of a 21-amino-acid insert present in LynA and absent in LynB. Here, we demonstrate the LynA and LynB are differentially regulated in immune cells. Phosphorylation of LynA at Tyrosine 32 in its unique region causes LynA to be rapidly, and selectively, poly-ubiquitinated by an E3 ligase, c-Cbl, and degraded. We show that differential expression of c-Cbl in macrophages and mast cells controls LynA protein levels, degradation, and signaling responses following Src-family kinase activation. Furthermore, we created novel knockout mice to study the roles LynA and LynB play in regulating autoimmune disease. Using these novel mice, we show that LynB prevents the development of splenomegaly and autoimmunity by limiting myeloid cell expansion and B cell activation. We also demonstrate that LynB-deficient mice have elevated responses to Toll-like receptor activation. Together, these results indicate that LynA and LynB are differentially regulated and have unique roles in the immune response. Therefore, understanding LynA and LynB signaling and regulation could yield targets that limit inflammation but preserve normal immune function.

TABLE OF CONTENTS

LIST OF TABLES

LIST OF FIGURES

CHAPTER 1: Introduction

1.1 Receptor diversity, signaling commonalities

The cells that comprise the immune system are diverse in nature, spanning short-lived innate immune cells such as neutrophils, which circulate through blood and lymph, patrolling for signs of infection and tissue damage, to long-lived tissue-resident lymphocytes and macrophages, which maintain tissue homeostasis while also acting as sentinels for infection. The diversity of immune cells allows the immune system to accomplish a diverse set of responsibilities, including, but not limited to, protecting against and eliminating pathogens, managing a diverse microbiota [1], directing organ development [2], eliminating apoptotic cell debris [3-5], preventing and eliminating cancerous cell growth [6-8], facilitating wound repair [9, 10], and monitoring and directing synaptic transmission and neuronal function [11]. To accomplish these varied tasks, immune cells express a panoply of receptors that respond to diverse environmental cues and subsequently direct immune function. Suprathreshold receptor ligation initiates signaling that directs an appropriate immune response. Ensuring that cues sensed by these receptors are properly integrated and regulated is absolutely critical to ensure that inflammation driven by an immune response is limited in scope to prevent tissue damage. Diseases such as cancer [7], lupus [12, 13], atherosclerosis [14] and other autoinflammatory diseases, and can occur when these systems are improperly regulated.

Intracellular tyrosine kinases are important mediators of immunoreceptor signal transduction and regulate immune-cell activation, proliferation, survival and the immune response to pathogens [15]. The transfer of the terminal phosphate of ATP to a tyrosine residue on a protein substrate results in changes in conformation and protein-protein interactions that act as signals to direct cellular function [16]. Although the growth, survival, and proliferation functions of tyrosine kinases are important in all cells, immune cells employ peculiar binding motifs, alternative expression of kinase family members, and additional receptor families for additional functionalities such as phagocytosis, antigen-specific signaling, and polarization. In lymphocytes, Src-family kinases (SFKs) initiate signaling downstream of T- and B-cell receptors by phosphorylating immunoreceptor tyrosine-based activation motifs (ITAMs), which lead to the activation of the tandem-SH2-containing tyrosine kinases Syk and Zap-70 [17, 18]. Together, these

tyrosine kinases activate FAK-family tyrosine kinases (FAK, Pyk2) and Tec-family tyrosine kinases (Btk, Itk, Tec [19]). Parallel pathways are activated upon Fc-receptor engagement in myeloid and NK cells. ITAM-coupled receptor activation and tyrosine kinase signaling is a major driver of the anti-pathogen response and can induce T cell activation, proliferation and degranulation; production of antibodies by B cells, pathogen engulfment (phagocytosis) by myeloid cells, and cytokine release and degranulation by NK cells [18, 20-23]. Janus-Kinase (JAK) activation downstream of membrane-proximal tyrosine kinase activation is critical for activation of Signal Transducer and Activator of Transcription (STAT) proteins that mediate growth, differentiation, and polarization [24] of immune cells in response to cytokines. Other receptor-tyrosine kinases such as Flt3, c-Kit, and Tyro/Axl/Mer control cell survival, differentiation and many other essential functions of immune cells [25, 26]. Despite the many inputs that engage tyrosine kinases and an intense research focus on the tyrosine kinases involved in immune activation, we are still discovering elements of the interactions and dynamics of tyrosine kinases that have profound effects on immune regulation [19, 22, 27-29]. Understanding the dynamics, kinetics, substrates, and scaffolding interactions of tyrosine kinases is critical to developing therapeutics that modulate immune function [13, 29, 30]. The research presented in this dissertation provides new insights into tyrosine kinase regulation and function in immune cells.

1.2 The Src-family kinases: structure and activation

1.2.1 Family members and structure

The SFKs in particular are critical for many aspects of immune activation. The SFKs comprise a group of eight evolutionarily and structurally related nonreceptor-tyrosine kinases [31-33]. The SFKs can be divided into two families differentiated by sequence similarity. The Lyn subfamily includes Lyn, Hck, Lck and Blk, while the Src subfamily includes Src, Yes, Fyn and Fgr [32]. Different immune cells express different SFKs, lending diversity to the regulation of similar signaling pathways. Notably, T cells primarily express Lck and Fyn, B cells primarily express Blk, Lyn, and Fyn, while myeloid cells express various combinations of Lyn, Hck, Fgr, Fyn and Src [32].

The SFKs share a similar domain structure (**Figure 1.1A**), with N-terminal palmitylation/myristylation sites followed by a disordered (or loosely ordered), unique region, Src-homology (SH)3, and SH2 domains, and ending with a two-lobed kinase domain. Lipidation anchors the SFKs to the inner leaflet of the plasma membrane and ensures proper microlocalization within membrane subdomains [34, 35]. The unique region is the least conserved element of the SFKs. Although other domains of the SFKs have been crystallized and structurally characterized, the unique region is relatively disordered, and not amenable to crystal structure analysis. Therefore, there is little structural information about the unique region. However, studies have shown that this region mediates important protein-protein interactions; for instance, the unique-region of Lck contains a Zinc-clasp structure that mediates the interaction of Lck with the T-cell coreceptors CD4 and CD8 [36, 37]. In most SFKs, the unique region may be post-translationally modified by phosphorylation or carbohydrate conjugation [38-40] to alter kinase function and interactions. In addition, the unique region can make intramolecular contacts that may alter kinase activity [41, 42]. Portions of this dissertation expand our knowledge on how the unique region regulates kinase function.

The SH3 and SH2 domains are well characterized structurally and have both regulatory and protein-protein interaction functions [43]. The SH3 binds intramolecular polyproline motifs [44] that keep the kinase in a closed confirmation, but also binds extramolecular polyproline motifs that help transmit signals. Similarly, the SH2 domain binds intra- and extra-molecular phosphorylated tyrosines [45] that serve similar purposes. The kinase

domain is responsible for transferring the terminal phosphate of ATP to a tyrosine residue on substrate proteins, which initiates signaling or alters protein structure [43].

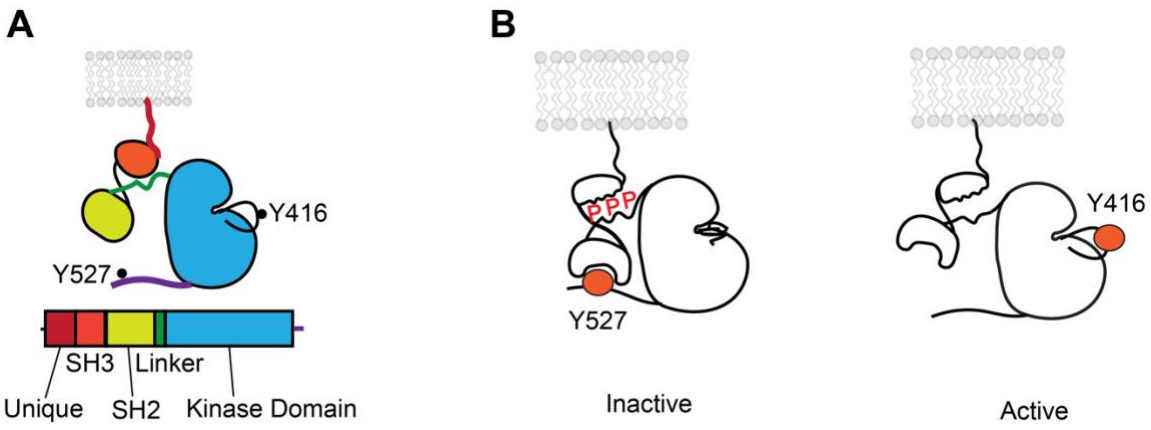

Figure 1.1. SFK structure and conformations. **(A)** Schematic of SFK structure **(B)** SFK in both inactive and active conformations, illustrating intramolecular interactions between the SH3 domain and polyproline motifs (P P P) in the linker region; and the SH2 domain bound to phosphorylated (red circle) Y527.

1.2.2 Intrinsic regulation of SFK activation

The kinase activity of the SFKs is subject to intramolecular regulation. In the inactive state, the SFKs are kept in a closed conformation that limits full kinase activity by blocking substrate binding and protein-protein interactions. (**Figure 1.1B**). In this state, the SH3 domain is bound to poly-proline motifs in a linker region that connects the SH2 domain to the kinase domain [46]. Similarly, the SH2 domain is bound to a phosphorylated tyrosine, tyrosine 527 (Y527 in the classical chicken, c-Src, numbering), on the C terminus [47, 48]. Activation of the kinase requires Y527 dephosphorylation, which opens the kinase and allows the SH3 domain to bind polyproline motifs in other proteins, further promoting an active conformation [49]. Phosphorylation of a tyrosine in the activation loop, Y416 (**Figure 1.1B**), is required for full kinase activity. The activation loop is important for binding magnesium, Mg^{2+}, that coordinates ATP binding in the active site. Phosphorylation at Y416, often provided via trans-autophosphorylation from other SFKs, induces a structural change that allows ATP and ligand binding in the active site of the kinase domain [50, 51]. Although full activation requires dephosphorylation of Y527 *and* phosphorylation of Y416, SFKs can adopt many conformations along a continuum of activation, with varied effects on kinase activity [52-54]. Additionally, post-translational modifications of other sites on the kinase can modulate kinase activity. Portions of this dissertation discuss some of these regulatory sites and mechanisms.

1.3 Regulation of SFK signaling and immune activation

1.3.1 Kinetic segregation and receptor clustering

Balancing Y527 and Y416 phosphorylation is critical for regulating the signaling ability of the SFKs. In immune cells, dephosphorylation of Y527 is primarily provided by the receptor-tyrosine phosphatases CD45 (Ptprc) and CD148 (Ptprj) [28, 55-57] and phosphorylation of Y527 is maintained by the kinase Csk [58]. The balance between CD45/148 and Csk regulates the pool of active SFK within the cell and subsequent downstream signaling generated by the SFKs.

Although CD45 and CD148 are required to initiate the process of SFK activation, both phosphatases also have the ability to dampen receptor signaling by dephosphorylating the SFK activation-loop tyrosine, Y416, and the ITAMs themselves [59]. Therefore, phosphatase localization and activity must be regulated to ensure maximal SFK signal

transduction. Kinetic segregation (**Figure 1.2A**) is a useful model that explains many aspects of how CD45/148 localization permits SFK activation and signal transduction. While most ITAM-coupled receptors have relatively small extracellular domains, on the order of ~5 nm [60], CD45 and CD148, have tall and rigid extracellular domains, 20-50 nm in length.[57, 61]. At steady-state, diffusion of phosphatases and receptors in two dimensions across the plasma membrane promotes a basal level of tonic signaling as CD45/148 dephosphorylate SFK Y527, and also limits the amplification of this signaling by dephosphorylating Y416, and ITAMs. However, when ITAM-coupled receptors are engaged by ligands, the bulky extracellular domains force the phosphatases to become excluded from a zone of diffusing ITAM-coupled receptors, known as the immunological/ phagocytic synapse [62, 63]. SFKs entering this exclusion zone are initially dephosphorylated at Y527 by the excluded phosphatases, and then subsequently protected by the absence of phosphatase in the synapse, allowing for ITAM phosphorylation and activation of Syk/Zap-70 which activates further downstream signaling [63]. Removing the bulky extracellular domain of CD45 and CD148 has been shown to alter phosphatase localization and abrogate SFK-mediated signaling.

The degree of receptor clustering (**Figure 1.2 B-C**) influences signaling outcomes in immune cells as well. While low-valency (nanoclustering) receptor ligation can exclude CD45/148 and activate the SFKs, it is not enough to induce cellular activation [62, 64, 65]. Signaling events and Zap-70 recruitment are partially controlled in T cells by the degree of receptor clustering [65]. Phagocytic cells, such as neutrophils and macrophages, have the ability to identify ITAM-receptor ligands associated with intact pathogens by sensing the degree of ITAM-clustering as a proxy for the size of the interacting surface. For instance, neutrophil extracellular trap (NET) release is more likely to occur in response to large fungal hyphae than smaller yeast cells [66, 67]. Similarly, the production of reactive oxygen species (ROS) and IL-6 in macrophages is dependent on stimuli size [62].

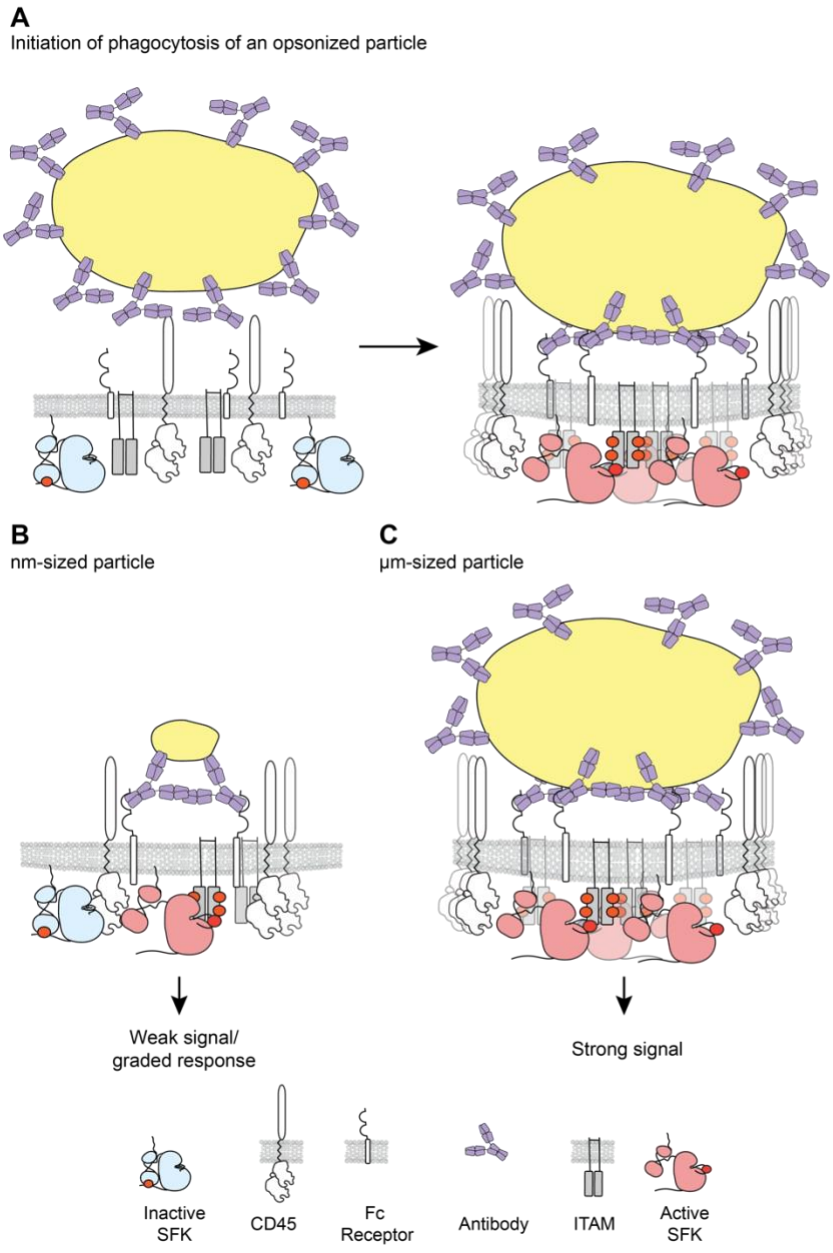

Figure 1.2. Kinetic segregation and receptor clustering. **(A)** Schematic of kinetic segregation illustrating phosphatase exclusion during Fc Receptor mediated formation of a phagocytic synapse. **(B-C)** Receptor clustering increases the degree of phosphatase exclusion and SFK activation.

1.3.2 Limitations of the kinetic segregation model

Although kinetic segregation is a useful model for understanding many aspects of SFK regulation, several studies have suggested that additional regulatory mechanisms influence immune activation. The phosphatases CD45 and CD148 are exceptionally efficient enzymes (Tanya Freedman, data unpublished). CD45 is also one of the most abundant proteins on the immune cell surface [68]. The high efficiency and expression of CD45 results in a considerable pool of active SFKs within resting cells [69]. Because this pool of active SFK is unable to induce effective downstream signal activation, additional regulatory elements must be present that regulate SFK activation and signaling. Pivotal studies using macrophages and T cells from Csk^{AS} transgenic mice have revealed other regulatory elements important for signal transduction following SFK activation. The Csk^{AS} system utilizes a designer version of Csk that can be specifically inhibited by the small molecule 3-IB-PP1 (**Figure 1.3**) [70]. In both T cells and macrophages that express Csk^{AS}, 3-IB-PP1 treatment induces robust SFK activation in the absence of any phosphatase exclusion or receptor ligation. Despite this strong initiation of signaling, Csk-inhibition fails to generate downstream markers of cellular activation, such as MAPK or Akt activation-loop phosphorylation, in both T cells and macrophages [22, 71]. In T cells, this signaling blockade can be overcome by cotreating with small molecules that induce remodeling of the actin cytoskeleton [71]. Actin corrals can restrict receptor diffusion and prevent full-scale receptor clustering, and the importance of actin in restricting cellular activation by limiting receptor diffusion is supported by other work [72-74]. Interestingly, in macrophages, actin remodeling fails to restore cellular activation in response to 3-IB-PP1-induced SFK activation, showing that regulation of SFK signaling differs by cell type. In macrophages, the signaling blockade is restored by pretreating (priming) the cells with inflammatory cytokines, which induces changes in protein expression, particularly the upregulation of the SFKs Lyn and Hck [22]. The ability of the SFKs to induce downstream signal transduction in primed macrophages upon 3-IB-PP1-induced activation was further shown to depend on Lyn. Actin-restricted receptor diffusion and regulation of the protein levels of receptors and signaling molecules are two mechanisms that work in concert with phosphatase exclusion to regulate SFK activation and signaling. The difference in SFK signaling between macrophages and T cells, illustrated by studies with Csk^{AS} mice, show that SFK signaling is also regulated in a cell-specific manner. Portions of this dissertation expand on some of the regulatory

mechanisms that function independently of kinetic segregation to control SFK signaling in different cell types.

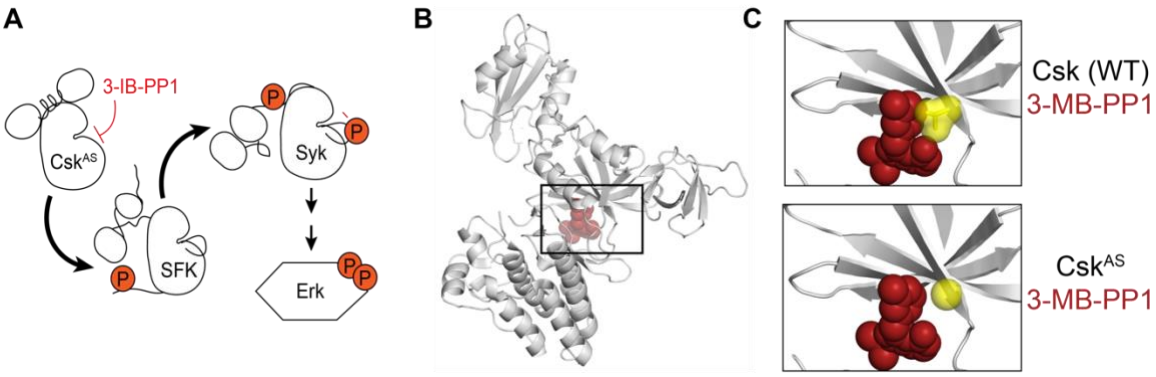

Figure 1.3 The analog-sensitive kinase Csk^{AS}. (A) The analog-sensitive kinase Csk^{AS} is inhibited by the bulky PP1 analog 3-IB-PP1, leading to Src family kinase (SFK) activation and subsequent activation of Syk tyrosine kinase. **(B)** Crystal structure of Csk (gray; PDB ID: 1K9A;[75]) modeled with the ATP binding site occupied by a bulky analog of the kinase inhibitor PP1 (3-MB-PP1; red). The box outlines the zoomed images in the following panel. Image rendering and modeling was performed in Pymol.**(C)** Zoomed views of wild-type (WT) and (modeled) Csk^{AS} with the gatekeeper (residue 266) highlighted in yellow. Threonine-to-glycine substitution of the gatekeeper residue (T266G) enlarges the ATP binding pocket, accommodating the bulky inhibitor. Wild-type Csk and endogenous kinases are not as sensitive to bulky inhibitor analogs

1.3.3 Non-receptor phosphatases and ubiquitin ligases

Additional regulatory mechanisms both prevent and dampen signal transduction by the SFKs. Non-receptor phosphatases such as SHP-1/2, PTPN22 (also called Lyp in humans or PTP-Pep in mice), and SHIP-1 are important regulators of SFK- and tyrosine-kinase signaling. In immune cells, SHP-1 and SHP-2 associate with immunoreceptor tyrosine inhibitory motifs (ITIMs) present within receptors such as FcγRIIb and Sirpα [76, 77]. ITIMs contain a single tyrosine site of phosphorylation, that, like ITAMs, is predominantly phosphorylated by the SFKs [18]. Upon ITIM phosphorylation, the SH2 domains found within SHP-1 and SHP-2 bind the phosphorylated ITIMs and are recruited from the cytoplasm to the plasma membrane, into close proximity to the SFKs, Syk/Zap-70 and phosphorylated ITAMs, which can be subsequently dephosphorylated by the SHP-1 and SHP-2 phosphatase domains. In accordance with kinetic segregation, failure to exclude ITIM-coupled receptors from the immunological synapse can dampen SFK signaling and cellular activation [78, 79]. The importance of SHP-1 to immune regulation is especially illustrated by the stark phenotype of SHP-1^{KO} mice [80]. Due to inflammation triggered by unrestrained myeloid activation and proliferation, SHP-1^{KO} mice develop pneumonia and skin lesions that have led this mouse strain to be commonly referred to as the “motheaten” mouse. Although SHP-2^{KO} mice suffer from embryonic lethality, this is not a result of immune activation but rather due the importance of SHP-2 for gastrulation. Interestingly, selective deletion of SHP-2 in T, B and myeloid cells has revealed contrasting roles for SHP-2 in both limiting ITAM and cytokine receptor signaling, and promoting activation of mitogen-activated protein kinase (MAPK) signaling pathways, lending complexity to the regulatory mechanisms that control immune activation [81, 82].

Ubiquitin ligases are important regulators of tyrosine kinase activity. The conjugation of ubiquitin to proteins can lead to conformational changes, cellular re-localization and protein degradation by both the lysosome and proteasome [83]. The Cbl family of ubiquitin ligases, which include the proteins c-Cbl and Cbl-b, are especially important regulators of both the SFKs and other tyrosine kinases in immune cells [84]. Both c-Cbl and Cbl-b contain structural elements that mediate strong interactions with the SFKs, including an SH2-like domain that can bind phosphorylated tyrosines on the SFKs, poly-proline motifs that can interact with the SFK SH3 domain, and tyrosine phosphorylation

sites that can interact with the SFK SH2 domain [84-86]. In addition, c-Cbl requires phosphorylation by SFKs to become activated [87, 88]. The importance of c-Cbl and Cbl-b in regulating SFK signaling has been demonstrated in both mice and humans. Mutations in c-Cbl that abrogate ubiquitin-ligase activity are found in leukemias, leading to increased SFK-mediated phosphoinositide 3-kinase (PI3K) signaling and cancer cell growth [89, 90]. Similarly, deletion of c-Cbl and Cbl-b in immune cells alters antigen receptor signaling in T cells, impairing receptor internalization, promoting cellular proliferation and causing defective positive selection in T cells [91-93]. Ubiquitin ligase activity by c-Cbl and Cbl-b also regulates B-cell-receptor recycling and localization, and the germinal center response [94, 95], as well as myeloid C-type lectin and Fc Receptor signaling [96-100].

1.4 Role of the SFK Lyn in immune signaling

1.4.1 Multiple roles for Lyn in regulating immune function

Lyn has long been a kinase of interest to immunologists. The *lyn* gene was first identified in 1987 via a cDNA screen as putative tyrosine kinase with similar structure to the previously identified SFKs Yes, Lck, Src and Fgr [101], and its tyrosine kinase activity was demonstrated shortly thereafter [102]. In 1991 Lyn was shown to be expressed in B cells, co-immunoprecipitate with the B cell receptor (BCR), and become phosphorylated following BCR stimulation. Crosslinking the BCR was shown to activate Lyn and cause it to bind the non-catalytic subunit of PI3K [103, 104]. Similarly to the BCR, Lyn could be co-immunoprecipitated with the ITAM-coupled FcεR in mast cells, activated following FcεR crosslinking, leading to the activation of phospholipases [105-107]. Further research showed that Lyn was expressed in platelets and associates with CD36, was expressed in monocytic cells [108, 109] and activated downstream of GM-CSF-receptor ligation [110].

These early studies suggested that by activating PI3K and phospholipase signaling downstream of ITAM-coupled receptors and cytokine receptors, Lyn functions redundantly to other SFKs in immune cells. However, in 1995 the development of gene targeting in embryonic stem cells allowed Lyn^{KO} mice to be created. Studies from these mice revealed that Lyn had a unique role in *suppressing* immune function. Using Lyn^{KO} mice, the Dunn group discovered that Lyn was required for the proper development of several types of immune cells [111]. Like some of the previously described severely immunocompromised mice at that time, such as the Btk^{KO} and motheaten ($SHP\text{-}1^{KO}$) mice, Lyn^{KO} mice had a marked reduction in B cells, resulting from a defect in B cell development, particularly in the transition of Pro/Pre-B cells to mature B cells. In addition, at roughly 10 months of age the Lyn^{KO} mice developed symptoms similar to the human autoimmune disease, systemic lupus erythematosus (SLE). Despite the defect in B cell formation and maturation, Lyn^{KO} plasma cells produced increased levels of circulating antibodies and produced anti-nuclear antibodies. The production of autoreactive antibodies that become deposited in the kidney promotes inflammation and kidney damage (glomerulonephritis). In parallel studies [112], The Yamamoto group demonstrated similar findings (defects in B cell maturation and the development of Lupus-like pathologies), but also noted the development of splenomegaly in Lyn^{KO} mice,

largely due to the increased presence of Mac-1+ (CD11b+/CD18+) cells, including monocytes, granulocytes and innate-like B-1 B cells. These two pivotal studies demonstrated that Lyn has a surprising role in negatively regulating the immune system, in contrast to the other SFKs expressed in immune cells.

A number of proteins and signaling cascades were shown to be critical for driving autoimmunity in the absence of Lyn. Cytokines like IL-6, BAFF, and IFN-γ ,[113, 114] and cytokine receptors, such as the IL-5Ra [115] were shown to promote autoinflammation and myeloproliferation in Lyn^{KO} mice. Proteins associated with actin rearrangement like Ezrin [116] and signaling proteins downstream of Lyn, including PI3K and Btk, have also been shown to mediate autoimmune disease in Lyn^{KO} mice.

Components of Toll-like Receptor (TLR) signaling, including the adaptor proteins MyD88 [117, 118] and CARD9 [119] , and the transcription factor IRF5 [120] were also shown to promote disease in the absence of Lyn. The Toll-like receptors are a group of receptors that sense components of bacterial, fungal and viral antigens, including lipopolysaccharides (LPS) derive from gram-negative bacteria, and single-stranded DNA derived from bacteria and viruses. The link between Lyn and TLR signaling was first illustrated in 1993, when Lyn was shown to co-immunoprecipitate with CD14, and be activated following LPS treatment of human monocytes [121]. However, a clear understanding of Lyn's role in TLR signaling remains elusive, likely due to differences in TLR signaling in different cell types. Lyn-deficient dendritic cells have elevated signaling responses and secrete more cytokines following treatment with ligands that activate the MyD88-dependent TLR4 (LPS) and TLR9 (CpG) [117, 119, 122]. Lyn has been shown to both positively and negatively regulate plasmacytoid dendritic cell (pDC) TLR signaling, depending on the method of TLR-agonist treatment [117, 123]. When pDCs are treated with CpG, Lyn is required for Type I Interferon production because Lyn promotes proper endosomal tracking and delivery of CpG to endosomal TLR9 [123]. Likewise, research has demonstrated conflicting roles for Lyn in macrophage TLR signaling. Some studies have demonstrated a negative role for Lyn in TLR4-related signaling [124], while others have demonstrated a minimal role for Lyn in the macrophage response to TLR receptor activation [119]. Finally, Lyn has been shown to be required for optimal cytokine release and downstream signaling in response to LPS treatment in mast cell [125].

TLRs themselves and TLR signaling are strongly linked to autoimmune and autoinflammatory diseases in both humans and mice. Lupus patients have increased TLR4, TLR7 and TLR9 expression, which is associated with worse lupus pathology [126, 127]. Overexpression of TLR7 and chronic TLR7 and TLR9 signaling induces autoimmune disease in mice [128-130]. Similarly, TLR4 is required for kidney pathology in some mouse autoimmune disease models [131]. Portions of this dissertation present new evidence examining the role for Lyn in TLR signaling and autoimmune disease development.

In mature follicular B cells, Lyn deletion causes both a delay and an amplification of BCR signaling, while simultaneously making cells more resistant to apoptosis, pushing cells towards an activated state, and promoting differentiation to plasma B cells [12, 132]. While initial animal studies were made using germline deletion of Lyn, genetic deletion of Lyn solely in B cells using Cre recombinase under the CD79a promoter showed that Lyn^{KO} B cells alone could induce autoimmunity and myeloproliferation [118]. Parallel studies using selective deletion of Lyn in dendritic cells via CD11c-cre revealed a critical role for dendritic-cell involvement in Lyn-mediated suppression of autoimmunity [117]. Lyn^{KO} conventional dendritic cells (cDC's) express higher levels T-cell-costimulatory molecules such as CD80 and CD86 and secrete higher levels of cytokines in response to TLR ligation.

While the proteins and cell types involved in autoimmunity development in Lyn-deficient mice were being discovered, so were the proteins involved in Lyn-mediated immune suppression. Early work defined the ability Lyn to co-immunoprecipitate and phosphorylate CD22 and FcγRIIb on B cells and mediate recruitment and phosphorylation of the phosphatases SHP-1, SHP-2, and SHIP-1 [112, 133, 134]. The integrin CD11b was shown to recruit Lyn and SHP-1 and dampen B cell and dendritic cell activation [119, 135]. Furthermore, Lyn-deficiency has been shown to mediate human SLE pathogenesis. Some patients with lupus have decreased B-cell-Lyn expression or altered Lyn trafficking [136-138]. Polymorphisms in the *LYN* gene are also enriched in patients with lupus [139], suggesting that like mice, Lyn plays a prominent negative role in human immunoreceptor signaling.

While Lyn is most well-known for its role in negatively regulating immunoreceptor signaling, Lyn does have prominent roles in promoting cellular activation as well. In contrast to follicular B cells, B1 B cells, which respond to T cell-independent antigens, require Lyn for downstream signaling in response to BCR ligation [140]. In B1 B cells, CD148 preferentially activates Lyn upon BCR ligation. CD148 is highly expressed in B cells and myeloid cells, and in macrophages, Lyn is activated more rapidly than other SFKs [22] as well. Similarly to BCR signaling, Lyn has positive and negative roles in mast-cell-FcεR1 signaling. The different roles for Lyn in FcεR1 signaling likely depend, at least in part, on the strength of stimulation [141]. In mast cells, Lyn is required for MAPK/Erk and Akt activation in response to low concentrations of stimuli, yet also required for effectively regulating/dampening MAPK and Akt activation in response to high stimuli concentrations. FcγR-mediated phagocytosis-induced signaling is defective in Lyn^{KO} macrophages as well [142]. Lyn^{KO} mice are also less able to survive infection with certain pathogens, including *Salmonella typhimurium* and *Pseudomonas aeruginosa* [119, 143-145]. In both respiratory and enteric infection models, Lyn^{KO} mice suffer from increased bacterial burden and increased cytokine secretion. While increased cytokine production in response to pathogens may result from a lack of negative regulation, Lyn appears required for proper pathogen phagocytosis and killing [144]. The susceptibility of Lyn^{KO} mice to pathogenic infection highlights both the positive and negative functions of Lyn in immunoreceptor signaling. Understanding how Lyn balances these functions, especially with regard to how Lyn regulates signaling across different cell types, is critical to understanding the contexts in which immunoreceptor signaling promotes diseases such as autoimmunity.

1.4.2 Alternative splicing of lyn: LynA and LynB

In 1991 mRNA from the *lyn* gene was shown to produce two alternatively spliced proteins, LynA and LynB [146]. LynA and LynB differ by the presence of a 21-amino acid insert located in the unique region of LynA, but absent in LynB. Alternative splicing of *lyn*, and the amino-acid sequence of the unique region present in LynA, is highly conserved throughout mammals, from primates to rodents and marsupials (**Figure 1.4**) [147].

The Yamamoto group was the first to demonstrate that LynA and LynB are differentially regulated, noting that the protein levels of LynA were selectively downregulated upon antigen stimulation in B cells [148]. In agreement with the Yamamoto study of LynA and LynB in B cells, Freedman et. al [22]. demonstrated that LynA was actively degraded upon pan-SFK activation in macrophages. The Freedman lab further demonstrated that LynA protein levels were critical for determining the sensitivity threshold for downstream signaling in macrophages in response to SFK activation. The evidence suggesting that LynA may activate downstream signaling more readily than LynB is consistent with other studies in mast cells [149] and MDA-MB-231 breast cancer cells [150]. Lyn^{KO} mast cells lentivirally-reconstituted with LynA showed greater phospholipase activation and more readily degranulated upon FcεR ligation, than those reconstituted with LynB. Conversely, LynB more readily phosphorylated inhibitory proteins such as SHIP-1, suggesting that LynB might play a more prominent role in inhibitory signaling [149]. Similarly, MDA-MB-231 breast cancer cells selectively expressing LynA have a more invasive phenotype than those selectively expressing LynB [150].

SFK signaling induces many aspects of the immune response. As such, SFK signaling must be efficiently regulated to insure proper control of inflammation and tissue damage. Kinetic segregation, the degree of receptor clustering, ubiquitin ligases and phosphatases all work in concert to regulate SFK signaling. The SFK Lyn is particularly required for negatively regulating SFK and ITAM-related signaling. The transcript for Lyn encodes two proteins, LynA and LynB. This dissertation expands on the regulatory mechanisms that control LynA and LynB signaling, and the role the two proteins play in the development of autoimmunity.

A

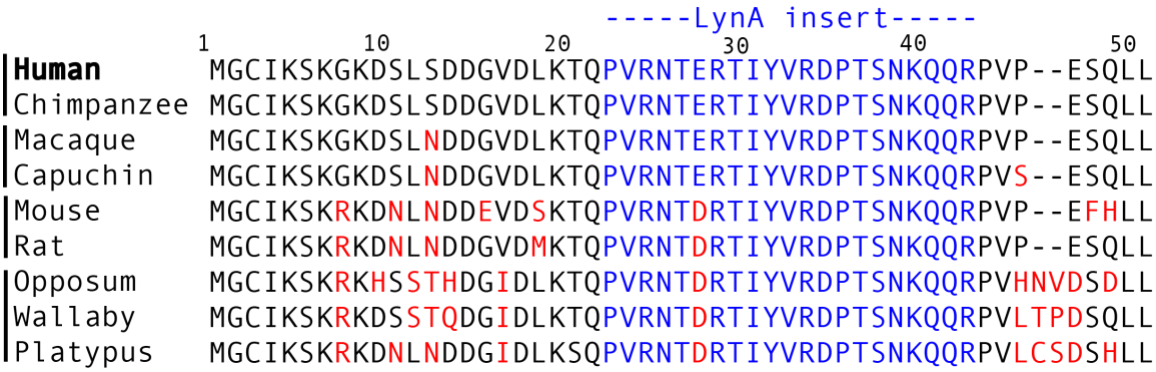

Figure 1.4 LynA is highly conserved across species (A) Sequence alignment of ape (human, chimpanzee), monkey (rhesus macaque, capuchin), rodent (mouse, rat), and marsupial (opossum, wallaby, and platypus) N-terminal Lyn protein sequences. Differences from human sequence are marked in red. The LynA insert is marked in blue. Sequences obtained from the Universal Protein Resource (Uniprot Entries: P07948, H2R453, F7BV42, A0A6J3JBZ6, P25911, Q07014) and Suthers et. al. [147]

1.5 Footnotes

Portions of this text were adapted from:

Brian BF 4th, Guerrero CR, Freedman TS. Immunopharmacology and Quantitative Analysis of Tyrosine Kinase Signaling. Curr Protoc Immunol. 2020 Sep;130(1):e104. doi: 10.1002/cpim.104. PMID: 32931655; PMCID: PMC7583487.

Author contributions: BFB, CRG and TSF wrote the manuscript.

CHAPTER 2: Methods

2.1 Tools for studying tyrosine kinase signaling

Numerous tools exist for studying the actions of tyrosine kinases in immune cells, including genetic methods, such as small interfering RNA (siRNA) knockdown and CRISPR/Cas9-based gene editing, small-molecule inhibitors, and designer kinases. Each approach has advantages and disadvantages with regard to specificity, temporal control, and likelihood of triggering compensatory mechanisms **(Table 2.1)**.

Method	Advantages	Disadvantages
Small-molecule inhibitors	Inexpensive, Rapid inhibition, No genetic compensation	Poor selectivity, Low solubility of inhibitors
Knockout models	Specificity, No barrier to studies *in vivo*	Transcriptional/Post-translational compensation that leads to altered signaling, Time/labor intensive, Expensive to maintain
Analog-sensitive kinases	Rapid kinase inhibition, No transcriptional feedback, Portable and robust	Time- and labor-intensive design/screening
Immunoblotting	Detection of low-abundance proteins, Wide compatibility	Low throughput, Limited by availability of validated, site-specific antibodies
Non-targeted proteomics	Unbiased, Can reveal novel phosphorylation sites	Limited quantification (no protein standards), Limited sensitivity, so might miss low-abundance proteins and rare events
Targeted proteomics	Precise quantification, even of low-abundant proteins or phosphorylation events, Does not rely on availability of antibodies	Time- and labor-ine assay development, Limited scope

Table 2.1: Advantages and disadvantages of different methods for studying tyrosine kinase signaling

Genetic methods are attractive options for studying kinase function because of their inherent specificity and stability. While knockout gene-editing strategies are valuable because they offer complete disruption of kinase signaling, siRNAs offer inducible control over kinase-signaling disruption and supplement knockout strategies when a knocking out a given kinase may be lethal to a cell or animal. siRNAs and genetic knockouts are routinely used to investigate the importance of specific kinases in immune cells. For instance, mice in which the SFK Lyn has been knocked out (Lyn^{KO}) have become important models of autoimmune disease after studies revealed the importance of Lyn as a negative regulator of B- and dendritic-cell activation [12, 151]. Tyrosine-kinase knockouts can also be coupled to *Cre-lox* and FLP-FRT systems for cell-specific knockout [117, 118]. The advent of CRISPR-Cas9 gene editing has facilitated the substitution of specific amino acid residues in knock-in models, allowing researchers to dissect novel elements of tyrosine kinase function [152]. The major drawback of genetic knockout and knockdown models for studying kinase signaling is that cells often develop compensatory mechanisms for coping with the loss of given kinase. These feedback (or, in cell lines and aging animals, cellular-evolutionary) effects may mask the normal signaling contributions and scaffolding interactions of the kinase of interest [153, 154].

Small-molecule inhibitors have facilitated the study of kinases in many aspects of immune activation. Kinase inhibitors generally function by competing with ATP for access to the active site, preventing substrate phosphorylation [155]. Although many compounds are marketed for inhibition of specific kinases, caution should be used when choosing an inhibitor and interpreting its effects on signaling. ATP-binding sites are highly conserved across the kinome [156], and most inhibitors target multiple kinases, either within a family or in different branches of the kinome [157]. Researchers should familiarize themselves with these off-target effects and use the lowest effective concentration of inhibitor to disfavor weaker binding interactions. Furthermore, many kinase inhibitors are poorly soluble in aqueous buffers, necessitating formulation for *in vivo* experiments or pre-treatment for *in vitro* experiments [158, 159]. A final consideration when working with ATP-mimetic inhibitors is that these inhibitors typically bind and may even induce the active conformation of the kinase. This can lead to a paradoxical increase in typical readouts of kinase activation (e.g. phosphorylation of the activation-loop tyrosine) and may even ultimately promote signaling due to release of

autoinhibition. Careful controls, for example assaying phosphorylation of inhibitory/activating sites on the kinase and direct substrates should be probed along with downstream readouts of cell activation. Ultimately, however, small-molecule inhibitors for many kinases are well characterized, commercially available, and require little up-front investment of time or resources. Moreover, a pharmacological approach can uniquely enable the study of transient effects with high kinetic fidelity and minimal regulatory compensation. Inhibitors are thus powerful tools for dissecting kinase contribution to immune activation. Inhibitors also have the advantage of potentially preserving scaffolding interactions of the target protein, unlike genetic knockout and knockdown methods.

Chemical-genetic methods for studying kinase signaling in immune cells combine the specificity of gene editing with the temporal control of small-molecule inhibitors. In one approach, kinases are sensitized to a bulky analog of an ATP-competitive kinase inhibitor by substituting a smaller amino-acid side chain for the usual aliphatic, polar, or bulky gatekeeper residue [160]. Since the gatekeeper is not directly involved in ATP binding, the “analog-sensitive” (^{AS}) kinase is functionally active until the designer inhibitor is added [161]. This chemical-genetic approach can be used in transfected/transduced cells or incorporated into the genome of a model animal as a transgene or knock-in. Since endogenous kinases have more occlusive gatekeeper residues, the engineered kinase-inhibitor pair is much more specific than traditional kinase inhibition. Importantly, analog-sensitive kinase inhibition has the additional advantage over genetic or siRNA knockout approaches in that normal kinase function in the absence of inhibitor will allow direct comparison of cells pre- and post-treatment. This real-time component also minimizes the likelihood of compensatory transcriptional changes and other adaptations in primary cells or animals and selective pressure and evolution in cell lines. This approach has been used to identify the specific roles for Zap-70 in T-cell activation and Csk in T-cell and macrophage activation, and has been applied to other kinases as well [22, 71, 162]. Furthermore, although many kinase inhibitors blunt signaling, some kinases, such as Csk, have negative-regulatory functions. Inhibition of analog-sensitive Csk (Csk^{AS}) with 3-IB-PP1 leads to robust Src-family kinase (SFK) *activation* [22, 71]. Inhibition of this negative-regulatory kinase can be used as potent stimuli of cellular

signaling and can be combined with other kinase inhibitors to elucidate kinase contributions to cellular activation and protein dynamics [27].

Although some information can be gleaned from unbiased total-protein and pan-phosphotyrosine detection methods, immunoblotting is typically most effective when applied as a targeted, relatively low-throughput process, requiring antibodies raised against unique peptide sequences or sites of posttranslational modification. The best antibodies have minimal cross-reactivity with other molecules in the cell. Small-volume, higher-throughput apparatuses are available, but these systems are less amenable to combining antibodies and resolving multiple species in a single blot. Despite these caveats, immunoblotting remains a robust, sensitive, and adaptable technique [163]. If epitope-specific antibodies are unavailable, immunoblotting can be combined with immunoprecipitation. For example, total protein immunoprecipitation can be followed with a pan-phosphotyrosine blot, and molecular-weight can be used to infer the identity of phosphorylated protein [22]. Alternatively, cyanogen-bromide fragmentation [164] can resolve phosphorylation of individual sites on multiply-phosphorylated proteins.

Freed of the requirement for specific antibodies, liquid chromatography mass spectrometry (LC-MS/MS) is an excellent exploratory technique for quantifying poorly-studied proteins and sites of post-translational modification. This methodology is especially useful for multiply-modified proteins that cannot easily be probed by blotting. Advances in LC-MS/MS have allowed researchers to quantify tyrosine phosphorylation via targeted and unbiased approaches [165-167]. Proteomics approaches use databases to identify enzyme-digested peptides following resolved by LC-MS/MS. Unbiased LC-MS/MS can identify novel sites of phosphorylation in a cell lysate or but may miss low-abundance peptides. In contrast, targeted approaches using isotope-labeled reference peptides are highly sensitive and can be used to quantify abundance or novel sites of post-translational modification in both cell lysates, but also *in vitro* kinase assays using recombinant or purified proteins.

Work presented in this dissertation uses knockout and knockdown models, CRISPR-Cas9 gene editing, analog-sensitive kinases, small-molecule inhibitors, immunoblotting and mass spectrometry to dissect the unique regulatory mechanisms and functions of LynA and LynB in immune cells.

2.2 Experimental methods

2.2.1 Mice

C57BL/6-derived *Csk*^{AS} mice are hemizygous for the *Csk*^{AS} BAC transgene on a *Csk*$^{-/-}$ background, as described previously [22, 71]. *Csk*^{AS}*Cblb*$^{-/-}$*(Csk*$^{-/-}$*)* mice were generated by crossing *Cblb*$^{-/-}$ female mice from M. Farrar (University of Minnesota) [91] with *Csk*$^{+/-}$ and *Csk*^{AS} male mice from our colony and then crossing *Csk*$^{+/-}$*Cblb*$^{-/-}$ *with Csk*^{AS}*Csk*$^{+/-}$ *Cblb*$^{-/-}$ mice. Due to sterility of *Cbl*$^{-/-}$ male mice, we were not able to produce a sustained lineage of *Csk*^{AS}*Cbl*$^{-/-}$*(Csk*$^{-/-}$*)* mice, but we obtained three individuals by crossing *Cbl*$^{-/-}$ female mice from E. Peterson (University of Minnesota) [168] with *Csk*$^{+/-}$ and *Csk*^{AS} male mice from our colony and then crossing *Cbl*$^{+/-}$*Csk*$^{+/-}$ *with Csk*^{AS}*Cbl*$^{+/-}$ mice. All mice were housed in specific pathogen-free conditions and genotyped using real-time PCR (Transnetyx, Inc., Memphis, TN). All animal use complies with University of Minnesota (UMN) and National Institutes of Health (NIH) policy (Animal Welfare Assurance Number A3456-01). UMN is accredited by AAALAC, and all animal use was approved by the UMN Institutional Animal Care and Use Committee (IACUC, protocol # 1910-37487A). Animals are kept under supervision of a licensed Doctor of Veterinary Medicine and supporting veterinary staff under strict NIH guidelines.

2.2.2 DNA constructs and mutagenesis

Plasmids containing c-terminally His_6V5-tagged mouse LynA and LynB were gifts from J. Rivera/R. Suzuki (National Institutes of Health) [149]. Myc-tagged mouse memCsk^{AS} [also referred to as Lck11-CskAS, 70] and Xpress-tagged human c-Cbl and Cbl-b [169] were gifts from A. Weiss (University of California, San Francisco). Untagged mouse Hck^{56+59}, Hck^{56}, Fgr, and FynT (Fyn), and human FynB were gifts from C. Lowell (University of California, San Francisco.) Site-directed mutagenesis was performed using QuikChange Lightning (Agilent Technologies, Santa Clara, CA) and was used to prepare the point mutants referenced in the main text, and also to introduce stop codons removing epitope tags from Fgr, LynA, and LynA^{Y32A}. Sequences of all constructs were verified by Sanger sequencing (GENEWIZ, South Plainfield, NJ).

2.2.3 Jurkat cell lines and transfection

The Jurkat T-cell strains Clone E6-1 [170] and JCaM1.6 (Lck-deficient) [171, 172] were gifts from the laboratories of A. Weiss (University of California, San Francisco) and Y. Shimizu (University of Minnesota), respectively. Both cell lines were authenticated by

STR profiling and tested negative for mycoplasma (ATCC, Manassas, Virginia). Jurkat cell lines were cultured in RPMI-1640 medium supplemented with 5-10% fetal calf serum (Omega Scientific, Inc., Tarzana, CA) and 2 mM glutamine, penicillin and streptomycin (Sigma-Aldrich, St. Louis, MO) as described previously [173]. Jurkat and JCaM1.6 cells were transiently transfected via electroporation, as described previously [173]. Briefly, cells were grown overnight in antibiotic-free RPMI-1640 medium supplemented with 10% fetal bovine serum (Omega Scientific) and 2 mM glutamine (RPMI10). Batches of 15 M cells were resuspended in RPMI10 with 10-15 µg plasmid DNA per construct. Cells were rested, electroporated at 285 V/10 ms in a BTX square-wave electroporator (Harvard Apparatus, Holliston, MA), resuspended in RPMI10, and allowed to recover overnight. One million live cells were then resuspended in phosphate-buffered saline (PBS), rested for 30 min at 37°C, and stimulated.

2.2.4 Microscopy

Jurkat cells were transfected with a membrane-anchored Csk^{AS} (memCsk^{AS}), c-Cbl, and LynB (to ensure a response to 3-IB-PP1) along with constructs encoding the unique regions of LynA, LynB and $LynA^{Y32A}$ fused to eGFP. A construct containing eGFP alone was used as a control. 24 hours after transfection, cells were filtered to remove clumps of dead cells and resuspended in PBS containing Hoechst Stain (Thermo Fisher) and incubated for 30 min at 37°C in a 96-well plate. Cells were then treated with 3-IB-PP1 at 37°C for 5 min before quenching with ice cold PBS and collected by centrifuging for 5 min x 1500 rpm at 4°C. Cells were resuspended in ice cold PBS pipetted onto glass slides and coverslipped directly before imaging. Cells were imaged using a Leica DM600B epifluorescent microscope using DAPI and GFP channels. Exposure times for GFP were set to normalize the brightness of the GFP across the different transfection conditions, as cell-to-cell expression was variable. Images were pseudocolored and merged using ImageJ software (NIH) with the Fiji plugin [174].

2.2.5 Preparation and flow cytometry of myeloid cells

BMDMs were prepared using standard methods [56]. Briefly, bone marrow was extracted from femura and tibiae of mice aged 6-8-weeks. After hypotonic lysis of erythrocytes, BMDMs were derived on untreated plastic plates (BD Falcon, Sigma-Aldrich) by culturing in Dulbecco's Modified Eagle Medium (DMEM, Corning Cellgro,

Corning, NY) containing approximately 10% heat-inactivated fetal calf serum (Omega Scientific), 0.11 mg/ml sodium pyruvate (Corning), 2 mM penicillin/streptomycin/L-glutamine (Sigma-Aldrich), and 10% CMG-14-12-cell-conditioned medium as a source of M-CSF [175]. After 6 or 7 days cells were resuspended in enzyme-free ethylenediaminetetraacetic acid (EDTA) buffer and replated in untreated 6-well plates (BD Falcon, Sigma-Aldrich) at 1 M cells per well in unconditioned medium with or without priming in 25 U IFN-γ (PeproTech, Rocky Hill, NJ). Bone-marrow-derived mast cells were prepared as described previously [176], as above except for the substitution of 10 ng/ml IL-3 (PeproTech) for CMG-14-12-conditoned medium. After 5 weeks, cells were subjected to flow-cytometry analysis (LSRFortessa, Becton Dickinson, Franklin Lakes, NJ) and found to be uniformly positive for FcεRIα (Mar-1, FITC-labeled, #134305) and c-Kit (2B8, APC-labeled, #105811), both from BioLegend (San Diego, CA). Cells were rested or primed overnight before stimulation.

2.2.6 siRNA knockdown of c-Cbl and Cbl-b

The siRNA sequence for knockdown of mouse c-Cbl was adapted from human siRNA. Cbl-b siRNA was designed using the Integrated DNA Technologies double-stranded siRNA design tools (IDT, Skokie, IL). Control double-stranded RNA from IDT was not predicted to be complementary to any sequence in human, mouse, or rat transcriptomes. The effective siRNA sequences from among those we tested are: c-Cbl guide sequence CCUACCAGGACAUUCAGAAAGCUUU (passenger sequence AAAGCUUUCUGAAUGUCCUGGUAGG), Cbl-b guide sequence (CUGACUUCUUGGUAUCUGAUAUATA (passenger sequence UAUAUAUCAGAUACCAAGAAGUCAGGU). Aliquots of 2 M BMDMs in 100 μl opti-MEM (ThermoFisher, Waltham, MA) were transfected with 1 μM siRNA via electroporation at 400 V/10 ms using a BTX square-wave electroporator. Cells were then plated on 150 mm untreated cell culture dishes and rested in 10 ml DMEM-10 for 30 min before adding 10 ml DMEM-10 supplemented with 10% CMG-14-12-cell-conditioned medium as a source of M-CSF. Transfections were pooled from several cuvettes to obtain enough cells for several stimulation conditions. After 24 h cells were resuspended in enzyme-free EDTA buffer and replated in untreated 6-well plates (BD Falcon, Sigma-Aldrich) at 1 M cells per well in unconditioned medium. Cells were used 48 h after transfection.

2.2.7 saRNA enrichment of c-Cbl

An saRNA sequence designed to upregulate transcription of c-Cbl was designed using an algorithm published previously [177]. c-Cbl-targeting saRNA "CBL-Tr-NM_005188-Pr-30-Cp-0" with guide sequence UCAAUUCUAGAUAAAGGCG (passenger sequence CGCCUUUAUCUAGAAUUGA) was ordered from IDT with 2' O-methylated uracil tails (mUmU) to increase transfection efficiency. On the first day of transfection, aliquots of 10^5 mast cells were resuspended in 400 µl mast-cell medium in a 24-well plate and mixed with 100 µl saRNA+lipofectamine 2000 or 3000 for a final concentration of 5 nM saRNA. Cells were then rested overnight before a second transfection with 100 µl saRNA+lipofectamine. On day three the cells were transferred into fresh mast cell medium and rested overnight. On the day of the experiment, mast-cell aliquots from the same saRNA condition were pooled, resuspended in 50 µl DMEM, and rested 2 h before stimulation.

2.2.8 Cell stimulation and immunoblotting

BMDM stimulations have been described previously [22]. After resting as described above, 1 M live Jurkat cells, mast cells, or adherent BMDMs were treated at 37°C in DMEM with 10 µM 3-IB-PP1, a gift from K. Shokat (University of California, San Francisco). Signaling reactions were quenched by placing on ice and lysing cells in sodium dodecyl sulfate (SDS) buffer (128 mM Tris base, 10% glycerol, 4% SDS, 50 mM dithiothreitol (DTT), pH 6.8). Whole-cell lysates were prepared for immunoblotting by sonicating with a Bioruptor (Diagenode, Inc., Denville, NJ) for 3 min and boiling for 15 min. For immunoblotting 0.25 M cell equivalents were run in each lane of a 7% NuPage Tris-Acetate gel (Invitrogen, Carlsbad, CA) and then transferred to an Immobilon-FL PVDF membrane (EMD Millipore, Burlington, MA). REVERT Total Protein Stain (LI-COR Biosciences, Lincoln, NE) was used according to the standard protocol to quantify lane loading. After destaining, membranes were treated with Odyssey Blocking Buffer (TBS) for at least 1 h. Blotting was performed using standard procedures, and blots were imaged on an Odyssey CLx near-infrared imager (LI-COR). Antibodies for immunoblotting were purchased from Cell Signaling Technology (Danvers, MA), ProMab Biotechnologies (Richmond, CA), Thermo Fisher Scientific (Waltham, MA), Abcam (Cambridge, UK), Santa Cruz (Dallas, TX), and LI-COR Biosciences.

2.2.9 Quantification, statistics, and image processing

Immunoblots were analyzed by densitometry from ImageStudio software (LI-COR Biosciences). Images were background-subtracted, and bands of the appropriate molecular weight were demarcated and analyzed for each gel lane. Each value was corrected for the total lane protein content (REVERT TPS), with the exception of pErk1/2, which was corrected with reference to total Erk1/2. Data were further normalized to a control condition to show relative changes from a reference state, each-condition t=0 or reference-condition t=0 as indicated. For all figures, n values are biological replicates, reflecting independent experiments from different individual mice (except where indicated if sufficient numbers of animals were not available), different days and/or batches of cells, stimulus preparations, and experimental workflows. Statistical analysis was performed using Prism Software (Graphpad, La Jolla, CA). Significance was assessed using one- or two-way ANOVA analysis with Tukey's or Sidak's correction for multiple comparisons as indicated in the figure legends, with analysis of the mean at each time point or condition. Error bars in each figure represent standard error of the mean from at least three independent experiments. Asterisks reflect specified P-values. Figures were further prepared using Adobe Creative Cloud software (San Jose, CA). Where appropriate, images were optimized by applying brightness/contrast changes to the whole image. No gamma or other nonlinear correction was applied. Images were rotated for figure preparation only after densitometry analysis.

2.2.10 Preparation of macrophage samples for targeted mass spectrometry analysis

Csk^{AS}c-$Cbl^{+/-}$ BMDMs were rested or treated 15 s with 3-IB-PP1, washed with ice-cold PBS, and lysed in 1% Lauryl Maltoside Buffer containing 150 mM NaCl, 0.01% sodium azide, and protease and phosphatase inhibitors (MSSAFE, Sigma-Aldrich, St. Louis, MO). After scraping the plates, cells and detergent were sonicated with a Diagenode biorupter for 5 min with a 50% duty cycle. The lysate was then cleared by centrifugation for 15 min at 14,000 rpm (16.1x g) at 4°C in a tabletop centrifuge. Lysates were precleared for 30 min at 4°C with Protein G Sepharose beads (Sigma-Aldrich) and normal rabbit serum (Jackson ImmunoResearch, West Grove, PA). LynA-specific antibody [22] (C13F9, Cell Signaling) was pre-bound to Protein-G-Sepharose beads for

at least 2 h. A bicinchoninic acid (BCA) protein assay was performed on the whole-cell lysates (Thermo Fisher) to ensure that equal amounts of protein from untreated and 3-IB-PP1-treated cells would be subjected to immunoprecipitation. Lysates were then mixed continuously with antibody and beads for 2 h at 4°C to immunoprecipitate LynA. Samples were applied to micro bio-spin chromatography columns (Bio-Rad, Hercules, CA), washed, and eluted with SDS Sample Buffer containing 125 mM Tris, 10% glycerol, 5% 2-mercaptoethanol, and 25% SDS. Samples were then concentrated to 40 µl using Ultracel-3K centrifugal spin columns (EMD Millipore). Each 40 µl immunoprecipitate sample was then resolved by gel electrophoresis. A calibration curve with a bovine serum albumin (BSA) standard curve was used to ensure that equal mass quantities of immunoprecipitated protein in the untreated and 3-IB-PP1-treated samples would be subjected to trypsin digest. For this calibration, we ran 0.05 - 20 µg BSA or the immunoprecipitate samples on a 10% Mini-PROTEAN TGX gel (Bio-Rad) at 170 V. Total protein was visualized without fixation using SimplyBlue Safestain (Thermo Fisher) according to manufacturer's instructions. Following staining, the gel was washed 2 x 1 h with water and imaged on a LI-COR Odyssey. The staining intensities were quantified by densitometry, and the BSA signals vs. mass quantities were fit to a linear function (GraphPad Prism). This function was then used to quantify the mass quantity of total protein in each immunoprecipitates. Gel pieces including the lower-MW (nonubiquitinated) Lyn species and higher-MW (polyubiquitinated) species were excised, spiked with the isotope-labeled LynA Y32 phosphopeptide [H]TI[pY]VRDP[$^{13}C_5{}^{15}N_1$]TSNK[OH] (Sigma-Aldrich), and subjected to in-gel digestion with TPCK-treated sequencing-grade trypsin (Promega, Madison, WI) and STAGE Tip peptide cleanup as previously described [178] except that iodoacetamide was used as the alkylating reagent. Digested samples were submitted for identification at the University of Minnesota's Center for Mass Spectrometry and Proteomics [179].

2.2.11 Mass spectrometry of cellular LynA immunoprecipitates

Peptide separations were performed on an Easy-nLC 1000 HPLC (Thermo Scientific) and loaded directly onto a 75 cm x 100-µm internal diameter fused silica PicoTip Emitter (New Objective, Woburn, MA), packed in-house with ReproSil-Pur C18-AQ (1.9 µm particle, 120 Å pore; Dr. Maish GmbH Ammerbuch, Germany) heated to 55°C. Peptide elution was performed using a tripartite gradient, decreasing the fraction of Buffer A

(0.1% formic acid in water) and increasing the fraction of Buffer B (0.1% formic acid in acetonitrile) at a flow rate of 300 nl/min (Step 1: 5-10% Buffer B over 5 min, Step 2: 10-16% B over 40 min, and Step 3: 16-26% B over 5 min).

The column was mounted in a nanospray source directly in line with an Orbitrap Fusion mass spectrometer (Thermo Scientific). Spray voltage was 2.1 kV in positive mode, and the heated capillary was maintained at 275 °C. The acquisition method combined two scan events corresponding to a full scan event and a parallel reaction monitoring (PRM) event targeting the singly-, doubly-, and triply-charged precursor ions of the three phosphorylated peptides without scheduling. The full scan event employed a *m/z* 380-1500 mass selection, an orbitrap resolution of 60,000 (at *m/z* 200), a target automatic gain control (AGC) value of 4e5, and maximum fill times of 50 ms. The PRM event employed an orbitrap resolution of 30,000 (at *m/z* 200), a target AGC value of 5e4 with a maximum ion injection time of 54 ms. The precursor ion of each targeted peptide was isolated using an isolation window of 1.6 *m/z*. Fragmentation was performed with a HCD collision energy of 30% and MS/MS scans were collected using a scan range from 100-1000 *m/z*. PRM data were collected in centroid mode. Data analysis was performed using manual integration using Thermo Xcalibur Qual Browser and Skyline [179, 180]. Peak searches were performed using PEAKS Studio X (Bioinformatics Solutions, Waterloo, Ontario). Experiments were run in triplicate, and the entire experiment was performed independently twice. Figures highlight one of these biological replicates, but the conclusions from the two sets of experiments are consistent.

2.2.12 LynA kinase reactions and preparation for mass spectrometry analysis

Purified recombinant Hck and GST-tagged LynA (Novus Biologicals, Centennial, CO and Thermo Fisher, respectively) were thawed and diluted in kinase buffer (25 mM Tris, pH 7.5; 10 mM MgCl2; 100 uM Na3VO4) for reactions titrating LynA or keeping LynA fixed and titrating Hck. Kinase assays (40 µl total volume, containing 50-1000 ng LynA or 250 ng LynA + 0-1000 ng Hck) were initiated by adding ATP to final concentration of 100 µM and then incubated at 30°C. An endpoint of 20 min was chosen based on a previous autophosphorylation study of recombinant Hck [38]. Reactions were stopped by adding 40 µl quenching solution (1% formic acid, 99% acetonitrile) and then frozen on dry ice. Samples were lyophilized and reconstituted in a 25 µl total volume of 7 M urea; 2 M

thiourea; 0.4 M Tris, pH 7.5; 20% acetonitrile, 4 mM tris(2-carboxyethyl)phosphine (TCEP), and 5 mM EDTA and incubated at 37°C for 45 minutes. Iodoacetamide was added to a final concentration of 8 mM and incubated in the dark for 30 min. After this alkylation step, 50 µl water was added to reduce the urea concentration below 2 M. Trypsin was then added to each sample (1:80 trypsin: protein) and incubated at 37°C for 18 h. Samples were dried and then desalted using a C18 stage-tip prior to the mass spectrometry run.

2.2.13 Creation of LynA^{KO} and LynB^{KO} mice

LynA^{KO} was induced using two gRNAs to delete 77 bp encompassing portions of the unique LynA insert in mouse lyn exon 2 (5'-GAUCUCUCACAUAAAUAGUU-3') and the following intron 2 (5'-CCAUGCUCCGAUCCUACUGU-3'). NHEJ then induced a frame shift that resulted in a premature stop codon after amino-acid residue 77.

LynB^{KO} was induced using one gRNA (5'-GUUCGGUCAGUAUUACGUAC-3') to make a cut near the LynB splice site in exon 2. A donor oligonucleotide (5'-AAAAGGAAAGACAATCTCAATGACGATGAAGTAGATTCGAAGACTCAACCAcTgCGTAATACTGACCCAACTATTTATGTGAGAGATCCAACGTCCAATAAACAGCAAAGGCCAGTAAG-3') was supplied to induce two single-nucleotide substitutions via HDR (lower-case letters in the sequence) that ablated the LynB splice site and a SnaBI restriction site. gRNA's were designed using CRISPOR.org [181]

3-weeks old C57BL/6J female mice were purchased from The Jackson Laboratory and adapted to University of Minnesota animal facilities 3-4 days before the first hormone injection. The stud C57BL/6J male mice were obtained from the Jackson Laboratory directly. The recipient females CD-1 mice at 38-49 days old was purchased from the Charles River Laboratory. The animal protocols used for all mutant mice generation were approved by the Institutional Animal Care and Use Committee (IACUC).

Microinjection of zygotes: The C57BL/6J females at 3-4 weeks old were superovulated by intraperitoneal injection of 5 IU pregnant mare serum gonadotropin, followed by injection of 5 IU human chorionic gonadotropin 48 hrs. later (both hormones from National Hormone & Peptide Program, Torrance, CA, USA), and they were immediately

crossed to C57BL/6J stud males. The next day, mouse zygotes were obtained from superovulated C57BL/6J females. For $LynA^{KO}$, the zygotes were injected with mixture of 30 ng/ul Cas9 protein, 3.5 ng/ul sgRNA each (2 sgRNA). For the LynB point mutation, the zygotes were injected with mixture of 30 ng/ul Cas9 protein, 3.5 ng/ul each of 2 sgRNA, and 7 ng/ul of ssODN (120bp) donor as the point mutation template [182]. CRISPR reagents were designed by University of Minnesota Genome Engineering Shared Resources (GESR) and purchased from IDT. All CRISPR reagents were tested and validated on NIH 3T3 cells before the zygote injection. And all the CRISPR reagents were resuspended in the injection buffer (10 mM Tris-HCl, 0.25 mM EDTA, pH 7.4) for the zygote injection

Toe DNA from the resulting pups was isolated using DNeasy Blood & Tissue Kit (Qiagen, Hilden, Germany) and subjected to an intermediate topo cloning step (Invitrogen, Carlsbad, CA) to insert PCR products into a plasmid for PCR sequencing (GeneWiz, South Plainfield, NJ) and digestion. A 500 bp segment in wild-type *lyn* encompassing the LynB splice site and the LynA unique insert was amplified using the following PCR primers: Forward 5'-acaaccgagatgtcctgct-3' Reverse 5'-agccagattatccctaaaatctctaca-3'. SnaBI (New England Biolabs, Ipswich, MA) cleavage of this product (recognition site TAC/GTA) generated two 250 bp fragments. In $LynA^{KO}$ a Cas9 double-cut deletion yields a shorter (~423 bp) PCR product that retains sensitivity to SnaBI cleavage. In $LynB^{KO}$ an HDR-induced mutation in the SnaBI site yields a 500 bp PCR product insensitive to SnaBI.

2.2.14 Tissue preparation and flow cytometry

Spleens were excised from mice and cut into <1mm pieces before being digested for 30 min in RPMI 2% FBS, 0.2 mg/mL collagenase type IV (Sigma-Aldrich, St. Louis, MO), 37.5 ug/mL DNAse I (Worthington Biochemical, Lakewood, NJ), 1 U/mL Heparin D Sodium (Sigma-Aldrich, St. Louis, MO), 1 mM $CaCl_2$ and 1 mM $MgCl_2$. Single-cell suspensions were prepared by filtering digested spleens through 70 µm filters (Celltreat, Pepperell, MA). Antibody master mixes were prepared in PBS 2% FBS, 2mM EDTA. Antibodies used are enumerated in **Table 2.2**. For myeloid-cell-staining, cells were stained in 100 µL master mix at 37 °C for 30 min. For T and B cell panels, cells were stained at 4 °C for 30 min. Following surface staining for myeloid and B cell panels, cells

were fixed and permeabilized using BD Biosciences Fix/Perm kits according to manufacturer's instruction. Intracellular staining of CD206 and Intracellular Ig occurred at 4 °C overnight. For FoxP3 staining, cells were fixed and permeabilized using Tonbo Biosciences Transcription factor staining kit according to manufacturer's instruction. Following intracellular staining, cells were washed with permeabilization buffer and resuspended in PBS 0.5% paraformaldehyde. Data was acquired using a BD Fortessa X-30 and analyzed using Flowjo.

Marker	**Clone**	**Source**	Color(s)
XCR1	ZET	Biolegend	FITC, APC
CD45	30-F11	Biolegend	A700, BUV496
PDCA-1	927	Biolegend	BV421
I-A/I-E	M5/114.15.2	Biolegend	BV510
CD206	C068C2	Biolegend	BV650
CD64	X54-5/7.1	Biolegend	BV711
Ly6C	HK1.3	Biolegend	BV785
TLR4	SA15-21	Biolegend	Biotin
TLR9	S18025A	Biolegend	FITC
TLR2	CB225	Biolegend	PE
CD14	Sa14-2	Biolegend	APC/Fire-750
CD115	AFS98	Biolegend	PE-Cy7
CD38	90	Biolegend	FITC, APC
GL7	GL7	Biolegend	PerCP-Cy5.5
CD69	H1.2f3	Biolegend	BV650
CD138	281-2	Biolegend	BV711
CXCR5	L138D&	Biolegend	PE
NK1	PK136	Biolegend	BV421
CD62L	MEL-14	Biolegend	BV510
CD69	H1.2f3	Biolegend	BV650
PD-1	29F.1A12	Biolegend	BV786
IgM	RMM-1	Biolegend	PE-Cy7
Ly6G	1A8	Tonbo Biosciences	PerCP-Cy5.5
CD80	16-10A1	Tonbo Biosciences	PE
CD86	P03.1	Tonbo Biosciences	PE
TCRβ	H57-597	Tonbo Biosciences	FITC, APC
FoxP3	3G3	Tonbo Biosciences	PerCP-Cy5.5, PE-Cy7
CD44	IM7	Tonbo Biosciences	PE-Cy7, PerCP-Cy5.5
Ghost Dye Red 780		Tonbo Biosciences	
CD16/32	2.4G2	Tonbo Biosciences	
CD11b	M1/70	BD Biosciences	BUV395, A700
CD11c	HL3	BD Biosciences	BUV737
IgD	11-26c.2a	BD Biosciences	BV786
B220	RA3-6B2	BD Biosciences	BUV395
Intracellular Ig	550589	BD Biosciences	PE
CD4	GK1.5	BD Biosciences	BUV395
CD8a	53-6.7	BD Biosciences	BUV737
MerTK	DS5MMER	Invitrogen	PE-Cy7

Table 2.2: Antibodies used for flow cytometry

2.2.15 ex vivo splenocyte stimulation

Spleens were excised from mice and placed in ice-cold RPMI, 2% FBS, 2 mM penicillin and streptomycin. Spleen tissue was mechanically disrupted using a 100-mm cell strainer (Corning) on a 50 ml tube, using a plunger of a 1 ml syringe. During and following processing of the spleen, strainers were flushed with ice-cold RPMI to acquire all cells. After processing, single-cell suspensions were counted and kept at 4˚C before proceeding with the in vitro stimulation. Stimulation and staining of cells were performed in 96-wells V-bottom plates (Nunc), using $2x10^6$ cells per well in 50 µL RPMI. Cells were placed in a 5% CO_2 37 °C incubator for 1 hr prior to treatment. CpG (IDT) and LPS (Invivogen) were diluted in RPMI 2-5% FBS and added by pipetting 50 ul of stimulus (in a 2-fold concentration) to the wells containing 50 ul of sample. 30 min. after stimulation, Brefeldin A and monensin (eBioscience) were added. 30 min. prior to the end of stimulation, Live/dead stain (Tonbo Biosciences) was added. Treatment was quenched at 4 hrs. by adding paraformaldehyde (PFA) to a final concentration of 1.6% and fixing at room temperature for 15 min. in the dark. Following fixation, cells were washed twice with BD Biosciences Fix/Perm diluent and by centrifuging at 0.4 x g for 5 min. and dumping supernatant. Cells were then mixed with staining master mix diluted in BD Biosciences Fix/Perm diluent overnight at 4 °C. Following intracellular staining, cells were washed twice with permeabilization buffer and resuspended in PBS, 0.5% PFA. Data was acquired using a BD Fortessa X-30 and analyzed using Flowjo.

2.2.16 Anti-Nuclear Antibody Staining

Kallestad HEp-2 (Bio-Rad, Cat. No. 30472) was used to detect Anti-Nuclear antibody staining according to the manufacturer's instruction, modified to detect mouse IgG. Briefly, wells were incubated with 40 µL mouse serum, diluted 40x in phosphate-buffered saline + 1% Bovine-serum albumin, at room temperature for 20 min. After incubation, slides were washed in PBS for 10 minutes and incubated with 30 µL FITC-labeled goat-anti-mouse IgG (Jackson ImmunoResearch, Cat. No. 115-095-164) diluted 200x and DAPI () diluted 10,000x for 20 min. at room temperature, followed by a 10 min. PBS wash. Slides were then mounted and coverslipped and viewed on an Olympus BX51 fluorescent microscope equipped with a digital camera and DP-BSW software (Olympus). Images were quantified, pseudocolored, and merged using ImageJ software (NIH) with the Fiji plugin.

2.2.17 Histology

Kidneys and spleens were snap-frozen in optimal cutting temperature compound and 5-μm sections were H&E stained. The presence and severity of nephritis was evaluated in a blinded fashion (as previously described [183]) by a pathologist. Scoring of glomerulonephritis and interstitial nephritis on a 0-3 scale (0=absent, 1=mild, 2=moderate, 3=severe) for glomeruli was based on glomerular size, glomerular hypercellularity, and presence of glomerular sclerosis, and for interstitial disease was based on the degree of inflammatory infiltrate and alteration in tissue architecture.

2.3 Footnotes

Portions of this text were adapted from:

Brian BF 4th, Guerrero CR, Freedman TS. Immunopharmacology and Quantitative Analysis of Tyrosine Kinase Signaling. Curr Protoc Immunol. 2020 Sep;130(1):e104. doi: 10.1002/cpim.104. PMID: 32931655; PMCID: PMC7583487.

Author contributions: BFB, CRG and TSF wrote the manuscript.

CHAPTER 3: Unique-region phosphorylation targets LynA for rapid degradation, tuning its expression and signaling in myeloid cells

3.1 Introduction

Phosphorylation of immunoreceptor tyrosine-based activation motifs (ITAMs) by Src-family kinases (SFKs) is the first enzymatic step in the activation of an innate immune response during a pathogen encounter. Initiation of cell-activating signaling typically occurs within clusters of ITAM-coupled receptors such as FcγR [184] or the hemi-ITAM Dectin-1 [81, 185], nucleated by highly multivalent immunoglobulin-G-decorated pathogens or fungal cell-wall β-glucans respectively. Together, SFKs and phosphorylated ITAMs trigger activation of the tyrosine kinase Syk [18]. The SFKs and Syk then drive activation of membrane-proximal signaling through adaptor proteins, cytoskeleton-modulating proteins, such as the FAK/Pyk2 kinases and Paxillin, and Tec kinases, which activate second-messenger pathways via phosphoinositide 3-kinase (PI3K) and phospholipases Cγ (PLCγ1/2). These early events ultimately lead to downstream signaling through Erk1/2 and other pathways [18]. As the byproducts of activated macrophages can be toxic (*e.g.* release of reactive oxygen species) and drive inflammation (*e.g.* release of tumor necrosis factor α), the responsiveness of innate immune cells is tightly regulated [62, 186-188].

Multiple mechanisms work together to tune the responsiveness of macrophages and other myeloid cells, including negative regulation by the phosphatases CD45 and CD148 [61, 62, 189], cytoskeletal barriers to diffusion [74], signaling via immunoreceptor tyrosine inhibitory motifs (ITIMs) [190] and inhibitory ITAMs [191, 192], and degradation and sequestration of signaling molecules targeted for polyubiquitination by ubiquitin ligases [193, 194]. The SFKs, which in myeloid cells typically include Fgr, Fyn, two transcripts of Hck, and two splice forms of Lyn, may also have positive and negative functions [149, 151, 190, 195]. Layered onto the traditional positive- and negative-regulatory roles of the SFKs, activated LynA (the longer of the two Lyn splice forms) is rapidly and specifically targeted for polyubiquitination and degradation, forming the basis of a signaling checkpoint that blocks spurious macrophage activation [22]. This checkpoint can be bypassed when LynA is upregulated, with LynA acting as a rheostat to tune macrophage sensitivity. For instance, LynA is transcriptionally upregulated when

macrophages are treated with interferon (IFN)-γ, and these primed cells have a lower threshold for SFK-mediated signaling [22]. The molecular mechanism that selectively targets LynA for polyubiquitination has not been elucidated previously.

Unlike Dectin-1 and FcγR signaling in macrophages, which are typically triggered in the context of pathogen-induced μm-scale clusters of receptors [22, 61, 62], mast-cell FcεR signaling has a low threshold for activation; small or even monovalent antigen-IgE complexes can induce a signaling response in the context of a cell-particle interaction [196-198]. Supporting this more permissive signaling function, the binding dynamics of Syk with FcεRI in mast cells is unaffected by the size of receptor aggregates [199]. Like macrophages, mast cells express LynA, and the disparity in the receptor sensitivity of these two cell types has not previously been explained.

This chapter describes the mechanism by which activated LynA is selectively recognized and rapidly degraded, thereby tuning both its steady-state expression and its activation kinetics in a cell-specific manner. To reveal the requirements for LynA degradation, we synchronized receptor-independent SFK activation using the designer inhibitor 3-IB-PP1 [70, 200, 201], which specifically inhibits a variant of the SFK-inhibitory kinase Csk (Csk^{AS}) [22, 70, 71]. Csk is responsible for phosphorylating a key inhibitory tyrosine in the C-terminal tail of all the SFKs. Inhibiting Csk^{AS} with 3-IB-PP1 disrupts the dynamic equilibrium between Csk and the phosphatases CD45 and CD148, which dephosphorylate the inhibitory tyrosine, leading to rapid and robust SFK activation [202, 203]. Using this model, we discovered that 3-IB-PP1-induced SFK activation leads to the phosphorylation and activation of the E3 ubiquitin ligase c-Cbl [87, 204] and the preferential polyubiquitination and degradation of LynA in macrophages, but it was not clear whether these two events were linked. Using knockout and overexpression models coupled with quantitative targeted mass spectrometry and analyses of protein abundance and cell signaling, we now demonstrate that c-Cbl controls the steady-state expression of LynA and mediates its rapid degradation upon activation in macrophages. LynA is targeted by c-Cbl in response to phosphorylation of tyrosine 32 (Y32) within the LynA unique region mediated by LynA, LynB or the shorter isoform of Hck. This recognition mode is distinct from the slower-phase action of c-Cbl and other E3 ligases on LynB and the other SFKs [22, 96, 205] . Finally, we have discovered that the LynA

checkpoint is cell-specific. In mast cells, which express very little c-Cbl but abundant Cbl-b, LynA is not rapidly degraded upon activation, a function that can be rescued by induced overexpression of c-Cbl. The differential regulation of c-Cbl and LynA may drive mast cells toward a lower activation threshold than macrophages.

3.2 Results

3.2.1 c-Cbl mediates steady-state and activation-induced degradation of LynA in macrophages

Our lab reported previously that activated LynA is rapidly polyubiquitinated and degraded in Csk^{AS} macrophages treated with the Csk^{AS} inhibitor (SFK activator) 3-IB-PP1 [22]. To identify the E3 ubiquitin ligase that mediates this degradation, we tested the functions of c-Cbl and Cbl-b, known modulators of ITAM signaling in both adaptive and innate immune cells [190, 193, 206]. We first used small interfering (si)RNAs to knock down the expression of c-Cbl and Cbl-b. Csk^{AS} BMDMs were transfected with non-targeting control RNA (ctrl) or with siRNA constructs targeting c-Cbl or Cbl-b. Rested transfectants were then treated with 3-IB-PP1 to induce SFK activation. Immunoblots of siRNA-transfected BMDM lysates **(Figure 3.1A)** showed modest but specific knockdown of c-Cbl (70% reduced) and Cbl-b (60% reduced) proteins, without a corresponding increase in c-Cbl expression as a consequence of Cbl-b knockdown **(Figure 3.1B)**.

Loss of c-Cbl, but not Cbl-b, resulted in impaired degradation of LynA in the first few minutes of 3-IB-PP1 treatment and increased steady-state expression of LynA protein (**Figure 3.1C,D**). To further confirm the importance of c-Cbl, we bred *$Csk^{AS}Cbl^{-/-}$* and *$Csk^{AS}Cblb^{-/-}$* mice from existing *$Cbl^{-/-}$* [168] and *$Cblb^{-/-}$* [91] strains and used these mice to generate Csk^{AS}c-$Cbl^{-/-}$ and Csk^{AS}Cbl-$b^{-/-}$ bone-marrow-derived macrophages (BMDMs). Immunoblots of whole-cell lysates show the loss of expression of c-Cbl and Cbl-b in Csk^{AS}c-$Cbl^{-/-}$ and Csk^{AS}Cbl-$b^{-/-}$ BMDMs, respectively, compared to Csk^{AS} BMDMs **(Figure 3.2A-B)**. Resting (unprimed) BMDMs were then treated with 3-IB-PP1 to induce activation of the SFKs **(Figure 3.2A)**.

As in the cbl-knockdown experiments, knockout of c-Cbl profoundly impaired the degradation of activated LynA in the first few minutes of 3-IB-PP1 treatment, with LynA levels remaining at 100% after 1 min of exposure to 3-IB-PP1 in Csk^{AS}c-$Cbl^{-/-}$ BMDMs compared to 60% in Csk^{AS} BMDMs **(Figure 3.2C)**. Csk^{AS}c-$Cbl^{-/-}$ BMDMs also expressed 3-fold more LynA protein than Csk^{AS} at steady state **(Figure 3.2D)**. The impaired degradation and increased steady-state LynA expression together resulted in 6- to 8-fold elevations in LynA protein in the first minutes of 3-IB-PP1 treatment.

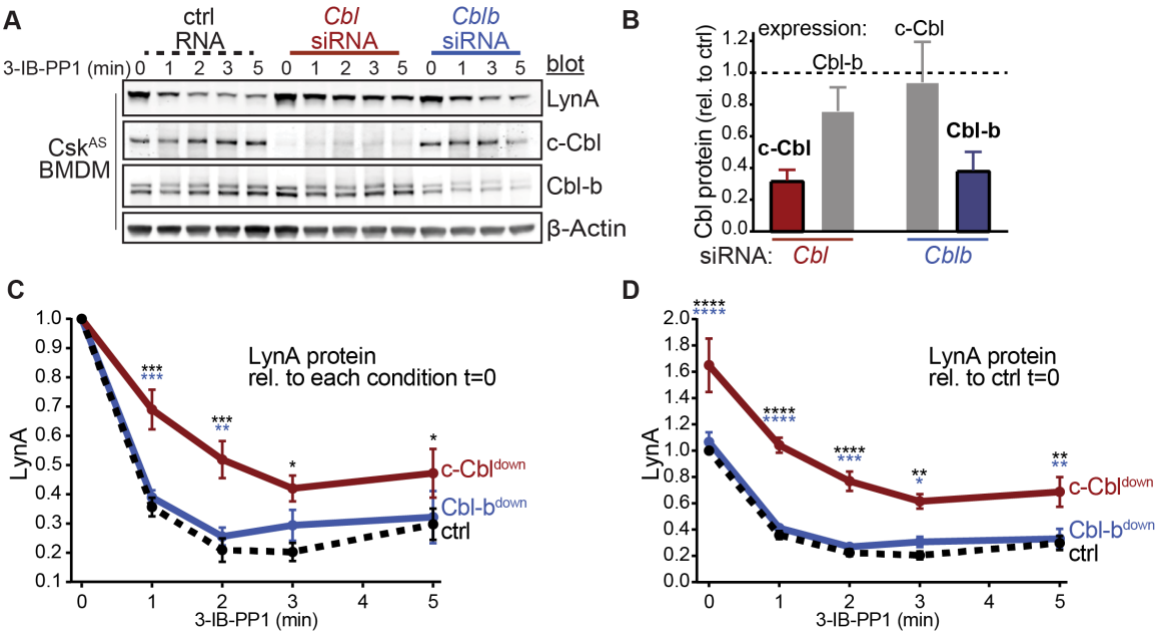

Figure 3.1. siRNA knockdown of c-Cbl expression in macrophages leads to steady-state upregulation and delayed degradation of LynA protein.
(**A**) Immunoblots showing LynA, c-Cbl, and Cbl-b protein in Csk^{AS} BMDMs transfected with non-targeting RNA (ctrl) or with siRNA constructs targeting *Cbl* or *Cblb* mRNA. Rested cells were treated with 3-IB-PP1 for the indicated times; β-Actin is shown as a loading control. (**B–D**) Quantification of relative c-Cbl, Cbl-b, and LynA protein, corrected for total protein content (TPS). SEM, n = 3. (**B**) Quantification of c-Cbl protein (red) and Cbl-b protein (blue), reported relative to their expression in ctrl BMDMs (dotted line). Remaining expression of the other Cbl family member is shown in gray. (**C–D**) Quantification of LynA, reported relative to the steady-state level in each siRNA condition (**C**) or relative to the level in the ctrl sample at steady state (**D**) in ctrl (black dotted), c-Cbl^{down} (red), and Cbl-b^{down} (blue) samples. Sig. from $ANOVA_2$-Tukey: [c-Cbl^{down} vs. ctrl, black asterisks], [c-Cbl^{down} vs. Cbl-b^{down}, blue asterisks]; ****p<0.0001, ***p=0.0001–0.0005, **p=0.0015–0.0058, * P=0.0105–0.0451. Other pairs ns.

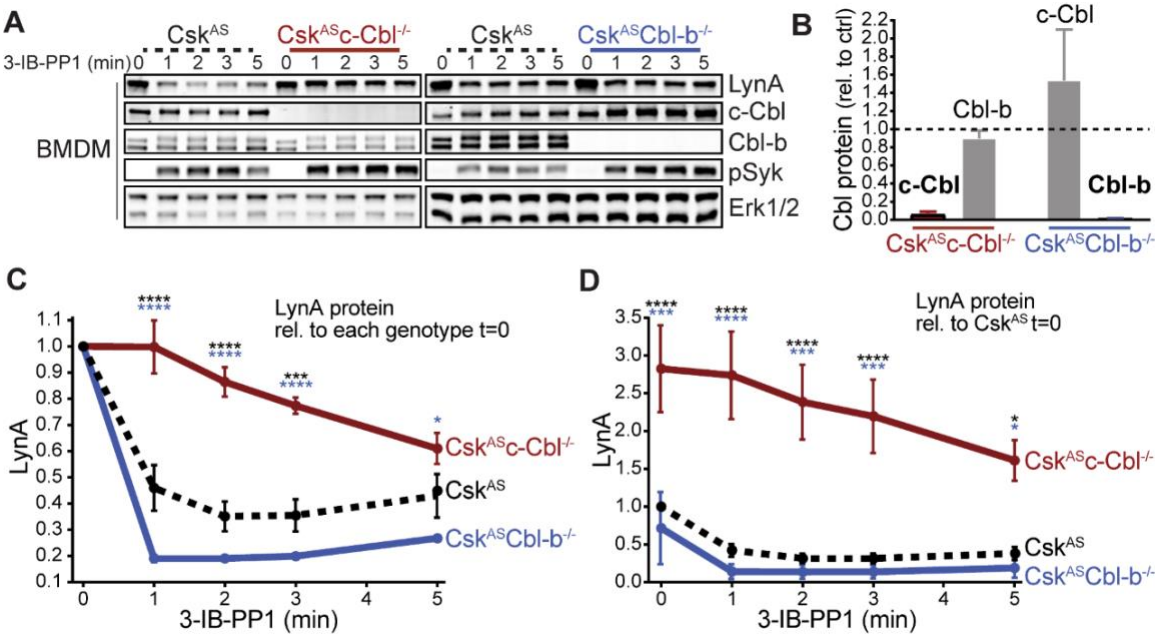

Figure 3.2. Loss of c-Cbl expression in macrophages leads to steady-state upregulation and delayed degradation of LynA protein. (A) Immunoblots showing LynA and Cbl protein in Csk^{AS}, Csk^{AS}c-$Cbl^{-/-}$, and Csk^{AS}Cbl-$b^{-/-}$ BMDMs treated with 3-IB-PP1 for the indicated times. Interdomain-B-phosphorylated Syk^{pY352} [17, 207, 208], an SFK target and prerequisite for Syk activation, is shown as a control for 3-IB-PP1-initiated signaling; total Erk1/2 is shown as a loading control. (B-D) Densitometry quantification of relative levels of Cbl and LynA protein, corrected for total protein content using REVERT Total Protein Stain (TPS). (B) Quantification of c-Cbl (red) and Cbl-b (blue) in Csk^{AS}c-$Cbl^{-/-}$ and Csk^{AS}Cbl-$b^{-/-}$ BMDMs relative (rel.) to their steady-state levels in Csk^{AS} BMDMs (dotted line). Expression of the other Cbl family member is shown in gray. Error bars reflect the standard error of the mean (SEM), n=4 from three Csk^{AS}c-$Cbl^{-/-}$ mice and n=3 from two Csk^{AS}Cbl-$b^{-/-}$ mice. (C-D) Quantification of LynA relative to the steady-state level in each genotype (C) or relative to the steady-state level in Csk^{AS} BMDMs (D). SEM, n=8 for Csk^{AS}, n=5 from three Csk^{AS}c-$Cbl^{-/-}$ mice, n=3 from two Csk^{AS}Cbl-$b^{-/-}$ mice. The significance (Sig.) from two-way ANOVA ($ANOVA_2$) with Tukey's multiple comparison test (-Tukey) are as follows: [Csk^{AS}c-$Cbl^{-/-}$ vs. Csk^{AS} black asterisks], [Csk^{AS}c-$Cbl^{-/-}$ vs. Csk^{AS}Cbl-$b^{-/-}$, blue asterisks]; **** P<0.0001, *** P=0.0001-0.0005, * P=0.0171-0.0459. Other pairs ns. Note: some of the error bars are smaller than the line width.

The effects of c-Cbl knockdown are blunted relative to Csk^{AS}c-$Cbl^{-/-}$ BMDMs, likely due to incomplete knockdown. As in the knockout experiments, LynA degradation in c-Cbl siRNA BMDMs was not fully eliminated but occurred on a much slower timescale, similar to the degradation of the other SFKs [22] **(Figure 3.1C-D).** Without c-Cbl upregulation in Cbl-b-knockdown BMDMs, we saw no increase in the LynA degradation efficiency or decrease in the steady-state level of LynA protein.

Although it has been reported previously that c-Cbl and Cbl-b have some redundant functions [92, 209], we were unable to detect any role for Cbl-b in suppressing the steady-state level or promoting the activation-induced degradation of LynA. Upon treatment for 1 min with 3-IB-PP1, LynA was 81% reduced in Csk^{AS}Cbl-$b^{-/-}$ compared to 60% in Csk^{AS} BMDMs **(Figure 3.2C)**. Although not statistically significant, steady-state expression of LynA was slightly depressed in Csk^{AS}Cbl-$b^{-/-}$ BMDMs **(Figure 3.2D)**. This increase in LynA degradation may be explained by a compensatory upregulation of c-Cbl protein expression in Csk^{AS}Cbl-$b^{-/-}$ BMDMs **(Figure 3.2B)**.

In the above experiments activating Syk phosphorylation was used as a control for 3-IB-PP1-induced SFK signaling. Notably, Syk phosphorylation is enhanced in 3-IB-PP1-treated Csk^{AS}c-$Cbl^{-/-}$ BMDMs, consistent with the higher expression level and longer half-life of LynA protein **(Figure 3.2A)**. Syk phosphorylation is also enhanced in 3-IB-PP1-treated Csk^{AS}Cbl-$b^{-/-}$ BMDMs, but this is likely due to the direct role of Cbl-b on Syk inhibition [210]. Activating phosphorylation of Erk1/2, a downstream signaling protein, is also complicated by the functions of the E3 ligases themselves. Erk phosphorylation in 3-IB-PP1-treated Csk^{AS}c-$Cbl^{-/-}$ BMDMs is impaired **(Figure 3.3)**, likely due to the loss of the adaptor function of c-Cbl in PI3K signaling [211, 212]. In 3-IB-PP1-treated Csk^{AS}Cbl-$b^{-/-}$ BMDMs, Erk1/2 phosphorylation, like Syk phosphorylation, is enhanced, again likely due to the negative-regulatory role of Cbl-b for Syk and other upstream signaling intermediates.

Overall, we conclude that c-Cbl is solely responsible for LynA-specific rapid degradation, whereas other E3 ubiquitin ligases can complement the canonical SFK-binding and -polyubiquitinating function of c-Cbl [96, 205], which mediates slower degradation of LynA and the other SFKs [22].

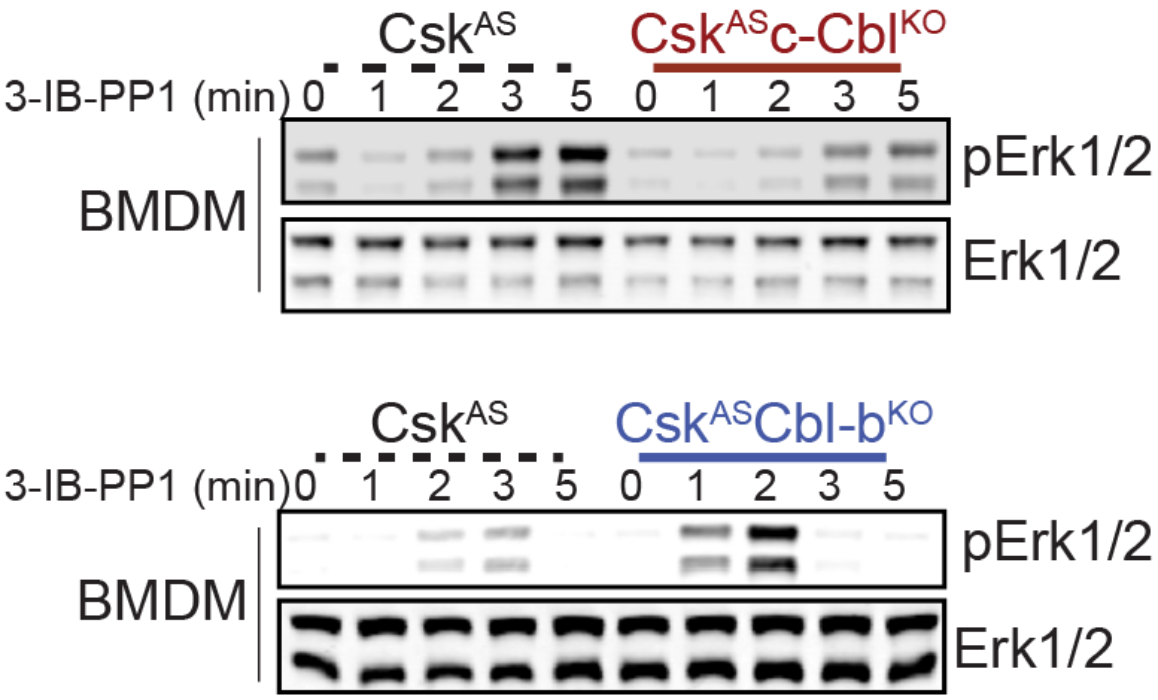

Figure 3.3. Paradoxical changes in Erk1/2 phosphorylation in Cbl-deficient cells obscure the contribution of LynA to signaling. Immunoblot showing impaired activating phosphorylation of Erk1/2pT202/pY204 (pErk1/2) in Csk^{AS}c-Cbl^{KO} BMDMs and enhanced Erk phosphorylation in Csk^{AS}Cbl-b^{KO} BMDMs compared to Csk^{AS} BMDMs treated with 3-IB-PP1.

3.2.2 A tyrosine residue in the unique-region insert of LynA is required for its rapid degradation

Susceptibility to rapid, activation-induced degradation differentiates LynA from the splice variant LynB and the other abundant SFKs in macrophages, Hck (59 and 56 kDa transcripts) and Fgr [151], which are degraded >10-fold more slowly than LynA during 3-IB-PP1 treatment [22]. The SFK FynT (Fyn) has also been reported to play an important role in macrophage inflammatory signaling [195]. We now confirm that, like Hck, Fgr, and LynB, macrophage Fyn is long-lived during 3-IB-PP1 treatment **(Figure 3.4A)**, although we have been unable to detect Fyn activation in response to 3-IB-PP1 [22]. We also tested degradation of transfected LynA in comparison with endogenous Fyn and Lck in Jurkat T cells cotransfected with c-Cbl and a membrane-localized variant of Csk^{AS} ($memCsk^{AS}$) [70], which sensitizes Jurkat cells to 3-IB-PP1, enabling synchronized SFK activation. As in macrophages, LynA is rapidly degraded in Jurkat cells treated with 3-IB-PP1, in contrast to longer-lived Lck [70] and Fyn **(Figure 3.4B)**. This highlights the unique susceptibility of LynA to rapid, c-Cbl-mediated degradation and suggests that cell types, such as T cells, that do not express Lyn may lack an analogous, rapid off-switch for SFK signaling.

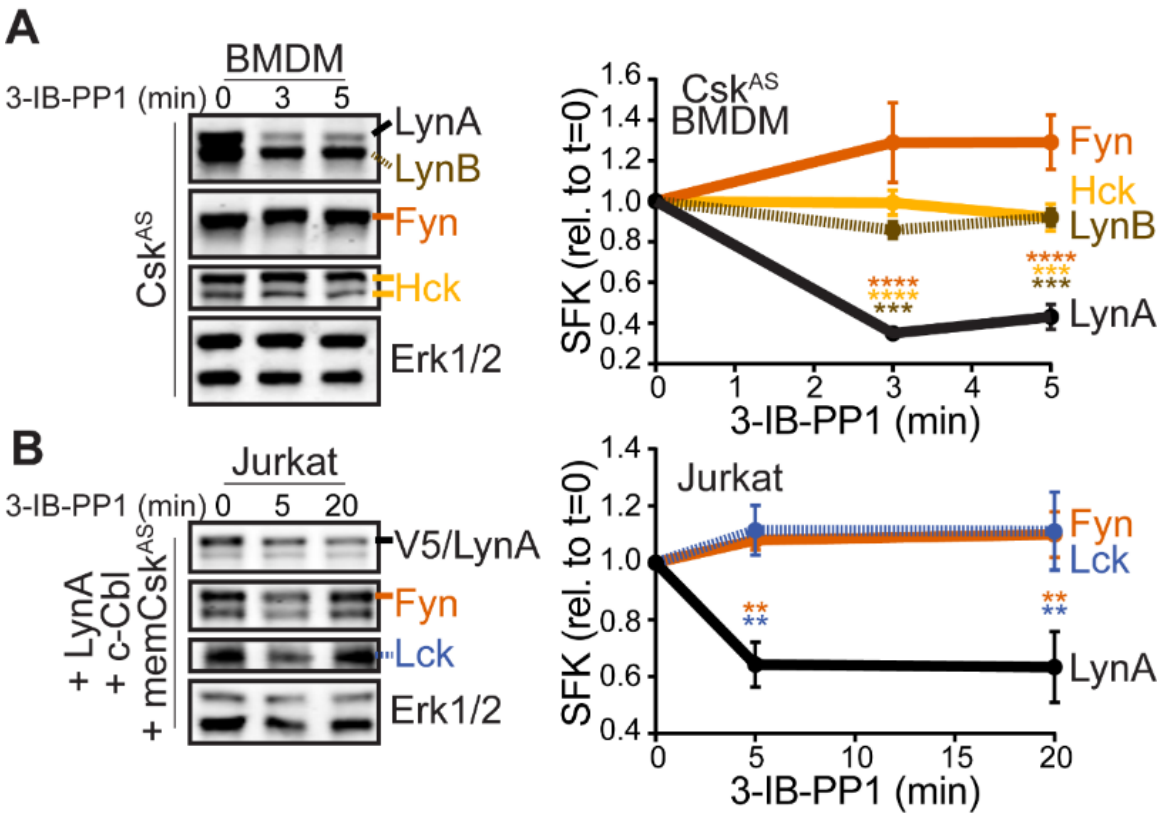

Figure 3.4. LynA is degraded more rapidly than Fyn and Lck during 3-IB-PP1 treatment. Immunoblots and quantification of SFK levels over the course of 3-IB-PP1 treatment. In both panels total Erk1/2 protein is shown as a loading control. Quantified values are corrected for total protein content (TPS) and reported relative to the steady-state level of each SFK. **(A)** Levels of Fyn (dark orange), Hck (light orange), LynA (black), and LynB (brown, dotted) protein in 3-IB-PP1-treated Csk^{AS} BMDMs. SEM, n=3. Sig. from $ANOVA_2$-Tukey: [Fyn vs. LynA, dark orange asterisks], [Hck vs. LynA, light orange asterisks], [LynB vs. LynA, brown asterisks]; **** P<0.0001, *** P=0.0006-0.0009, ** P=0.0034. **(B)** Levels of Fyn (dark orange) and Lck (slate) and His_6V5-tagged LynA (black) in 3-IB-PP1-treated Jurkat T cells cotransfected with $memCsk^{AS}$ and c-Cbl. SEM, n=4. Sig. from $ANOVA_2$-Tukey: [Lck vs. LynA, slate asterisks], [Fyn vs. LynA, dark orange asterisks]; ** P=0.0018-0.0048. Other pairs ns.

To determine which residues in the LynA protein mediate the unique interaction with c-Cbl, we undertook a mutational analysis. We were, however, unable to achieve expression of LynA variants in Csk^{AS} or $Csk^{AS}Lyn^{-/-}$ BMDMs [22] by transfection, Amaxa nucleofection, or lentiviral transduction, likely due to toxicity of overexpressed Lyn. As an alternative approach, we expressed LynA ectopically in Jurkat cells by transient cotransfection of His_6V5-tagged variants of Lyn along with a Cbl-family ligase and $memCsk^{AS}$. As a proof of principle for this model, we first transfected Jurkat cells with wild-type LynA, $memCsk^{AS}$, and either empty vector (ctrl), c-Cbl, or Cbl-b plasmid DNA **(Figure 3.5A)**, which increased c-Cbl expression 3-fold and Cbl-b 25-fold, respectively, over endogenous levels **(Figure 3.5B)**. Overexpressing one Cbl family member did not affect the abundance of the other. Phosphorylation of Erk1/2, via the combined effects of transfected LynA and endogenous Lck, demonstrates that 3-IB-PP1 was applied to all transfectants **(Figure 3.5A)**. As predicted, c-Cbl overexpression in Jurkat cells increased the rate of LynA degradation (30% depletion after 5 min treatment with 3-IB-PP1 in c-Cbl-overexpressing Jurkat cells compared to no detectable depletion in either ctrl or Cbl-b-overexpressing cells) **(Figure 3.5C)**. This observation is consistent with the knockout and siRNA experiments in BMDMs, demonstrating that Jurkat cells, which do not normally express Lyn, are capable of supporting rapid, c-Cbl-mediated degradation of LynA.

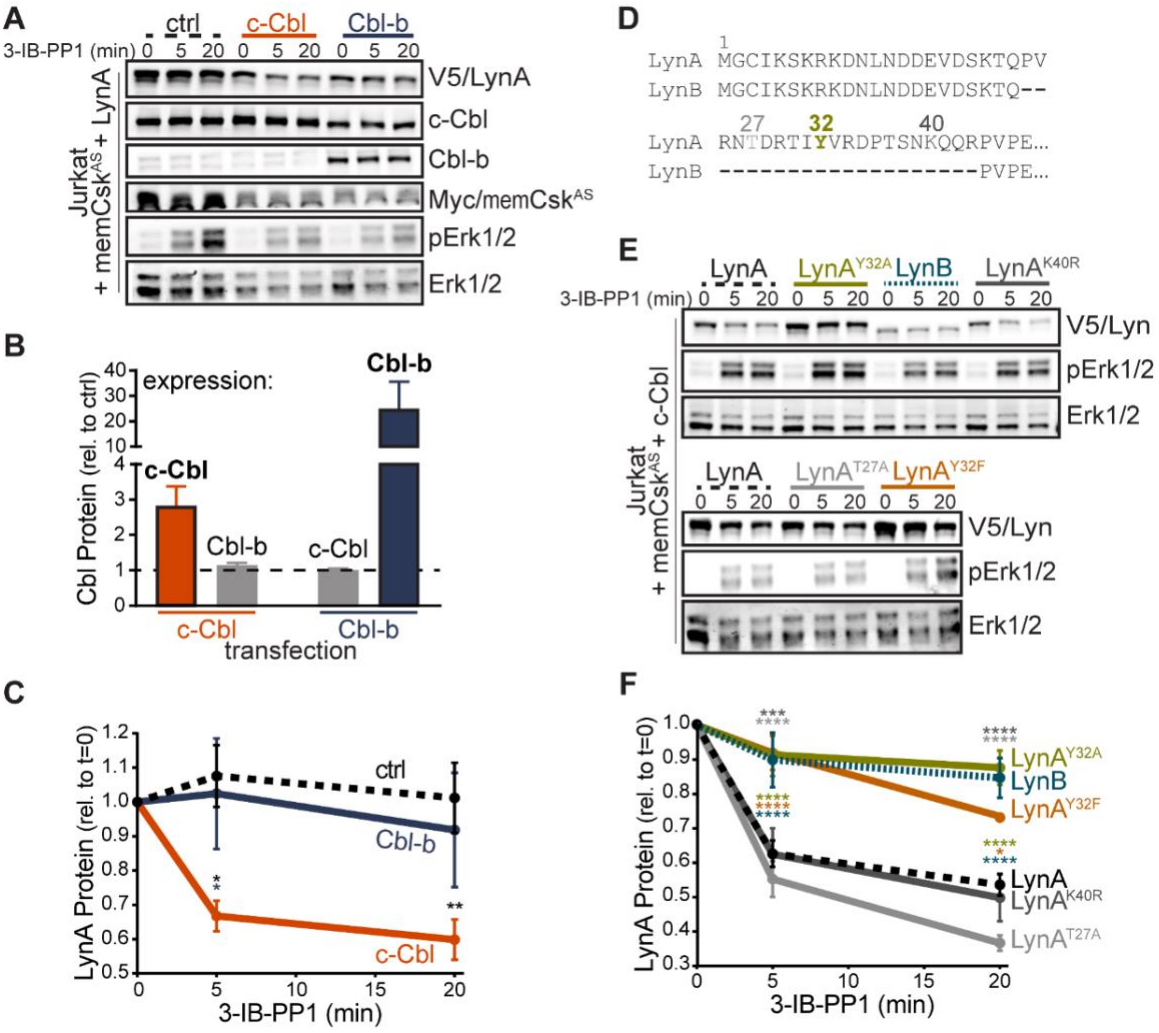

Figure 3.5. Unique-region tyrosine 32 is required for activation-induced degradation of LynA. (A) Immunoblots of Jurkat cells cotransfected with His_6V5-tagged LynA, Myc-tagged $memCsk^{AS}$, and either empty vector (ctrl), c-Cbl, or Cbl-b and treated with 3-IB-PP1. Phosphorylated $Erk1/2^{pT202/pY204}$ (pErk1/2) is shown as a qualitative control for 3-IB-PP1-initiated signaling from the combined effects of transfected LynA and endogenous Lck. As expect Total Erk1/2 is shown as a loading control. **(B-C)** Quantification of relative Cbl and V5-tagged LynA protein, corrected for total protein content (TPS). SEM, n=4. **(B)** Quantification of overexpressed c-Cbl (orange) and Cbl-b (dark blue) relative to endogenous (ctrl) levels (dotted line). Endogenous expression of the other Cbl family member in each condition is shown in gray. **(C)** Quantification of LynA protein during 3-IB-PP1 treatment relative to the steady-state level for transfections of empty-vector ctrl (black dotted), c-Cbl (orange), or Cbl-b (dark blue). Sig. from $ANOVA_2$-Tukey: [c-Cbl vs. ctrl, black asterisks], [c-Cbl vs. Cbl-b, blue asterisks]; ** P=0.0092, * P=0.0270-0.0102. Other pairs ns. **(D)** N-terminal amino-acid sequences of mouse LynA and LynB [146, 213], including the 21 amino-acid unique-region insert of LynA, highlighting residues Y32 (olive), T27 (light gray), and K40 (dark gray). **(E)** Immunoblots of 3-IB-PP1-treated Jurkat cells cotransfected with c-Cbl, Myc-tagged

memCsk^{AS}, and His_6V5-tagged Lyn constructs, including wild-type LynA, LynA^{Y32A}, LynB, LynA^{K40R}, LynA^{T27A}, or LynA^{Y32F}. **(F)** Quantification of protein levels of V5-tagged LynA (black dotted), LynA^{Y32A} (olive), LynB (teal dotted), LynA^{K40R} (dark gray), LynA^{T27A} (light gray), and LynA^{Y32F} (orange) over the course of 3-IB-PP1 treatment, corrected for total protein content (TPS) and reported relative to the steady-state level for each Lyn variant. SEM, n=7 for LynA, n=4 for LynA^{Y32A} and LynB; n=3 for LynA^{K40R}, LynA^{T27A}, and LynA^{Y32F}. Sig. from $ANOVA_2$-Tukey: [LynA^{Y32A} vs. LynA, olive asterisks], [LynB vs. LynA, teal asterisks], [LynA^{Y32F} vs. LynA, orange asterisks], [LynA^{K40R} vs. LynA^{Y32A}, dark gray asterisks], [LynA^{T27A} vs. LynA^{Y32A}, light gray asterisks], [LynB vs. LynA^{K40R}, P=0.013, 0.01], [LynB vs. LynA^{T27A}, P<0001], [Lyn^{Y32F} vs. LynA^{K40R}, P=0.012, 0.0157], [Lyn^{T27A} vs. LynA^{Y32F}, P<0.0001], [Lyn^{Y32A} vs. LynA^{K10R}, P<0.0001]; **** P<0.0001, *** P=0.0006, * P=0.0166. Other pairs ns.

LynB, which lacks a 21 amino-acid insert found in the unique region of LynA **(Figure 3.5D)**, was less efficiently degraded (10% depleted after 5 min treatment with 3-IB-PP1) than LynA (40% depleted after 5 min) in c-Cbl- and memCsk^{AS}-cotransfected Jurkat cells **(Figure 3.5E-F)**. Again, these data mirror our findings in Csk^{AS} BMDMs [22] and confirm that the unique susceptibility of LynA to rapid degradation is preserved in the Jurkat model. We hypothesized that the targeting site in LynA must lie within the unique-region insert (residues 23-43), absent in LynB [146, 213], which contains a tyrosine residue reported to be phosphorylated in cancer cells [Y32; 150, 214], a predicted threonine phosphorylation site [T27; NetPhos 3.1, 215] and predicted lysine ubiquitination site [K40; UbPred, 216] **(Figure 3.5D)**.

Substituting Y32 with either A or F blocked the rapid degradation of LynA **(Figure 3.5E)**, reducing the depletion after 5 min treatment with 3-IB-PP1 from 40% (LynA) to 10% (LynA^{Y32A}) or 8% (LynA^{Y32F}), levels indistinguishable from LynB (10%) **(Figure 3.5E-F)**. Substitution of Y32 did not alter the membrane localization of a unique-region construct at steady state or after 3-IB-PP1 treatment **(Figure 3.6A)**. Neither the predicted ubiquitination site mutation (LynA^{K40R}) nor the threonine phosphorylation site mutation (LynA^{T27A}) significantly affected the rate of LynA degradation **(Figure 3.5F)**.
As in BMDMs, the efficiency of Lyn degradation correlated with its steady-state expression in Jurkat cells. LynB is 2-fold and LynA^{Y32A} 3-fold more highly expressed than wild-type LynA, LynA^{K40R}, or LynA^{T27A} at steady state, resulting in 3- to 4-fold more protein remaining after 20 min treatment with 3-IB-PP1.

Overall, we conclude that the unique tyrosine residue Y32 in the LynA insert flags LynA for rapid, c-Cbl-mediated degradation and that this mechanism both determines the half-life of activated LynA protein during signaling and tunes its steady-state expression.

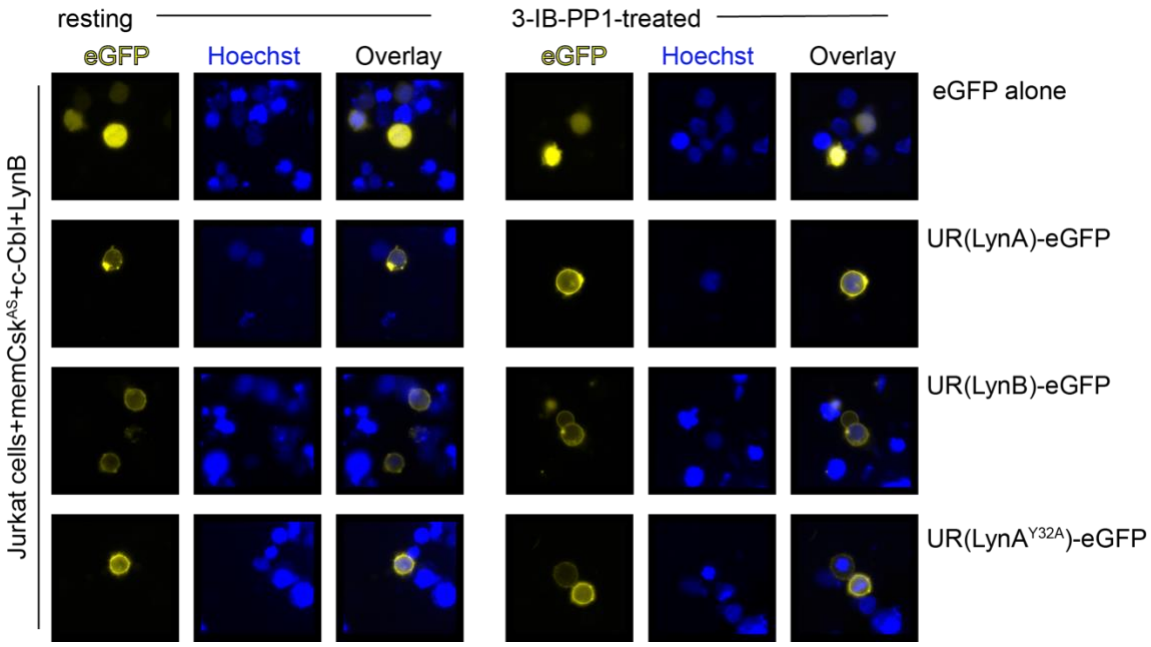

Figure 3.6. The unique regions of LynA, LynB, and LynA^{Y32A} are membrane-localized in resting and 3-IB-PP1-treated cells. Representative epifluorescence images of GFP-tagged unique-region (UR) constructs of LynA, LynB, and LynA^{Y32A}, showing localization in Jurkat cells before and after treatment for 5 min with 3-IB-PP1.

3.2.3 Phosphorylation on tyrosine 32 targets activated LynA for polyubiquitination

Although phosphorylated LynA^{Y32} has been found in liver and mammary tumor cells [150, 214], it has been unclear whether this posttranslational modification is functionally relevant in hematopoietic cells and whether Y32 is phosphorylated as a consequence of SFK activation. To probe for Y32 phosphorylation, we performed quantitative targeted liquid chromatography-coupled tandem mass spectrometry (LC-MS/MS) analysis of LynA immunoprecipitated from resting and 3-IB-PP1-treated BMDMs. We expected phosphorylation at this site to be transient due to the rapid degradation of LynA, and so we used a two-pronged approach to enrich potential Y32-phosphorylation: (i) Csk^{AS}c-Cbl$^{+/-}$ BMDMs were used to slow the rate of LynA polyubiquitination, and (ii) 3-IB-PP1 was applied as a 15 second pulse treatment. At this early time point, all SFKs are expected to be activation-loop phosphorylated, with only 20% of all LynA polyubiquitinated, as we have observed in wild-type BMDMs [22].

Lysates from resting and 3-IB-PP1-treated BMDMs, normalized for total protein content, were subjected to immunoprecipitation using a LynA-specific antibody [22] **(Figure 3.7A)**. Although some polyubiquitinated LynA species were generated, LynA was largely nonubiquitinated, as expected in Csk^{AS}c-Cbl$^{+/-}$ BMDMs pulse-treated with 3-IB-PP1. Bands from a Coomassie-stained gel containing nonubiquitinated and polyubiquitinated LynA were excised, normalized for protein content, and spiked with reference amounts of isotope-labeled control peptide corresponding to the tryptic fragment of Lyn encompassing pY32. These samples were then subjected to in-gel trypsin digestion and analyzed by LC-MS/MS. Peptides corresponding to phosphorylated and unphosphorylated LynA Y32, including the isotope-labeled standard, were detected in nonubiquitinated and polyubiquitinated LynA species from 3-IB-PP1-treated cells **(Figure 3.7C)**. We were able to resolve phosphorylated and unphosphorylated Y32 peptide and other potential phosphorylated species within the same tryptic peptide via their elution profiles: pY32 peptide coeluted with its isotopically labeled counterpart and these were clearly separated from unphosphorylated and threonine-phosphorylated species **(Figure 3.8A-F)**. The identity of each peptide was assigned via the MS/MS fragmentation pattern at the expected *m/z*.

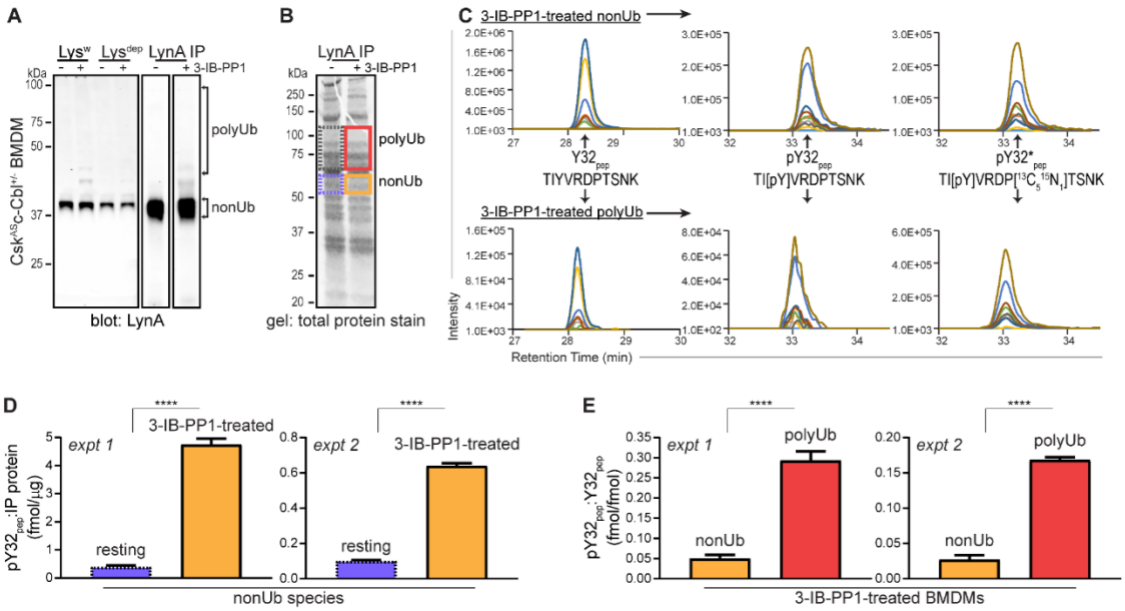

Figure 3.7. Tyrosine 32 is a site of activation-induced phosphorylation in macrophages. (A) Blots showing immunoprecipitation of LynA from Csk^{AS}c-$Cbl^{+/-}$ BMDMs with (+) or without (-) a 15 second treatment with 3-IB-PP1. Nonubiquitinated (nonUb) and polyubiquitinated (polyUb) LynA species in whole-cell and immunodepleted lysate (Lys^{w} and Lys^{dep}, respectively) and IP samples are shown. **(B)** Total-protein-stained gel showing regions excised for LC-MS/MS analysis of polyUb LynA (higher boxes) and nonUb LynA (lower boxes); box colors correspond to the bar graphs below. Total IP protein content was quantified by applying densitometry to the whole lane and assigned mass values using a BSA standard curve. Normalized amounts (based on the total IP protein content) were spiked with 125 fmol isotope-labeled control peptide ($pY32^{*}_{pep}$) corresponding to the phosphoY32-containing tryptic fragment of LynA and subjected to in-gel trypsin digestion and LC-MS/MS. **(C)** Tryptic peptides corresponding to IP-derived unphosphorylated-Y32-containing LynA peptide ($Y32_{pep}$), IP-derived phosphorylated-Y32-containing LynA peptide ($pY32_{pep}$), and added $pY32^{*}_{pep}$ were quantified by using parallel reaction monitoring (PRM) to trigger MS/MS spectra for peptide parent ions, 687.3267 and 690.3336 *m/z*, respectively. Extracted ion chromatograms (XICs) were derived from Skyline for MS/MS fragment ions corresponding to y and b ionic fragments from Y32, pY32, and pY32* peptides and used to quantify the ratios of $pY32_{pep}$:$pY32^{*}_{pep}$ or $pY32_{pep}$:$Y32_{pep}$. Ion-annotated Representative XICs are shown in Figure 3.8. Assignments of peptide species to specific phosphorylation states are shown in Figure 3.8. Detection of phosphorylated species in IP samples is shown in Figure 3.8.. **(D-E)** Quantitative analysis of Y32 phosphorylation in resting and 3-IB-PP1-treated BMDMs, including nonUb species from resting BMDMs (blue dotted), nonUb species from 3-IB-PP1-treated BMDMs (orange), and polyUb species from 3-IB-PP1-treated BMDMs (red). Although we analyzed a gel fragment that would contain any polyUb species in resting BMDMs (gray dotted), this species was sufficiently rare as to be unquantifiable. Error bars represent the standard deviation (stdev) of n=3 technical replicates. Data from two biological replicates are shown side by side. **(D)** Quantification of $pY32_{pep}$ in nonUb species from resting vs. 3-IB-PP1-treated BMDMs normalized to the total protein content of each IP. This analysis relies on an assumption equal amounts of total LynA in each sample, so this analysis was used only

to nonUb samples, which were roughly equally abundant in resting and 3-IB-PP1-treated BMDMs. Sig. from two-tailed t tests for each experiment: [nonUb resting vs. nonUb 3-IB-PP1-treated, asterisks]; **** P<0.0001. **(E)** Quantification of $pY32_{pep}$ in nonUb vs. polyUb species in 3-IB-PP1-treated BMDMs normalized to amount of unphosphorylated $Y32_{pep}$. Sig. from two-tailed t tests for each experiment: [nonUb resting vs. nonUb 3-IB-PP1-treated, asterisks]; **** P<0.0001.

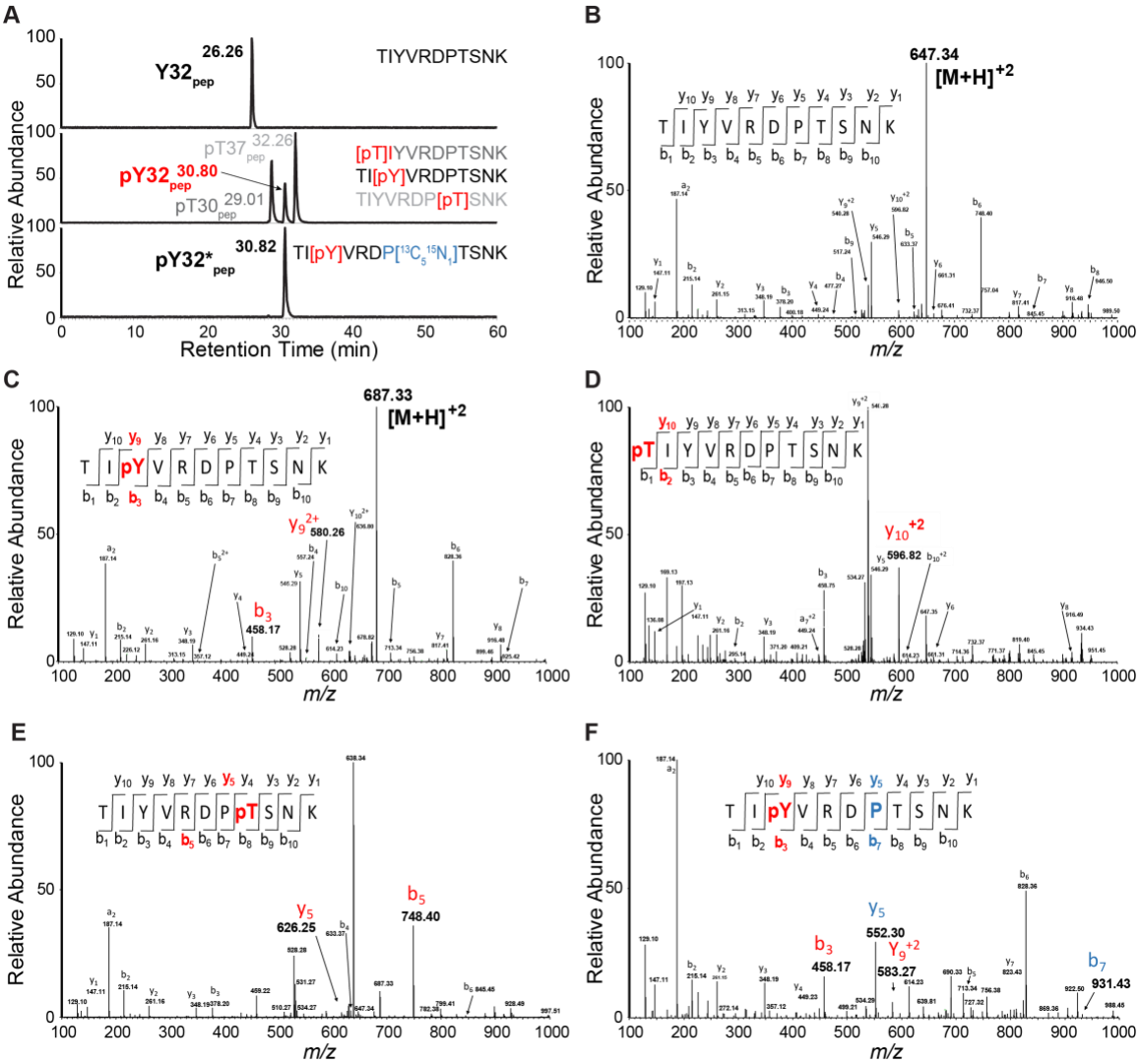

Figure 3.8. PRM chromatograms and spectra for unphosphorylated and phosphorylated LynA Y32 tryptic peptides.(**A**) PRM chromatograms illustrating resolution of synthetic phosphorylated and unphosphorylated peptides (top and middle panels), resolution of pY32 and synthetic threonine-phosphorylated (pT) species (middle panel), and coelution of unlabeled $pY32_{pep}$ with isotope-labeled $pY32^*_{pep}$ (middle and bottom panels). Species detected in LynA IPs ($Y32_{pep}$, $pY32_{pep}$, and $pY32^*_{pep}$) are indicated in bold type, phosphorylation sites are shown in red, and the isotope-labeled proline residue is shown in blue. (**B–F**) MS/MS spectra for synthetic peptides corresponding to tryptic peptides containing LynA Y32. The expected fragmentation pattern for each is indicated with phosphoions labeled in red/bold and isotope-labeled ions labeled in blue/bold. (**B**) MS/MS for $Y32_{pep}$ run at 647.3435 *m/z*. (**C**) MS/MS for $pY32_{pep}$ run at 687.3267 *m/z*, with highlighted fragment ions from phosphoY32. (**D**) MS/MS for $pT30_{pep}$ run at 687.3267 *m/z*, with highlighted fragment ions from phosphoT30. (**E**) MS/MS for $pT37_{pep}$ run at 687.3267 *m/z*, with highlighted fragment ions from phosphoT37. (**F**) MS/MS for $pY32^*_{pep}$ run at 687.3267 *m/z*, with highlighted fragment ions from phosphoY32 and the isotope-labeled proline residue.

In the LynA immunoprecipitates the tryptic peptide spanning residue 32 was phosphorylated at Y32 but not at T30 or T37. Search results in the PEAKS software package did not yield any matches for single or double threonine phosphorylation in combination with pY32, enabling complete analysis of LynA Y32 phosphorylation using an isotope-labeled pY32 peptide as the sole reference. Molar quantities of phosphorylated and unphosphorylated LynA Y32 peptide were derived by integrating the appropriate extracted ion chromatogram (XIC) peaks and correcting these values using standard curves with known molar ratios of unlabeled and isotope-labeled pY32 peptides. For some analyses, a second calibration curve was used to determine the molar quantities of unphosphorylated Y32 peptide.

We detected LynA Y32 phosphorylation in 3-IB-PP1-treated BMDMs in two independent experiments. After immunoprecipitation and sample processing, pY32 was 6- to 12-fold enriched in nonubiquitinated Lyn from 3-IB-PP1-treated BMDMs relative to resting BMDMs (**Figure 3.7D)**. LynA Y32 is therefore a site of inducible phosphorylation following activation of SFKs in primary macrophages. In resting BMDMs the vast majority of LynA is inactive [22] and therefore may be protected from bulk degradation by lack of phosphorylation of this site. Phosphorylated Y32 peptide was, however, detectable at low levels in resting BMDMs, supporting a model in which the bulk differences in the steady-state levels of LynA protein in cells lacking c-Cbl expression **(Figure 3.2)** are attributable to mass action, driven by degradation of small quantities of basally active LynA.

Although LynA Y32 phosphorylation was detected in activated but nonubiquitinated LynA, this effect was even greater in polyubiquitinated LynA, which was 6.0- to 6.4-fold enriched in Y32 phosphorylation relative to nonubiquitinated LynA (**Figure 3.7E)**. It is therefore likely that phosphorylation of LynA Y32 is an early consequence of SFK activation and a prerequisite for rapid polyubiquitination by c-Cbl.

3.2.4 Activated LynA induces its own degradation in trans

In macrophages and other hematopoietic cells SFKs are the first kinases to be activated upon ITAM-coupled receptor engagement, phosphorylating intracellular ITAMs, ITAM-associated Syk or Zap-70 [17, 207], and integrin-associated FAK or Pyk2 [18, 217]. We have reported that Syk and FAK are phosphorylated on activating tyrosine residues in Csk^{AS} BMDMs treated with 3-IB-PP1 [22]. To test whether these downstream kinases might participate in negative feedback leading to LynA degradation, we treated Csk^{AS} macrophages with competitive inhibitors of Syk [218], FAK/Pyk2 [219], or the SFKs themselves [220] in combination with 3-IB-PP1. As controls for on-target effects, we demonstrated that Erk1/2 and SFK activation-loop phosphorylation were blocked in samples cotreated with the pan-SFK inhibitor PP2, that Erk1/2 but not SFK activation-loop phosphorylation was blocked in samples cotreated with the Syk inhibitor BAY-61-3606, and that Paxillin phosphorylation was blocked in samples cotreated with the FAK/Pyk2 inhibitor PF-431396 **(Figure 3.9A)**. SFK inhibition via PP2 treatment abrogated LynA degradation **(Figure 3.9A-B)**. In contrast, LynA degradation was unaffected by Syk or FAK/Pyk2 inhibition. Together these data suggest neither Syk nor FAK/Pyk2 (or any off-target kinases inhibited by BAY-61-3606 and PF-431396) participates in a negative-feedback loop leading to LynA degradation, suggesting that the only upstream kinases, the SFKs, might phosphorylate LynA Y32 directly in cis or trans. This tight feedback circuit could explain the strikingly fast kinetics of LynA degradation.

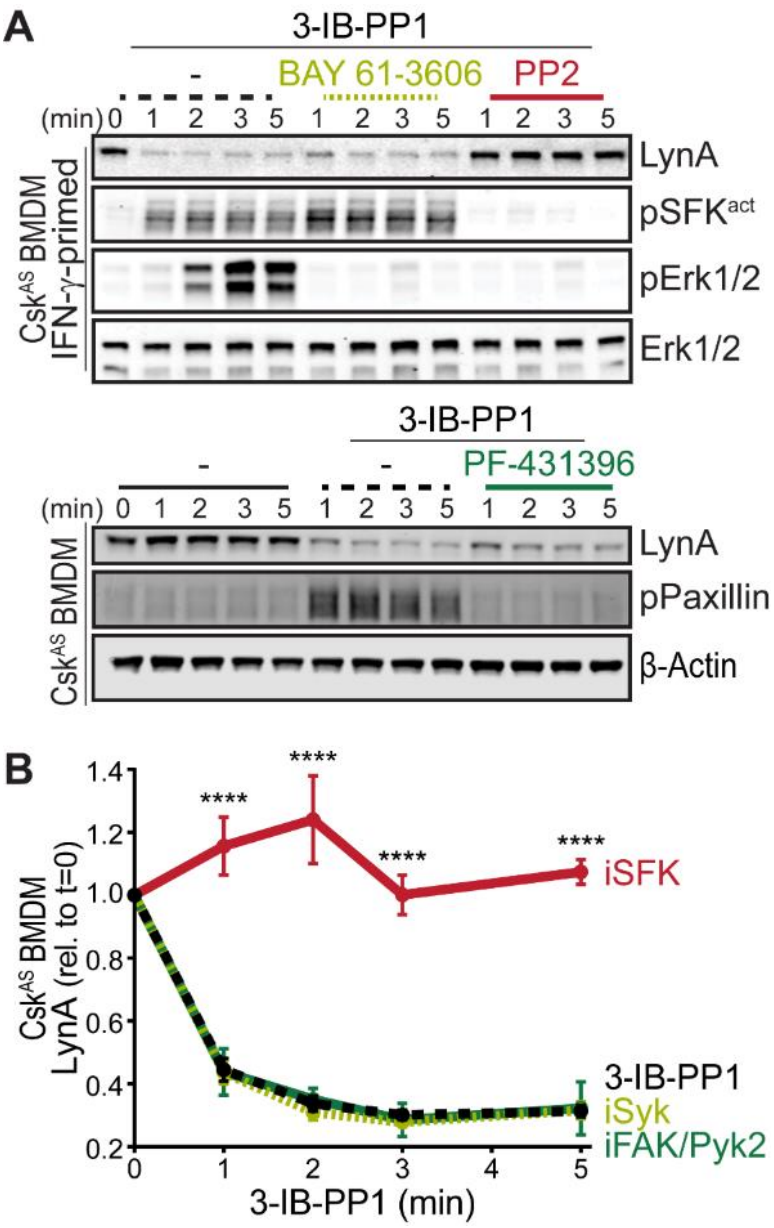

Figure 3.9. Syk, FAK, and Pyk2 kinase activities are not necessary for the rapid degradation of LynA. (A) Immunoblots showing expression of endogenous LynA protein in Csk^{AS} BMDMs treated with 3-IB-PP1 only or cotreated with 3-IB-PP1 and the Syk inhibitor BAY 61-3606, the SFK inhibitor PP2, or the FAK/Pyk2 inhibitor PF-431396. Activated signaling proteins including SFKs ($pSFK^{act}$, activation-loop-phosphorylation corresponding to Src^{pY416}), pErk1/2, and $Paxillin^{pY118}$ (pPaxillin) are shown as controls for inhibitor function; β-Actin and total Erk1/2 are shown as loading controls. **(B)** Quantification of LynA protein during 3-IB-PP1 treatment only (black dotted) or with the inhibitors BAY 61-3606 (iSyk, light olive), PP2 (iSFK, red), or PF-431396 (iFAK/Pyk2, green), corrected for total protein content (TPS) and reported relative to the steady-state level of LynA. SEM, n=3. Sig. from $ANOVA_2$-Tukey: [+PP2 vs. 3IB only, asterisks]; **** $P<0.0001$. Other pairs ns.

To investigate the role of LynA kinase activity in its degradation, we turned again to Jurkat-cell transfections, testing three functionally impaired variants of LynA: LynA^{T410K}, which has disrupted substrate recognition [221], and LynA^{Y397F}, which lacks the key autophosphorylation site that stabilizes the kinase active state and interacts with c-Cbl [31, 96, 202]. To minimize interference from T-cell endogenous SFKs, we used Lck-deficient JCaM1.6 cells; previous work has shown that endogenous Fyn does not independently activate the TCR signaling pathway in this cell line [171, 172]. When transfected into JCaM1.6 cells along with memCsk^{AS} and c-Cbl, only catalytically competent His_6V5-tagged LynA was subject to rapid, 3-IB-PP1-induced degradation **(Figure 3.10A)**; we did not detect degradation of the substrate-binding-impaired variant (T410K) or the activation-loop-mutated variant (Y397F). Zap-70 phosphorylation was only visible in JCaM1.6 cells transfected with wild-type LynA, demonstrating the functional impairment of LynA^{T410K} and LynA^{Y397F}.

We then transfected the same variants of LynA into Lck-expressing Jurkat cells **(Figure 3.10B)**. The presence of phosphorylated Zap-70 in all transfections demonstrates the expected activation of endogenous Lck in response to 3-IB-PP1 [70, 171, 222, 223]. Activated Lck, however, was unable to induce degradation of LynA, with no detectable loss of either catalytically-impaired variant **(Figure 3.10C)**. To ensure that the substrate-binding and conformational elements altered in the T410K and Y397F variants did not affect our results, we confirmed that the active-site mutant LynA^{K275R} was similarly resistant to 3-IB-PP1-induced degradation **(Figure 3.11)**.

We wondered whether mutation of Y32 disrupts the interaction between LynA and c-Cbl. To investigate this, we transfected Jurkat cells with memCsk^{AS} and c-Cbl, along with V5-tagged constructs for LynA, LynB and LynA^{Y32A}. We then treated these cells with 3-IB-PP1 to induce SFK and c-Cbl activation, and performed an immunoprecipitation for V5 (**Figure 3.12**). When we quantified the amount of c-Cbl co-immunoprecipitated with each Lyn construct, we saw that c-Cbl-association with Lyn increased upon 3-IB-PP1-treatment as expected (**Figure 3.12A**). However, we saw minimal differences in the ability of LynA, LynB, or LynAY32A to co-immunoprecipitate c-Cbl (**Figure 3.12C**). Lyn can interact with c-Cbl through multiple compensatory mechanisms. We wondered whether Lyn-SH3 domain binding to poly-proline motifs, Lyn kinase activity, and Lyn

activation loop phosphorylation were providing compensatory mechanisms that might obscure the effect of Y32 phosphorylation. To investigate this we made triple mutants, W100A/ T410K/ Y397F, of LynA, LynB and LynA^{Y32A} that would block the ability of Lyn's SH3 domain to interact with c-Cbl (W100A [224]), through substrate binding (T410K) or through activation loop phosphorylation (Y397F). We also co-transfected in LynA^{Y32A}, without a V5 tag to provide the necessary kinase activity required for c-Cbl activation (**Figure 3.12B**). Introduction of these three mutations had a stark effect on c-Cbl binding to all Lyn variants (**Figure 3.12C**). Although we still noticed an induction of c-Cbl binding for LynA and LynB upon SFK activation, the effect was minimal and seemed to be negated in the LynA^{Y32A} mutant. Thus, multiple mechanisms ensure c-Cbl's interaction with Lyn, apart from Y32 phosphorylation

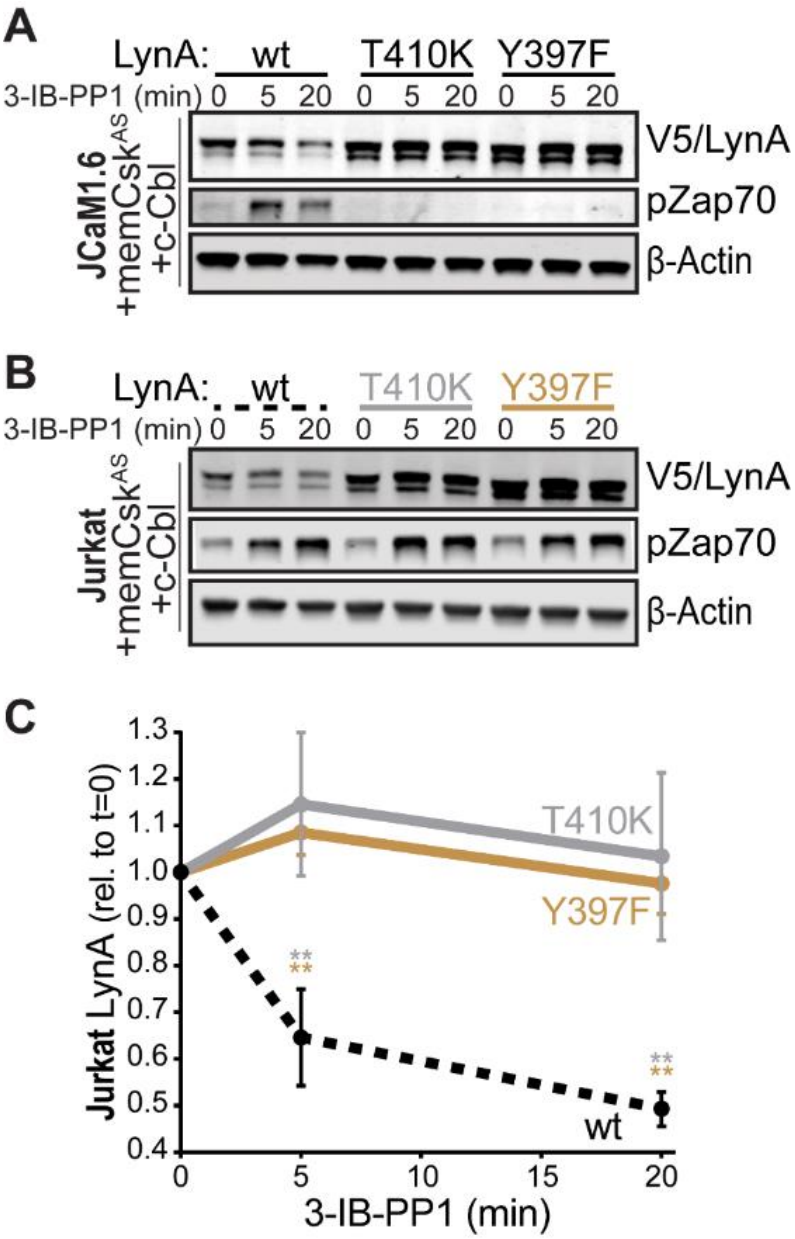

Figure 3.10. SFK activity is required for rapid degradation of LynA. (A) Immunoblots showing expression of transfected wild-type (wt), substrate-binding-impaired (T410K), or activation-loop-mutated (Y397F) His_6V5-tagged LynA protein coexpressed in JCaM1.6 cells with $memCsk^{AS}$ and c-Cbl and treated with 3-IB-PP1. Interdomain-B-phosphorylated Zap-70^{pY319} (pZap-70), an SFK target and prerequisite for Zap-70 activation, reflects the catalytic activity of LynA; β-Actin is shown as a loading control. **(B)** Overexpression of LynA variants in Jurkat cells. pZap-70 reflects 3-IB-PP1-induced Lck activation. **(C)** Quantification of V5-tagged LynA variants wt (black dotted), T410K (gray), and Y397F (orange) in Jurkat cells during 3-IB-PP1 treatment, corrected for total protein content (TPS) and reported relative to the steady-state level for each variant of LynA. SEM, n=3. Sig. from $ANOVA_2$-Tukey: [T410K vs. wt, gray asterisks], [Y397F vs. wt, orange asterisks]; ** P=0.0015-0.0083. Other pairs ns.

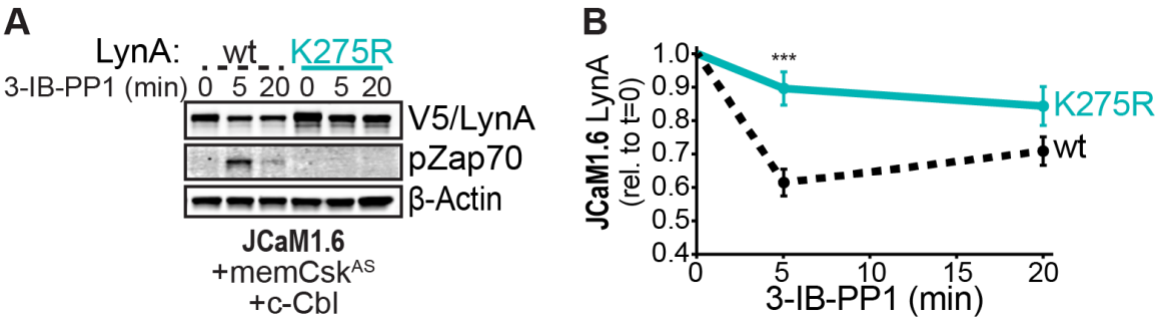

Figure 3.11. Catalytically dead LynA^{K275R} is not targeted for rapid degradation. (**A**) Immunoblots showing ectopic expression of wild-type (wt, black dotted) and active-site-mutated (K275R, cyan) His_6V5-tagged LynA protein coexpressed in JCaM1.6 cells with memCsk^{AS} and c-Cbl and treated with 3-IB-PP1. pZap-70 shows the impaired function of LynA^{K275R}; β-Actin is shown as a loading control. (**B**) Quantification of V5-tagged LynA protein corrected for total protein content (TPS), reported relative to the steady-state level for each LynA variant. SEM, n = 3. Sig. from $ANOVA_2$ with Sidak's multiple comparison test: [K275R vs. wt] ***p=0.0008.

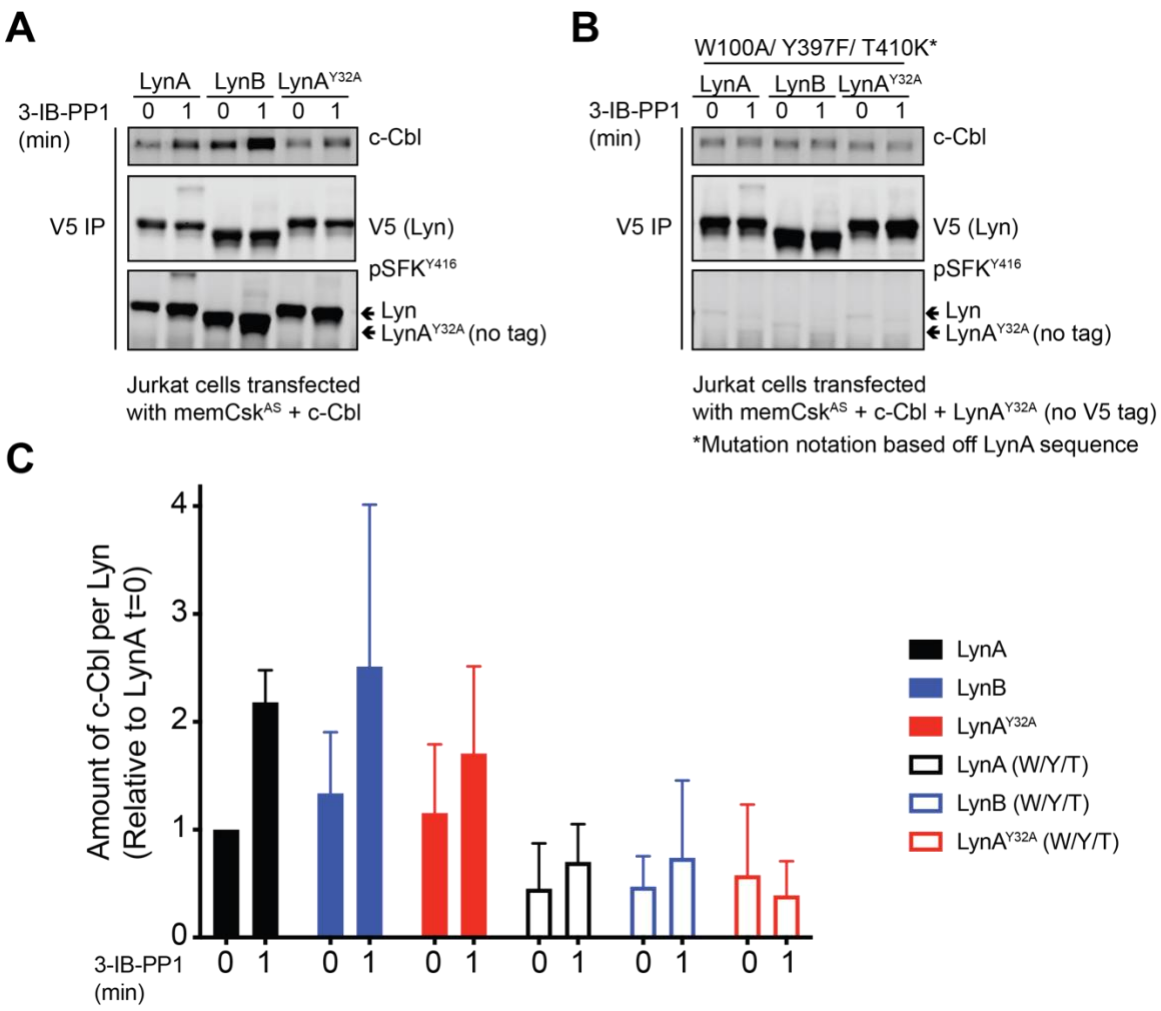

Figure 3.12. Mutating Y32 minimally disrupts c-Cbl binding to LynA. (A) Representative immunoblot of c-Cbl co-immunoprecipitation by V5-pulldown in Jurkat cells transfected with V5-tagged LynA, LynA^{Y32A} and LynB. **(B)** Representative immunoblot of c-Cbl co-immunoprecipitation by V5-pulldown in Jurkat cells transfected with V5-tagged LynA, LynA^{Y32A} and LynB with W100A/T410K/Y397F mutations to abolish SH3 binding (W100A), substrate binding (T410K) and activation-loop phosphorylation (Y397F). LynA Y32A (no V5 tag) was co-transfected to provide kinase activity necessary for c-Cbl activation. **(C)** Quantification of the amount of c-Cbl co-immunoprecipitated from Jurkat cells via V5-immunoprecipitation, relative to the amound of c-Cbl pulled down by unstimulated Jurkat cells transfected with LynA.

Observing that neither the Jurkat-cell SFKs (Lck/Fyn) nor the myeloid-cell SFK targets (Syk and FAK/Pyk2) participate in LynA degradation, we turned our focus to the major SFKs in macrophages. We showed above that wild-type LynA is degraded in 3-IB-PP1-treated Jurkat cells cotransfected with c-Cbl and memCsk^{AS}, suggesting that it can provide the sole initiating signal to trigger its own degradation, in (i) its ability to induce the phosphorylation of LynA Y32 and (ii) its ability to phosphorylate and activate c-Cbl. To determine whether this effect could be mediated by LynA and the other macrophage-expressed SFKs in trans, we performed experiments in which LynA^{T410K} (not degraded on its own during 3-IB-PP1 treatment) was coexpressed with kinase-active SFKs in Lck-deficient JCaM1.6 cells. LynA^{T410K} degradation thus reveals the ability of other SFKs to induce both LynA Y32 phosphorylation in trans and c-Cbl activation **(Figure 3.13)**. The composition of these transfected samples was assessed by immunoblotting for His_6V5-tagged LynA^{T410K} (for quantification in experimental samples) and wild-type His_6V5-tagged LynA (as a positive control). Wild-type LynA and LynA^{Y32A} were used for cotransfection as untagged constructs, so they could be resolved on LynA immunoblots **(Figure 3.13A)**. Expressed SFKs were visualized using antibodies specific for inactive and active SFKs, the V5 epitope tag, and/or individual SFKs **(Figure 3.13A)**. Cotransfected SFKs were classified by expression level, by ability to induce phosphorylation of the LynA^{T410K} activation loop (pLynA^{act}), of Zap-70 (at an activating SFK substrate site in interdomain B [17, 207]), and of c-Cbl at Y731 (an SFK- but not Syk-dependent site of phosphorylation [225]) **(Figure 3.13B)**.

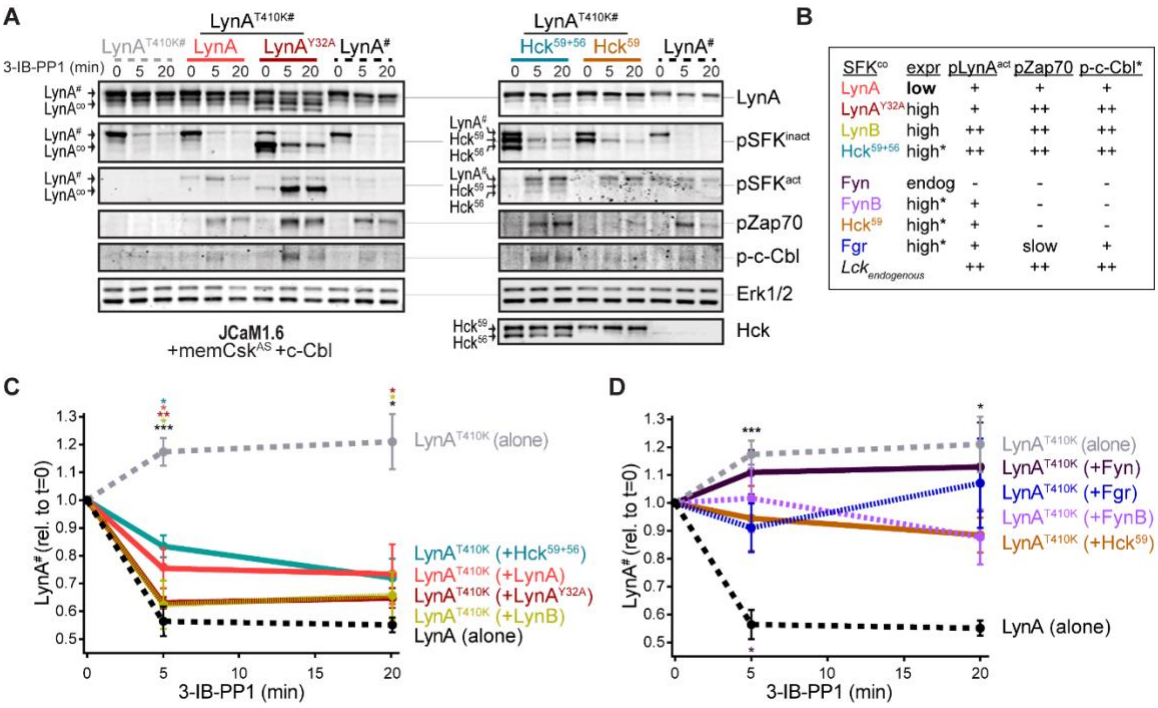

Figure 3.13. LynA, LynB, and Hck^{56kDa} can induce rapid degradation of cotransfected LynA in trans. (A) Representative immunoblots showing levels of non-intrinsically degradable His$_6$V5-tagged LynA^{T410K} (#) cotransfected with empty vector or active SFK (co) in memCsk^{AS}- and c-Cbl-expressing JCaM1.6 cells. Cotransfected SFKs include untagged LynA, untagged LynA^{Y32A}, His$_6$V5-tagged LynB, the long and short isoforms of Hck (Hck^{59+56}), the long isoform of Hck (Hck^{59}), FynT (Fyn), FynB, and Fgr. Endogenous FynT was also present. His$_6$V5-tagged LynA$^{T410K\#}$ (or wild-type LynA$^{\#}$ in the positive control condition) was quantified from a total LynA blot (top panel). Colors correspond to later figure panels. Coexpressed SFK was visualized via total SFK and pSFK^{inact} (inhibitory-tail phosphorylated SFK, corresponding to Src^{pY530}) blots as indicated. pSFK^{act} (activation-loop phosphorylated, corresponding to Src^{pY416}), pZap-70, and p-c-Cbl blots are used to show 3-IB-PP1-induced activity of the cotransfected SFK. Erk1/2 is shown as a loading control. When cotransfected with LynA^{T410K}, untagged wild-type LynA expression was expressed at very low levels, but its presence can be inferred based on induction of Zap-70 and c-Cbl phosphorylation with 3-IB-PP1 treatment. Endogenous Fyn was also present in the JCaM1.6 cells. **(B)** Comparison of the expression (expr) levels of cotransfected SFKs (SFK^{co}) and their ability to induce phosphorylation of the LynA^{T410K} activation loop (pLynA^{act}, the highest band in the pSFK^{act} blots), Zap-70^{pY319} and c-Cbl^{pY731} (p-c-Cbl) following 3-IB-PP1 treatment. If expression could not be directly compared with the wild-type LynA in the positive-control sample (*i.e.* all constructs except LynA and LynB, which could be compared directly via LynA and/or V5 blots), pSFK^{inact} and/or pSFK^{act} blots were used to provide a rough estimate of expression, with the caveat that these antibodies may recognize different SFK sequences with differing efficiency (marked with asterisks). Despite transfection, Fyn expression remained at endogenous levels (endog). The ability of endogenous Lck to phosphorylate the activation lop of LynA, interdomain B of Zap-70, and Y731 of c-Cbl was assessed in Lck-expressing Jurkat cells transfected with LynA^{T410K}. **(C-D)** Quantification of His$_6$V5-tagged wild-type LynA alone (black dotted, shown as a positive

control) or His_6V5-tagged $LynA^{T410K}$ alone (gray dotted) or cotransfected with the kinase-active SFKs. All LynA quantifications (#) are corrected for total protein content (TPS) and reported relative to the steady-state level for each transfection condition. SEM, n=5 for $LynA^{T410K}$ and LynA alone, SEM, n=4 for all others. Sig. from $ANOVA_2$-Tukey: [$LynA^{T410K}$ vs. LynA black asterisks], $LynA^{T410K}$ vs. $LynA^{T410K}$+LynA, coral asterisks], [$LynA^{T410K}$ vs. $LynA^{T410K}$+$LynA^{Y32A}$, wine asterisks], [$LynA^{T410K}$ vs. $LynA^{T410K}$+LynB, gold asterisks], [$LynA^{T410K}$ vs. $LynA^{T410K}$+Hck^{59+56}, teal asterisks], [Lyn vs. $LynA^{T410K}$+Fyn, dark purple asterisk]; *** P=0.0007, ** P=0.0017, * P=0.0180-0.0466. Other pairs ns. **(C)** Quantification of His_6V5-tagged $LynA^{T410K}$ cotransfected with SFKs that induce greater or equal Zap-70 phosphorylation than wild-type LynA alone, a combination of effects from protein expression and from the ability of each SFK to phosphorylate Zap-70. These include: untagged wild-type LynA (coral), untagged $LynA^{Y32A}$ (wine), His_6V5-tagged LynB (gold dotted), and Hck^{59+56} (teal). **(D)** Quantification of His_6V5-tagged $LynA^{T410K}$ cotransfected with SFKs that induce less pZap-70 than wild-type LynA alone: Hck^{59} (tan), Fgr (blue dotted), Fyn (purple), and FynB (light purple).

Cotransfected wild-type LynA, LynA^{Y32A}, and LynB were all capable of inducing the degradation of LynA^{T410K} in trans. Where depletion of LynA^{T410K} transfected alone was undetectable after 5 min of 3-IB-PP1 treatment, cotransfected wild-type LynA, LynA^{Y32A}, and LynB induced depletion of LynA^{T410K} by 20%, 37%, and 40%, respectively; wild-type LynA alone was depleted by 40% at the same time point **(Figure 3.13C)**. Although individual cells in a transiently transfected pool express varying levels of each construct, we were able to observe trends in bulk expression levels of cotransfected SFKs. As reported by the LynA immunoblots for wild-type LynA and LynA^{Y32A} **(Figure 3.13A)** and the V5 immunoblots for LynA and LynB, LynA^{Y32A} and LynB are more highly expressed than wild-type LynA. This is consistent with our previous observations **(Figure 3.5)**. This difference in expression could explain the effectiveness of LynA^{Y32A} and LynB in inducing degradation of LynA^{T410K}; the unique-region substitution in LynA^{Y32A} does not noticeably block this function or catalytic activity in general, at least compared to similarly expressed LynB. Potential differences in activity or signaling specificity, however, would be better investigated in a system that does not rely on overexpression.

Expression of Hck from a dual 59 kDa- and 56 kDa-expressing (Hck^{59+56}) plasmid induced depletion of LynA^{T410K} by 17% after a 5 min treatment with 3-IB-PP1 **(Figure 3.13C)**. Based on estimates from pSFK blots, both isoforms of Hck were expressed at high levels and pLynA^{act}, pZap-70, and p-c-Cbl were strongly induced **(Figure 3.13A-B)**. This activity, however, did not translate into a higher rate of LynA^{T410K} degradation than the poorly expressed, cotransfected wild-type LynA **(Figure 3.13A-B)**, suggesting that the ability to induce LynA degradation in trans depends on substrate specificity or other protein-protein interactions. Hck^{59} alone was able to phosphorylate the activation loop of LynA^{T410K} but unable to phosphorylate Zap-70 or c-Cbl **(Figure 3.13A,B,D)**. This suggests that the shorter isoform, Hck^{56} is the only one capable of inducing Zap-70 phosphorylation and LynA degradation.

Endogenous Fyn in Jurkat cells is not activated during 3-IB-PP1 treatment **(Figure 3.13A)**, and we were unable to increase Fyn expression or 3-IB-PP1-induced activation by cotransfection. We did, however, detect overexpression and 3-IB-PP1-induced activation of a cotransfected brain isoform of Fyn (FynB). Like Hck^{59}, FynB could induce

activation-loop phosphorylation of LynA^{T410K} **(Figure 3.13B)** but did not phosphorylate Zap-70 or c-Cbl or induce LynA^{T410K} degradation.

Although neither was able to induce degradation of LynA^{T410K}, Fgr and Lck were markedly different from Hck[59] and FynB in that, in addition to activation-loop-phosphorylating LynA^{T410K}, they were also capable of inducing Zap-70 and c-Cbl phosphorylation **(Figure 3.13B,D)**.

Overall, these results show that LynA degradation can be induced by SFK activity in trans. Activated LynA, LynB, and Hck[56] can all mediate LynA degradation to some extent, but Lyn appears to do this most efficiently, due either to faster activation kinetics or more efficient phosphorylation of LynA and c-Cbl.

3.2.5 Differential expression of c-Cbl tunes LynA protein levels and signaling in macrophages and mast cells

Analysis of data from the Immunological Genome Project (Immgen) shows that mRNA expression of Lyn and c-Cbl are differentially regulated across different cell types. Mast cells, for instance, express very low levels of c-Cbl mRNA **(Figure 3.14)** [226, 227], which translates into a low level of c-Cbl protein expression [228]. Cbl-b mRNA, in contrast, is abundant in mast cells.

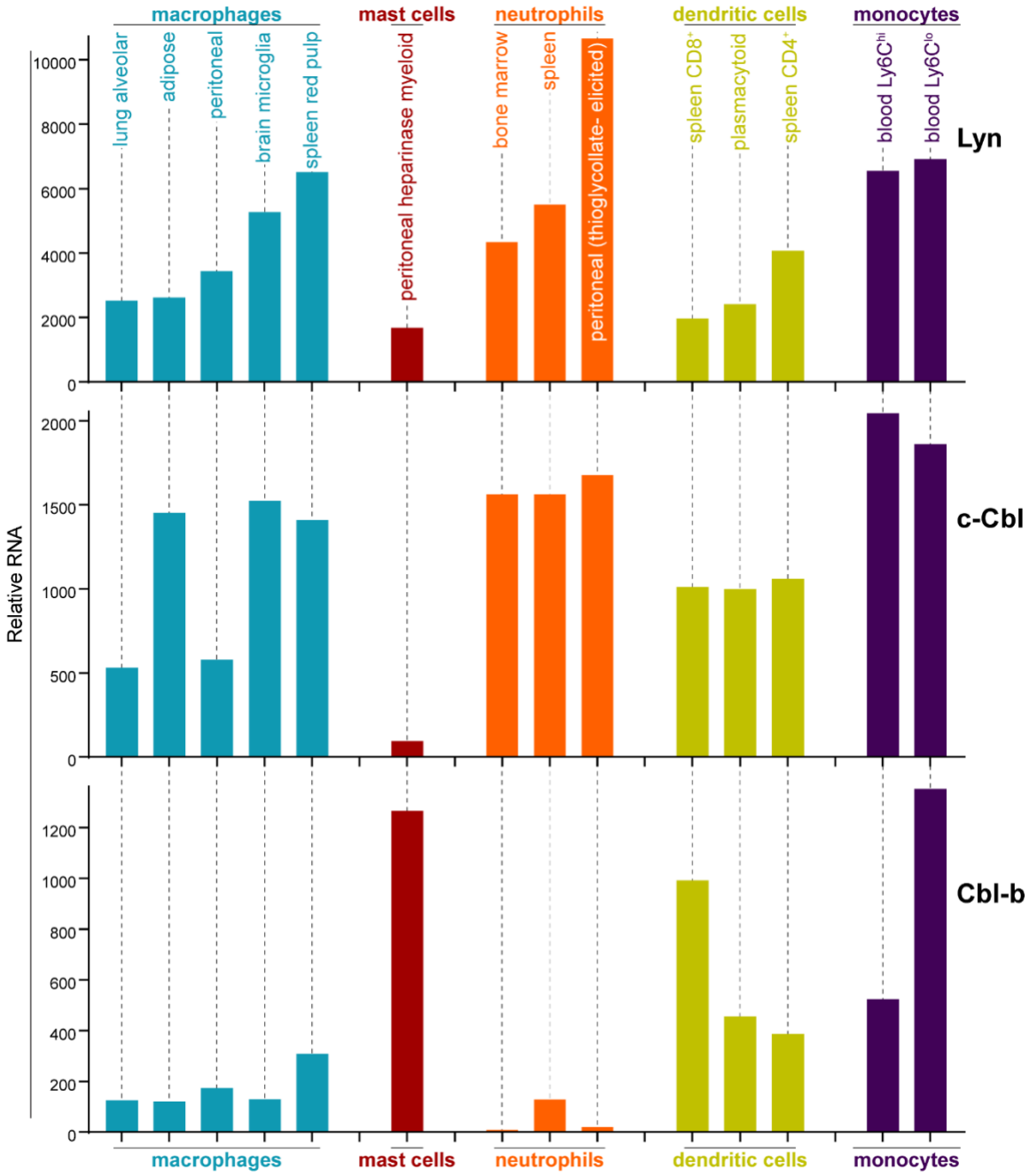

Figure 3.14. LynA, c-Cbl, and Cbl-b mRNAs are regulated differentially in myeloid cells. Mouse RNAseq data derived from the Immunological Genome Project [ImmGen, http://rstats.immgen.org/Skyline/skyline.html, 226, 227]. RNA levels of Lyn, c-Cbl, and Cbl-b are shown for macrophages, mast cells, neutrophils, dendritic cells, and monocytes.

As in macrophages, Lyn is a key regulator of mast-cell ITAM signaling [229], but the effect of disparate Cbl-family expression on LynA in the two cell types remains unknown. We generated bone-marrow-derived mast cells from Csk^{AS} mice and performed surface marker analysis as we had done already for BMDMs [22]. Csk^{AS} mast cells were homogenous in their expression of traditional mast-cell markers FcεR1α and c-Kit (CD117) [176] **(Figure 3.15A)**. We then used immunoblotting to compare the expression of Cbl and LynA protein in Csk^{AS} mast cells and BMDMs and found that mast cells express very little c-Cbl (20% of the level in rested macrophages) and relatively high levels of Cbl-b (80% of the level in rested macrophages) **(Figure 3.15B-C)**. Strikingly, low c-Cbl expression was accompanied by a complete resistance of LynA to degradation in the first 5 min of 3-IB-PP1 treatment **(Figure 3.15D)**. Mast cells also had increased steady-state expression of LynA (30% higher than in rested BMDMs) **(Figure 3.15E)**, despite low reported mRNA expression **(Figure 3.14)**. These combined effects resulted in 3-4x more LynA protein in mast cells than in rested BMDMs and 2x more than in primed BMDMs between 3 and 5 min of 3-IB-PP1 treatment. Mast cells also had a stronger signaling response to 3-IB-PP1. Although the kinetics of Erk phosphorylation in mast cells varied among experiments, induction of pErk1/2 was consistently higher in mast cells than in macrophages, including in primed BMDMs **(Figure 3.15F)**. We therefore hypothesized that cell-specific expression of c-Cbl tunes steady-state LynA protein levels and the persistence of that protein during activation. Since mast cells are less dependent on c-Cbl for positive signaling (*e.g.* as a scaffold in PI3K activation), long-lived LynA potentiates a strong response to 3-IB-PP1. Thus mast cells bypass the LynA signaling checkpoint by maintaining low levels of c-Cbl and therefore high levels of activated LynA.

The relationship between c-Cbl expression, LynA degradation, and sensitivity to SFK-mediated signaling suggests that the sensitivity of myeloid cells can be tuned by changes in c-Cbl expression at the mRNA and/or protein level. To test this effect, we transfected mast cells derived from Csk^{AS} bone marrow with a small activating (sa)RNA duplex [177, 230, 231] designed to increase the expression of c-Cbl. Transfection of this saRNA into mast cells increased the expression of c-Cbl protein 2-fold relative to mock-transfected cells **(Figure 3.15G)**. Csk^{AS} mast cells were then treated with 3-IB-PP1 for up to 15 min to activate SFKs and assess degradation of LynA and signaling potential as

reported by pErk1/2. Even this modest increase in mast-cell c-Cbl expression increased LynA degradation in response to 3-IB-PP1 and suppressed downstream phosphorylation of Erk1/2 **(Figure 3.15I-J)**. 3-IB-PP1 treatment for 15 min led to a 30% reduction of LynA protein in c-Cbl-overexpressing mast cells; LynA degradation at this time point was undetectable in control mast cells **(Figure 3.15I)**. Correspondingly, Erk1/2 phosphorylation was completely suppressed in mast cells treated with c-Cbl saRNA relative to control mast cells **(Figure 3.15J)**. Together, these data are consistent with a model in which differential expression levels of c-Cbl in myeloid cells regulates the activation response of LynA, working together with transcriptional regulation to tune myeloid-cell responsiveness to SFK-mediated signaling

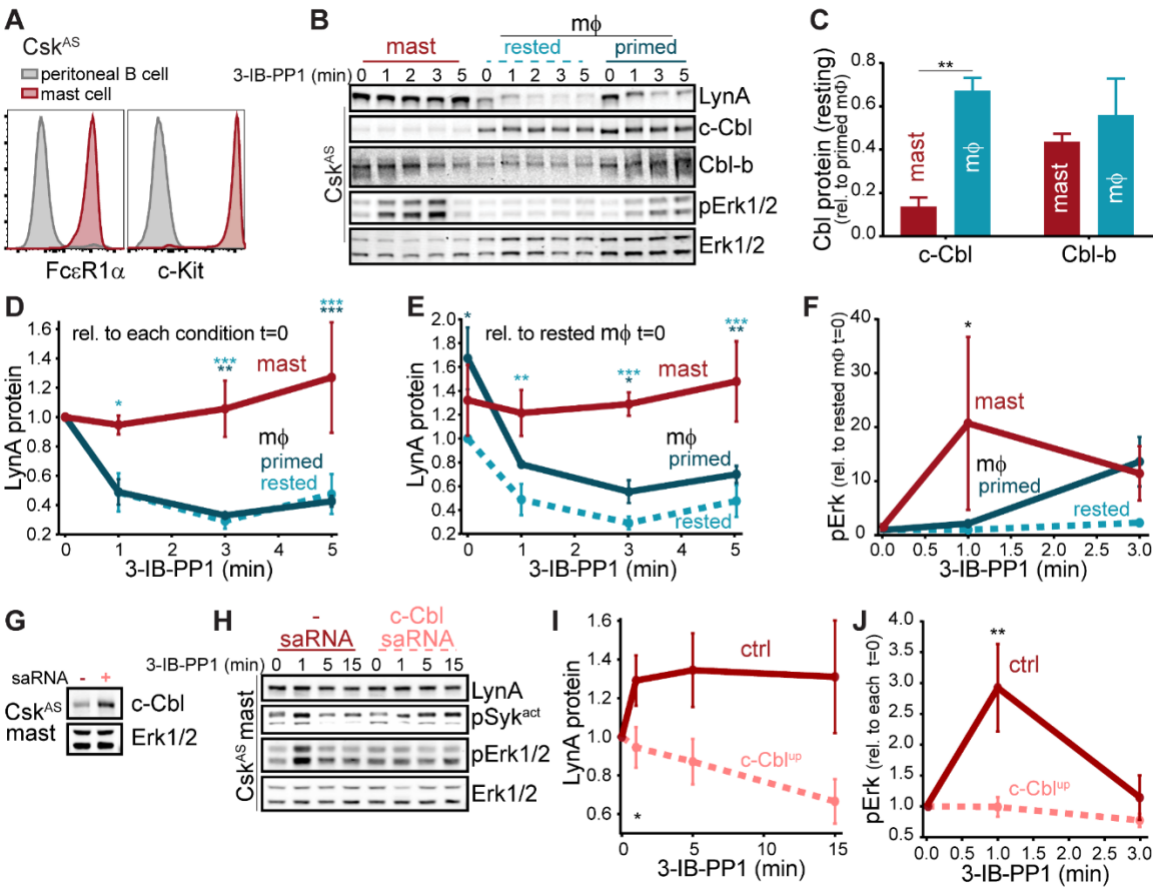

Figure 3.15. Differential expression of c-Cbl expression tunes LynA protein levels and SFK-mediated downstream signaling in macrophages and mast cells. (A) Flow cytometry showing surface expression of the mast-cell markers FcεR1α and c-Kit (CD117) in Csk^{AS} bone-marrow-derived mast cells (red) compared to a peritoneal B-cell control (gray). **(B)** Immunoblots of Csk^{AS} mast cells and BMDMs (mϕ) after resting or IFN-γ priming, showing the levels of LynA, c-Cbl, Cbl-b, and pErk1/2 during 3-IB-PP1 treatment; total Erk1/2 is shown as a loading control. **(C-F)** Quantification of c-Cbl, Cbl-b, LynA, and pErk in mast cells (red), IFN-γ-primed mϕs (dark teal), and rested mϕs (light teal). **(C)** Quantification of steady-state c-Cbl and Cbl-b protein in mast cells and rested mϕs, corrected for total protein content (TPS) and reported relative to levels in primed mϕs. SEM, n=3. Sig. from one-way ANOVA with Sidak's multiple comparison test: [mast vs. rested mϕs] ** P= 0.0035. Others pairs ns. **(D-E)** Quantification of LynA in mast cells and mϕs during 3-IB-PP1 treatment, corrected for total protein content (TPS) and reported relative to the steady-state level of LynA in each cell type **(D)** or relative to the steady-state level of LynA in rested mϕs **(E)**. SEM, n=3 for mast cells and primed mϕs, n=4 for rested mϕs. Sig. from $ANOVA_2$-Tukey: [mast vs. rested mϕs, light teal asterisks], [mast vs. primed mϕs, dark teal asterisks]; *** P=0.0004-0.0008, ** P=0.0025-0.0088, * P=0.0134-0.0466. Other pairs ns. **(F)** Quantification of pErk1/2 induction during 3-IB-PP1 treatment, corrected for total Erk1/2 expression and reported relative to the steady-state level of pErk1/2 in rested mϕs. SEM, n=3 for mast cells, n=4 for primed mϕs, n=5 for rested mϕs. Sig. from $ANOVA_2$-Sidak: [mast vs. rested mϕs, asterisk]; * P=0.0330. Other pairs ns. **(G)** Immunoblots showing steady-state expression of c-Cbl in Csk^{AS} mast cells

transfected in the presence or absence of Cbl-specific saRNA. Erk1/2 is shown as a loading control. **(H)** Immunoblots showing levels of LynA protein, pSyk, and pErk1/2 during 3-IB-PP1 treatment of saRNA-transfected or mock-transfected mast cells. **(I-J)** Quantification of LynA and pErk in mast cells with (pink) and without (red) saRNA-induced upregulation of c-Cbl. SEM, n=3. **(I)** Quantification of LynA protein during 3-IB-PP1 treatment, corrected for total protein content (TPS) and reported relative to the steady-state level for each transfection condition. Sig. from mixed-effects ANOVA analysis: * P= 0.0229. **(J)** Quantification of pErk1/2 induction during 3-IB-PP1 treatment in saRNA-treated and mock-treated mast cells, corrected for total Erk1/2 expression and reported relative to the steady-state level for each condition. SEM, n=3 for mast cells. Sig. from $ANOVA_2$-Sidak: ** P=0.0045.

3.3 Discussion

Polyubiquitination of kinases and adaptor proteins via the Cbl family can lead to their degradation, via the endolysosome or proteasome, and to non-degradation-mediated inhibition [84]. These E3 ligases must in turn be tightly regulated to prevent hyperresponsive or aberrant immune signaling while maintaining proper pathogen clearance [100]. Although highly homologous, c-Cbl and Cbl-b target different subsets of signaling proteins for inhibition and/or degradation [85, 232], with c-Cbl polyubiquitinating the SFKs, including Lyn [97, 233], and Cbl-b acting on ITAM-coupled receptors, Syk, and other kinases [100, 209, 210, 228]. c-Cbl binds via its PTB domain to the SFK activation-loop phosphotyrosine [96] and via its PXXP motifs to the SFK SH3 domain [205]. It is also a substrate, requiring phosphorylation to become fully activated. These binding interfaces promote common c-Cbl interaction with all the SFKs. In this chapter we report that c-Cbl targets LynA for rapid and specific degradation, a process that occurs with a half-life of a minute in BMDMs. In contrast, other E3 ligases contribute to the slower degradation mechanism shared among the other SFKs, including LynB, Fgr, Hck^{59}, Hck^{56}, Lck, FynB, and FynT, with the caveat that FynT does not seem to be activated in response to 3-IB-PP1. While overexpressed, transfected FynB was able to induce LynA Y416 phosphorylation (but not degradation), endogenously expressed Fyn (FynT) did not appear to be activated during 3-IB-PP1 treatment. FynB and FynT differ in their SH2 domain sequence, suggesting importance for Fyn SH2 in regulating Fyn activity.

c-Cbl is targeted to LynA via a noncanonical recognition site present in LynA but not the other SFKs. Although LynA and LynB have identical activation kinetics, lipidation sites, and activation-loop and SH3-domain sequences, LynA is degraded >10-fold more quickly than LynB in macrophages treated with the Csk^{AS} inhibitor/SFK activator 3-IB-PP1 [22]. Exploiting the similarity between LynA and LynB to make a limited set of point mutations, we have discovered that, while activation-loop phosphorylation and SH3-domain interactions mediate slower-phase targeting by c-Cbl and other E3 ligases, rapid degradation of LynA is triggered by an interaction peculiar to its unique-domain insert region.

We have discovered that Y32 in the unique-region insert of LynA is required for its rapid

degradation. This site is rapidly phosphorylated as LynA becomes activated, and this event marks LynA for c-Cbl-mediated polyubiquitination. Phosphorylation of LynA Y32 had been observed in neuroblastoma cell lines upon receptor-tyrosine-kinase activation [234]. In epidermoid carcinoma (A431) cells and breast tumor samples LynA Y32 is phosphorylated by the epidermal growth factor receptor (EGFR), allowing it to phosphorylate MCM-7 and stimulate cell proliferation [214]. We now present evidence of LynA Y32 phosphorylation in macrophages, where this potentially positive-regulatory function paradoxically induces LynA to trigger its own c-Cbl-mediated polyubiquitination and degradation, a process underlying its function as a rheostat controlling the LynA checkpoint.

Kinase-impaired variants of LynA are not rapidly degraded, a result confirmed in macrophages treated with the SFK inhibitor PP2. Catalytically active LynA and LynB, however, can induce degradation of catalytically impaired LynA in trans. Interestingly, the shorter isoform of Hck can also induce degradation of LynA, although less efficiently than Lyn itself. Degradation of LynA depends on a minimum of two phosphorylation events: the phosphorylation of LynA Y32 and activating phosphorylation of c-Cbl [87, 204]. The ability of individual Src family members to induce LynA degradation necessarily rely on the efficiency of these two processes. In cotransfection experiments, we found that some SFKs (FynB, Hck^{59}, Fgr, and Lck) were unable to induce degradation of kinase dead $LynA^{T410K}$ despite an increase in their own activation-loop phosphorylation and their ability to phosphorylate the activation loop of $LynA^{T410K}$. This suggests, perhaps surprisingly [235, 236], that these kinases are not localized away from LynA or otherwise lacking in activity. Instead, it is likely that the induction of LynA degradation occurs via specific protein-protein interactions and/or substrate recognition interfaces. Unlike FynB and Hck^{59}, Fgr and Lck were surprisingly able to phosphorylate c-Cbl, despite c-Cbl being reported to be a poor substrate for Lck and Zap-70 [204]. Again, this suggests that the substrate preferences of the Src family members are regulated. On the other hand, Syk and FynT have both been reported to phosphorylate and activate c-Cbl [204], but LynA degradation in 3-IB-PP1-treated BMDMs is unaffected by Syk inhibition and Fyn is not activated during 3-IB-PP1 treatment.

Rapid degradation of LynA is easily observed upon bulk SFK activation by 3-IB-PP1 but

also affects the steady-state level of LynA protein, likely due to the selective degradation of small amounts of basally active [22] LynA over time. Although the unique region of LynA lacks a c-Cbl consensus recognition motif [85], pY32 could serve as a docking site for the PTB domain of c-Cbl. In this ultrafast feedback process, activation-loop- and Y32-autophosphorylated LynA could efficiently phosphorylate and activate c-Cbl and facilitate its own degradation, potentially then releasing c-Cbl for other positive and negative regulatory signaling functions. Earlier work has shown that although the interactome of transfected LynA^{Y32F} in mammary adenocarcinoma (MDA-MB-231) cells more closely resembles that of wild-type LynA than LynB, some LynA interactions are lost [150]. It is also possible that, by analogy to a similarly situated but non-homologous phosphorylation site in Hck (pY29) [38], phosphorylation of LynA Y32 could be directly activating. The unique regions of LynA and LynB make distinct SH3-domain contacts [42], and phosphorylation could alter these interactions, leading to increased kinase activity. Hyperactivated LynA could then efficiently phosphorylate and activate nearby or pre-complexed c-Cbl, triggering its own degradation more aggressively than do the other SFKs.

LynA and LynB have been reported to interact with different subsets of proteins in mast cells and in triple-negative breast cancer cells, with LynA signaling via ITAM [149], cytoskeletal, and proliferative [150] pathways and LynB initiating negative feedback via ITIMs and phosphatases [149]. In mammary epithelial cells the ratio of LynA and LynB is actively regulated by Epithelial Splicing Regulatory Protein 1 (ESRP1), with LynA-upregulated tumors having the more invasive phenotype [150]. The positive-regulatory roles reported for LynA in mast and tumor cells complements our own observations that LynA degradation can block macrophage signaling through the Erk, Akt, and NFAT pathways, which cannot be rescued by active LynB [22].

Aberrant activation driven by ITAM signaling pathways in macrophages is a known driver of autoimmune and inflammatory disease, with activated macrophages accumulating in chronically inflamed tissues in the absence of an active infection [237]. Regulation of LynA protein expression and deactivation kinetics by c-Cbl could, via the LynA checkpoint, prevent the initiation of pathological signaling. The threshold for macrophage activation is modulated by changes to their local environment. For example, IFN-γ and

LPS polarize macrophages for a pro-inflammatory response, whereas IL-4 and IL-13 polarize macrophages for tissue repair (i.e. collagen deposition) and inflammatory resolution [4, 238]. We have reported that IFN-γ decreases the macrophage signaling threshold in part by increasing the expression of LynA [22]. Dynamic changes in SFK and c-Cbl levels could modulate the macrophage activation threshold, ensuring that macrophages respond appropriately during times of infection (low threshold) and limiting aberrant activation in response to cellular debris and small-scale antibody complexes during inflammatory resolution (high threshold).

Like macrophages, mast cells reside in nearly every bodily tissue and perform environment-specific functions in addition to sensing non-self [238, 239]. While macrophages have distinct anti-inflammatory roles as professional phagocytes in the silent clearance of apoptotic cells and agents of wound healing, mast cells are constitutively primed for ITAM-induced triggering, releasing preformed granules that contain inflammatory cytokines, chemokines, prostaglandins, and proteases. Pursuant to these differing functions, macrophages continuously gauge ITAM ligand valency (*i.e.* particle size) and have a relatively high basal threshold for inflammatory activation [22, 62], while mast cells can be triggered by small-scale receptor clustering induced by low-valency or even monovalent FcεR-IgE-allergen complexes [196, 197]. One striking difference between the macrophage and mast-cell ITAM regulatory machinery is that mast cells express almost no c-Cbl. In spite of low reported mRNA levels (Immgen, [226, 227]), mast cells constitutively express a high level of LynA protein, likely due to impaired steady-state degradation of basally active LynA. Furthermore, LynA is not degraded upon activation and 3-IB-PP1 triggers a stronger Erk phosphorylation response in the absence of ITAM-receptor ligation in mast cells than in rested macrophages.

Overall, we describe a model in which regulation of LynA and c-Cbl levels helps to determine an immune cell's potential for inflammatory ITAM signaling. Regulated degradation tunes down the LynA rheostat, blocking cell signaling via the LynA checkpoint at low cellular doses of LynA and overriding the LynA checkpoint at higher doses. In macrophages, this occurs on a continuum where LynA dose is highest in cells rendered more reactive by IFN-γ priming (polarization). Mast cells express almost no c-

Cbl and maintain high levels of LynA at steady state and over time, consistent with permissive signaling in the absence of a large-scale ITAM receptor clustering event nucleated by multivalent receptor ligation. Appropriate regulation of immune receptor thresholds is critical for maintaining the function of innate immune cells; threshold dysregulation can lead to chronic feedback loops that drive inflammatory signaling in autoimmune disease and conversely tumor-supporting immunosuppressive signaling [237]. Elucidating the mechanisms by which the LynA checkpoint is regulated may allow us to tune immune-cell sensitivity and reprogram pathological cells

3.4 Footnotes

Portions of this text have been previously published and adapted here:

Brian BF 4th, Jolicoeur AS, Guerrero CR, Nunez MG, Sychev ZE, Hegre SA, Sætrom P, Habib N, Drake JM, Schwertfeger KL, Freedman TS. Unique-region phosphorylation targets LynA for rapid degradation, tuning its expression and signaling in myeloid cells. Elife. 2019 Jul 8;8:e46043. doi: doi.org/10.7554/eLife.46043

Author contributions: BFB, ASJ, CRG, MGN, and ZES performed experiments. SAH PS, NH, JMD and KLS provided methodology and review. BFB performed experiments related to figures 3.1 – 3.13, 3.15. MGN assisted with experiments related to 3.1 – 3.13, 3.15. CRG performed experiments related to 3.7-3.8. ZES and JMD provided expertise related to figures 3.7-3.8. ASJ performed experiments related to Figure 3.13. SAH, PS, and NH provided expertise and reagents related to Figure 3.15. BFB and TSF conceptualized experiments and wrote the manuscript.

CHAPTER 4: CRISPR-based constraint of *lyn* splicing reveals a unique function of LynB in suppressing autoimmunity

4.1 Introduction

Autoimmune diseases comprise a spectrum of disorders in which the immune system mounts an improperly regulated immune response against self-antigens, or regulatory mechanisms fail to limit excessive inflammation [240-242]. The development and progression of autoimmunity can have many causes and drivers, including dysregulated immune-cell signaling [80, 111, 243]. Understanding how immunoreceptor signaling is regulated is imperative to develop therapies that limit immune activation but preserve the immune system's ability to eliminate pathogens.

The tyrosine kinase Lyn has been implicated in the development or progression of several autoimmune diseases, especially in human systemic lupus erythematosus (SLE). Polymorphisms in the *LYN* gene are risk factors for SLE [139, 244] and patients with lupus often have deficiencies in Lyn expression, signaling or trafficking [136, 138]. In both human and mice, Lyn is expressed in B cells and myeloid cells, as well as non-hematopoietic cells such as neurons and epithelial cells, and transmits signals downstream of a number of receptors, including immunoreceptor tyrosine-based activation motif (ITAM)-coupled receptors such as the B-cell receptor (BCR) [12, 104, 133] and Fc receptors (FcRs) [141]. Lyn also signals downstream of non-ITAM-coupled receptors such as integrins [245], and Toll-like receptors (TLRs) [117, 119]. Importantly, Lyn also associates with and signals downstream of immunoreceptor tyrosine inhibitory motif (ITIM) receptors such as CD22 [133, 246, 247], leading to the activation of phosphatases such as SHP-1 and SHIP-1, that act as important brakes on inflammatory signaling. Lyn is unique amongst the Src-family kinases in its ability to activate pathways that both promote and inhibit cellular activation [12, 151, 248]. Understanding how Lyn is able to mediate both positive and negative signaling in immune cells is critical for understanding the development and progression of autoimmune diseases and developing treatments that selectively suppress immune function.

In mouse models, global Lyn knock-out mice develop an age-onset autoimmune disease that partially resembles human SLE, including the production of anti-nuclear antibodies (ANAs), and the development of splenomegaly and glomerulonephritis [249]. Similar

phenotypes are observed in B cell-selective [118] and dendritic-cell-selective [114, 117] Lyn knockout (Lyn^{KO}) mice, underscoring that Lyn deficiency in multiple Lyn-expressing cell types contributes to the development of autoimmunity. The development of autoimmune disease in Lyn^{KO} mice can be abrogated by concomitantly knocking out downstream signaling proteins such as CARD9 [119], modulators of actin dynamics such as Ezrin [250], and TLR signaling components, such as MyD88 [117, 118, 183] and IRF5 [120], revealing that a wide array of activated signaling pathways contributes to disease development in the absence of Lyn.

MyD88 is an adaptor protein that links multiple TLRs, including TLR4 and TLR9, to downstream signaling and cellular activation [251]. TLR4 normally senses lipopolysaccharides generated by gram-negative bacteria and TLR9 normally responds to single-stranded DNA (ssDNA) with unmethylated CpG motifs often found in microbial DNA. Both TLR4 signaling and overexpression have been implicated in human SLE and mouse models of lupus [126, 128, 130, 131, 252]. Lyn has been shown to negatively regulate TLR4 and TLR9 signaling in dendritic cells [117, 119, 120]. However, Lyn has also been shown to positively regulate TLR4 signaling in mast cells and macrophages [124, 125]. A detailed, molecular understanding of how Lyn interacts with and differentially regulates TLR4 and TLR9 signaling in multiple cell types remains incomplete.

mRNA from the *lyn* gene can be alternatively spliced to produce two proteins, LynA (the longer isoform) and LynB. LynA contains a 21-amino-acid-insert near its N-terminus, in the unique region of the SFKs. Previous research suggests that LynA and LynB can interact with different proteins and modify different signaling pathways. Lentiviral expression of LynA or LynB in Lyn^{KO} mast cells revealed that LynA has a greater propensity to activate downstream signaling after FcεR ligation whereas LynB was better able to activate inhibitory phosphatases [149]. Similarly, breast cancer cells had a more invasive phenotype when reconstituted with LynA [150], suggesting that LynA associates more with activating signaling pathways than LynB. Furthermore, analysis of proteins that immunoprecipitate with LynA showed an enhancement of proteins related to cytoskeletal rearrangement, further suggesting differential interactomes of LynA and LynB. Additional data suggests that the 21-amino-acid-insert of LynA may make

important intramolecular contacts with other regulatory domains, including the Src-homology 3 (SH3) domain, that may further differentiate the regulatory mechanisms that control LynA and LynB activity [42].

Our previous research has uncovered unique regulatory mechanisms and functions of LynA and LynB that suggest unique roles in regulating immune function. Using Csk^{AS} transgenic mice, we identified a unique role for LynA in promoting macrophage pro-inflammatory signaling [22]. Csk^{AS} mice express a transgenic Csk mutant that can be specifically inhibited by the small molecule 3-IB-PP1 [70]. Treating Csk^{AS} macrophages with 3-IB-PP1 induces global SFK activation and rapid poly-ubiquitin-mediated degradation of LynA, which occurs on a much faster time scale than LynB and other SFKs expressed in macrophages [22]. The rapid degradation of LynA prevents activation of downstream proteins, such as MAPK/Erk and Akt. However, treating (priming) macrophages with inflammatory cytokines, such as IFN-γ, upregulates the protein levels of LynA and LynB and restores downstream signaling upon SFK activation. Elucidating how LynA and LynB may contribute differentially to macrophage activation and priming-dependent signaling has been complicated by a lack of genetic models that enable LynA and LynB to be studied independently.

To investigate the functions of LynA and LynB, we used CRISPR-Cas9 to create novel knockout models to study LynA and LynB independently. We show that $LynB^{KO}$ mice develop splenomegaly, produce anti-nuclear antibodies and develop glomerulonephritis, suggesting that LynB, in particular, has a negative regulatory role and prevents the development of autoimmune disease in mice. Furthermore, circulating immune cells in $LynB^{KO}$ mice also have increased expression of TLR4, but not other TLRs. Finally, we show the LynB-deficiency increases the responsiveness of certain immune cells to TLR4 and TLR9 stimulation, suggesting additional pathways negatively regulated by LynB.

4.2 Results

4.2.1 Generation of LynA^{KO} and LynB^{KO} mice

LynA is produced by splicing exon 2 and 3 of the *lyn* gene, whereas LynB is spliced from a cryptic splice site in exon 2 (**Figure 4.1A**). To generate LynA^{KO} mice we injected mouse embryos with preformed ribonucleoprotein complexes [182, 253] containing Cas9 and two guide (g)RNAs to induce two cuts in the region of the *lyn* exon 2 that encodes the unique insert of LynA, 3' of the cryptic LynB splice site (**Figure 4.1B**). Repair of the resulting deletion and double-strand break by non-homologous end joining (NHEJ) resulted in a deletion and frameshift, facilitating screening and ensuring selective loss of LynA expression. After implantation and birth, pups were screened via PCR and restriction digest; candidates yielding truncated PCR products (due to the exon-2 deletion) and maintaining a cut site for SnaBI near the LynB splice junction were found to be single-allele carriers of the LynA deletion and bred to homozygosity. Three founder candidates were verified by PCR sequencing. Of these, one mutation was sufficiently close to the exon-2 splice junction to disrupt LynB protein expression, and one initially bred slowly. Therefore, we proceeded with mice derived from a single founder, "LynA^{KO}(CRISPR)", in which the LynA sequence is scrambled after amino-acid residue 30, four residues into the LynA unique-region insert, followed by a premature stop codon after residue 77 **(Figure 4.2)**. LynB is unaffected LynA^{KO} mice.

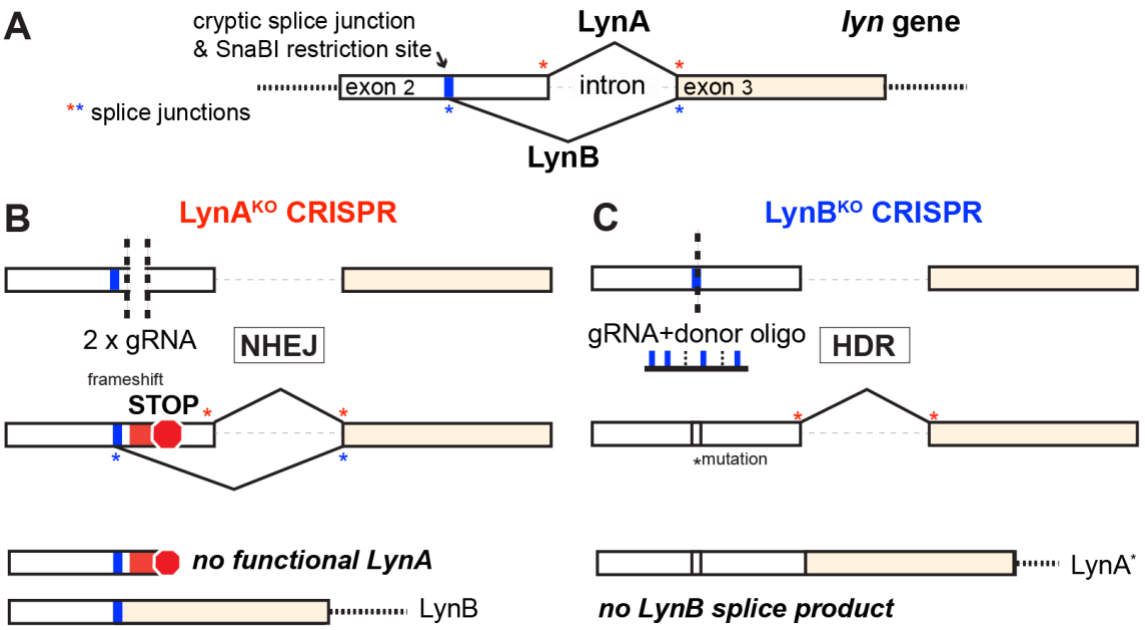

Figure 4.1. Generation of LynA^{KO} and LynB^{KO} mice
(A) A cryptic splice junction in exon 2 allows for alternative splicing of the *lyn* gene, producing LynA and LynB **(B)** LynA^{KO} mice were created using dual gRNAs and NHEJ, resulting in a deletion within the LynA insert sequence and a premature stop codon after the cryptic LynB splice acceptor site in exon 2. **(C)** LynB^{KO} mice were created using one gRNA and a donor oligonucleotide sequence encoding two point mutations: one to inactivate the LynB splice acceptor site and another (silent) mutation to ablate a SnaB1 restriction enzyme cleavage site for PCR-based screening. In the LynB^{KO} mice, LynA(*) is expressed with the unique-region substitution V24L.

WT mouse *lyn*

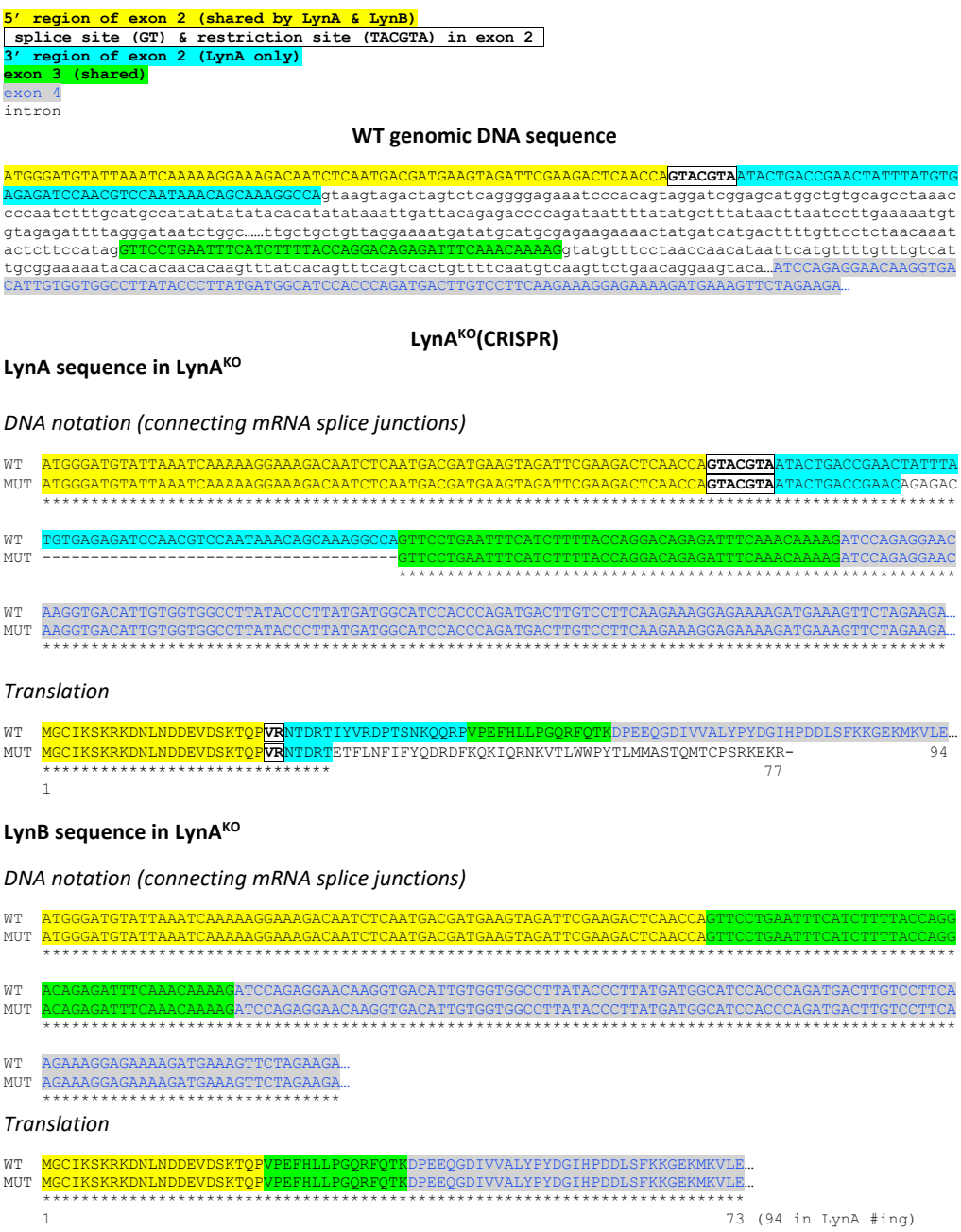

Figure 4.2. Genomic and protein sequence generated in LynA^{KO} mice. Genomic and proteins sequences of exon 2 (yellow) and exon 3 (green) of the mouse *lyn* gene, illustrating the cryptic LynB splice site (boxed) and LynA unique region (cyan), and illustrating the truncated protein products from CRISPR gene editing in the LynA^{KO} mice.

WT mouse *lyn*

5′ region of exon 2 (shared by LynA & LynB)
splice site (GT) & restriction site (TACGTA) in exon 2
3′ region of exon 2 (LynA only)
exon 3 (shared)
exon 4
intron

WT genomic DNA sequence

ATGGGATGTATTAAATCAAAAAGGAAAGACAATCTCAATGACGATGAAGTAGATTCGAAGACTCAACCAGTACGTAATACTGACCGAACTATTTATGTG
AGAGATCCAACGTCCAATAAACAGCAAAGGCCAgtaagtagactagtctcaggggagaaatcccacagtaggatcggagcatggctgtgcagcctaaac
cccaatctttgcatgccatatatatatacacatatataaattgattacagagaccccagataatttttatatgctttataacttaatccttgaaaaatgt
gtagagattttagggataatctggc……ttgctgctgttaggaaaatgatatgcatgcgagaagaaaactatgatcatgacttttgttcctctaacaaat
actcttccatagGTTCCTGAATTTCATCTTTTACCAGGACAGAGATTTCAAACAAAAGgtatgtttcctaaccaacataattcatgttttgtttgtcat
tgcggaaaaatacacacaacacaagtttatcacagtttcagtcactgttttcaatgtcaagttctgaacaggaagtaca…ATCCAGAGGAACAAGGTGA
CATTGTGGTGGCCTTATACCCTTATGATGGCATCCACCCAGATGACTTGTCCTTCAAGAAAGGAGAAAAGATGAAAGTTCTAGAAGA…

LynB^{KO}(CRISPR)
(no LynB due to mutation of splice site)

LynA sequence in LynB^{KO}

DNA notation (connecting mRNA splice junctions)

```
WT  ATGGGATGTATTAAATCAAAAAGGAAAGACAATCTCAATGACGATGAAGTAGATTCGAAGACTCAACCAGTACGTAATACTGACCGAACTATTTA
MUT ATGGGATGTATTAAATCAAAAAGGAAAGACAATCTCAATGACGATGAAGTAGATTCGAAGACTCAACCACTGCGTAATACTGACCGAACTATTTA
    ************************************************************************ * ************************
    1                                                                                                 95

WT  TGTGAGAGATCCAACGTCCAATAAACAGCAAAGGCCAGTTCCTGAATTTCATCTTTTACCAGGACAGAGATTTCAAACAAAAGATCCAGAGGAAC
MUT TGTGAGAGATCCAACGTCCAATAAACAGCAAAGGCCAGTTCCTGAATTTCATCTTTTACCAGGACAGAGATTTCAAACAAAAGATCCAGAGGAAC
    ****************************************************************************************************
    96                                                                                              190

WT  AAGGTGACATTGTGGTGGCCTTATACCCTTATGATGGCATCCACCCAGATGACTTGTCCTTCAAGAAAGGAGAAAAGATGAAAGTTCTAGAAGA…
MUT AAGGTGACATTGTGGTGGCCTTATACCCTTATGATGGCATCCACCCAGATGACTTGTCCTTCAAGAAAGGAGAAAAGATGAAAGTTCTAGAAGA…
    ****************************************************************************************************
    191                                                                                             284
```

Translation

```
WT  MGCIKSKRKDNLNDDEVDSKTQPVRNTDRTIYVRDPTSNKQQRPVPEFHLLPGQRFQTKDPEEQGDIVVALYPYDGIHPDDLSFKKGEKMKVLE…
MUT MGCIKSKRKDNLNDDEVDSKTQPLRNTDRTIYVRDPTSNKQQRPVPEFHLLPGQRFQTKDPEEQGDIVVALYPYDGIHPDDLSFKKGEKMKVLE…
    **********************:*****************************************************************************
    1                                                                                               94
```

Figure 4.3. Genomic and protein sequence generated in LynB^{KO} mice. Genomic and proteins sequences of exon 2 (yellow) and exon 3 (green) of the mouse *lyn* gene, illustrating the cryptic LynB splice site (boxed) and LynA unique region (cyan), and illustrating the resulting protein products of LynA^{V24L} from CRISPR gene editing in the LynB^{KO} mice.

To generate LynB^{KO} mice we used a single gRNA to induce a Cas9 cut near the cryptic LynB splice site in *lyn* exon 2. Homology-directed repair (HDR) was then templated from a donor oligonucleotide (**Figure 4.1C**) with two single-nucleotide substitutions, one to ablate the splice site and one silent mutation to ablate a SnaBI restriction site for restriction-based screening. Candidates resistant to SnaBI were found by PCR sequencing to be heterozygous for the splice-site mutation and were bred to homozygosity. We proceeded with the best breeder of two candidates. This strain bearing two alleles of "LynBKO(CRISPR)" results in expression of LynA with a conservative valine (V)-to-leucine (L) substitution at position 24 in the unique region; the SnaBI restriction-site mutation is silent **(Figure 4.3)**.

To test whether V24 substitution alters the function of LynA, we compared the signaling responses of LynA, LynA^{V24L} and LynA^{V24A}, transiently transfected into JCaM1.6 T cells, which lack the endogenous SFK Lck. In this model, activated LynA is required to initiate downstream signaling [27]. To induce LynA activation, we co-transfected JCaM1.6 cells with a membrane-localized variant of Csk (memCsk^{AS}) that is sensitized to inhibition via the small molecule 3-IB-PP1 [27, 70]. Addition of 3-IB-PP1 to memCsk^{AS}-transfected cells induces activation of the SFKs (including transfected LynA [27]) without the requirement for TCR crosslinking [70]. Downstream signaling, as assessed by Erk phosphorylation, was unaffected in LynA, LynA^{V24A} and LynA^{V24L}-expressing cells, but blocked in cells expressing a kinase-dead variant, LynA$^{T410K/Y397F}$, suggesting that LynA kinase activity and interactions with Syk and other substrates are not disrupted **(Figure 4.4A,B)**. To further investigate whether LynA^{V24L} substitution alters LynA regulation, we bred LynB^{KO} mice to Csk^{AS}-transgenic mice to generate Csk^{AS}LynB^{KO} mice. We have previously shown that LynA is rapidly degraded in Csk^{AS} bone-marrow derived macrophages (BMDMs) following treatment with 3-IB-PP1. We saw no difference in LynA degradation between Csk^{AS} and Csk^{AS}LynB^{KO} (**Figure 4.4C,D**), suggesting the V24L substation does not affect LynA regulation. To further control for any effect of this unique-region substitution on LynA function, we performed initial studies with mice produced from an F1 cross of homozygous LynA^{KO} and LynB^{KO} parents (F1: "AB^{hemi}"), which express LynA^{V24L} and LynB from one allele each **(Figure 4.5A)**. For simplicity, we refer to LynA protein in LynB^{KO} mice and cells simply as "LynA."

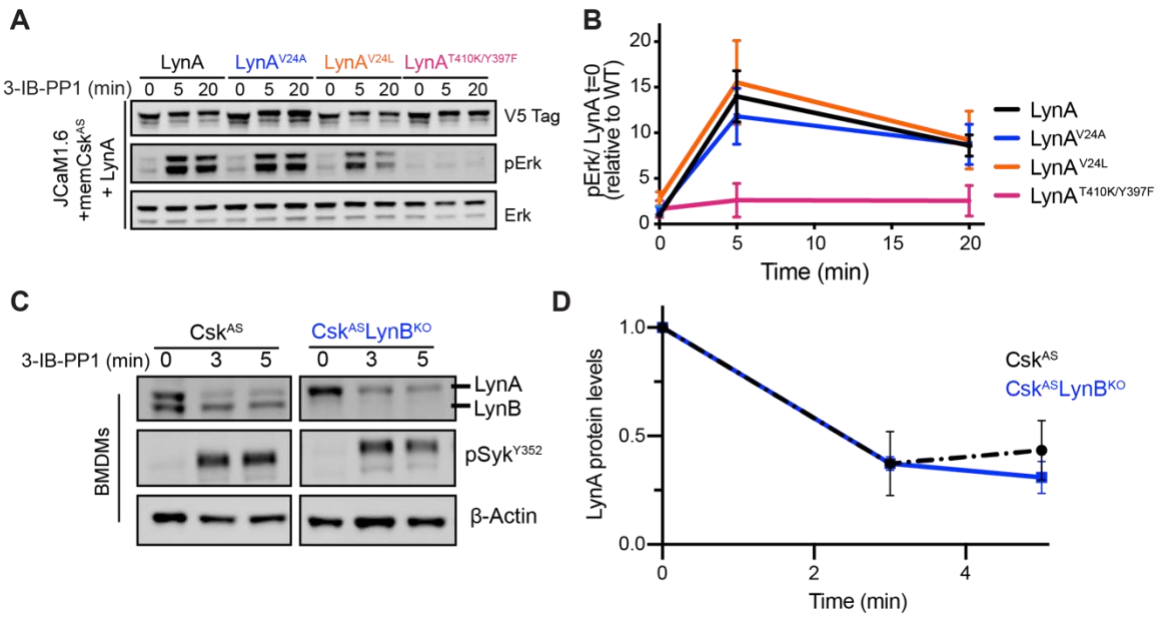

Figure 4.4. V24L substitution does not affect LynA degradation or signaling. (A) Representative immunoblot of JCam1.6 cells transfected with LynA, LynA^{V24A}, LynA^{V24L} and LynA$^{T410K/Y397}$ mutants along with membrane-anchored Csk^{AS} (memCsk^{AS}) and treated with Csk^{AS} inhibitor 3-IB-PP1. **(B)** Quantification of pErk activation in **(A)** normalized to the amount of LynA protein at t=0. **(C)** Representative immunoblot of Csk^{AS} and Csk^{AS}LynB^{KO} BMDMs treated with 3-IB-PP1. **(D)** Quantification of LynA degradation in Csk^{AS} and Csk^{AS}LynB^{KO} macrophages

We next probed Lyn protein expression in BMDMs from LynA^{KO} and LynB^{KO} mice and found the expected pattern of deficiency (LynA absent in the homozygous LynA^{KO} (LynA^{KO}LynB$^{+/+}$) and LynB absent in the homozygous LynB^{KO} (LynB^{KO}LynA$^{+/+}$) (**Figure 4.5B**). To our surprise, however, the protein level of the remaining Lyn isoform (LynB in the homozygous LynA^{KO} and LynA in the homozygous LynB^{KO}) was ~2.5x elevated relative to WT (**Figure 4.5B-D**), suggesting feedback compensation. Compensating for the loss of a SFK by upregulating other SFKs has been previously described [254]. However, we detected no differences in other SFK expression in BMDMs derived by LynA^{KO} and LynB^{KO} mice (**Figure 4.5B**)**.** We created hemizygous LynA^{KO}LynB$^{+/-}$ and LynB^{KO}LynA$^{+/-}$ mice by breeding the LynA^{KO} and LynB^{KO} homozygous mice to Lyn^{KO} mice, which lack both LynA and LynB due to a homozygous Neomycin insertion (Lyn^{KO}(NEO)) (**Figure 4.5A**) Mice that express only one allele of LynA or LynB (genotype LynA^{KO}(CRISPR)/Lyn^{KO}(NEO), protein-expression phenotype LynA^{KO}LynB$^{+/-}$ or genotype LynB^{KO}(CRISPR)/Lyn^{KO}(NEO), protein-expression phenotype LynB^{KO}LynA$^{+/-}$, express physiological levels of LynA and LynB, respectively (**Figure 4.5B-D**).

We have previously shown that priming macrophages for 12-16 hours with interferon (IFN)-γ induces transcriptional upregulation of Lyn. This response to inflammatory priming was preserved in all LynA^{KO} and LynB^{KO} BMDMs (**Figure 4.5E-G).**

We have previously shown that the ubiquitin ligase c-Cbl regulates the protein level of LynA in macrophages and that c-Cbl-expression controls the magnitude of LynA signaling. We wondered whether LynA deletion conversely feeds back to alter expression of c-Cbl. We probed BMDMs from knockout mice for expression c-Cbl, and the closely related E3 ligase Cbl-b, expression. We found that BMDMs from LynB^{KO} mice have increased levels of c-Cbl, while Cbl-b be levels were unaffected in LynA^{KO} and LynB^{KO} mice (**Figure 4.6**). This suggests that c-Cbl-expression levels are regulated in response to Lyn signaling and may act as a mechanism to control the level of Lyn signaling.

We performed future experiments using hemizygous mice, as opposed to the $LynA^{KO}LynB^{+/+}$ an $LynB^{KO}LynA^{+/+}$ homozygous mice. For simplicity, the hemizygous mice will be referred to as $LynA^{KO}$ and $LynB^{KO}$ in all future references in this chapter.

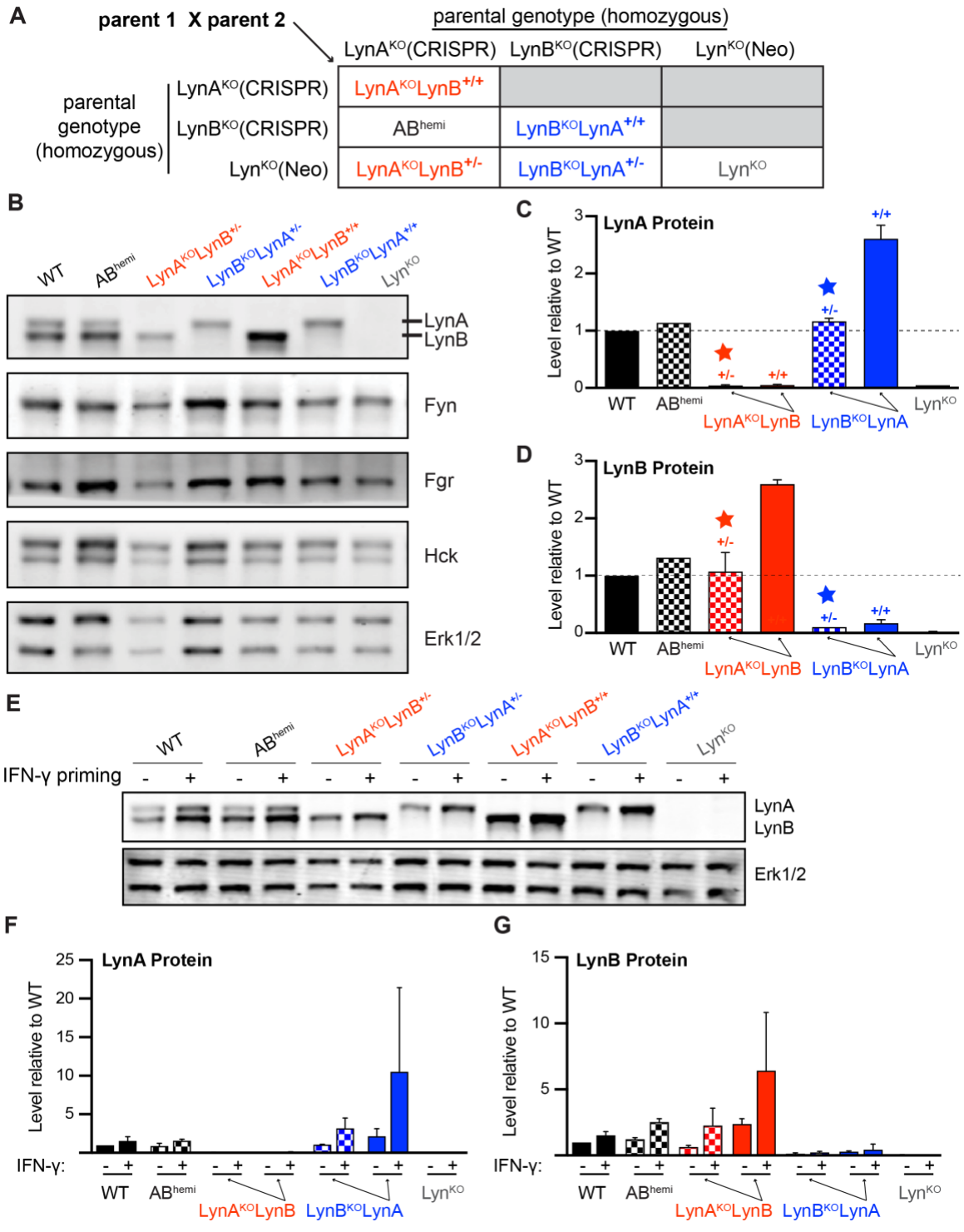

Figure 4.5. SFK expression and regulation is normal in LynA^{KO} and LynB^{KO} mice. **(A)** Breeding scheme used to generate LynA^{KO} and LynB^{KO} mice and AB^{hemi} mice. **(B)** Immunoblot showing Lyn, Fyn, Fgr and Hck expression in BMDMs from WT, LynA^{KO}, LynB^{KO} and AB^{hemi} and Lyn^{KO} mice. Erk1/2 is shown as a loading control. **(C)**

Quantification of LynA and **(D)** LynB protein levels in BMDMs derived from the breeding scheme in **(A)**. Stars represent hemizygous mice for the expressed isoform of Lyn, which will be used for all future experiment. Results from n=2 immunoblots. **(E)** Representative immunoblot of untreated and IFN-γ-treated BMDMs from CRISPR knockout mice. **(F)** Quantification of LynA protein and **(G)** LynB protein in IFN-γ-treated BMDMs, illustrating IFN-γ-dependent Lyn upregulation.

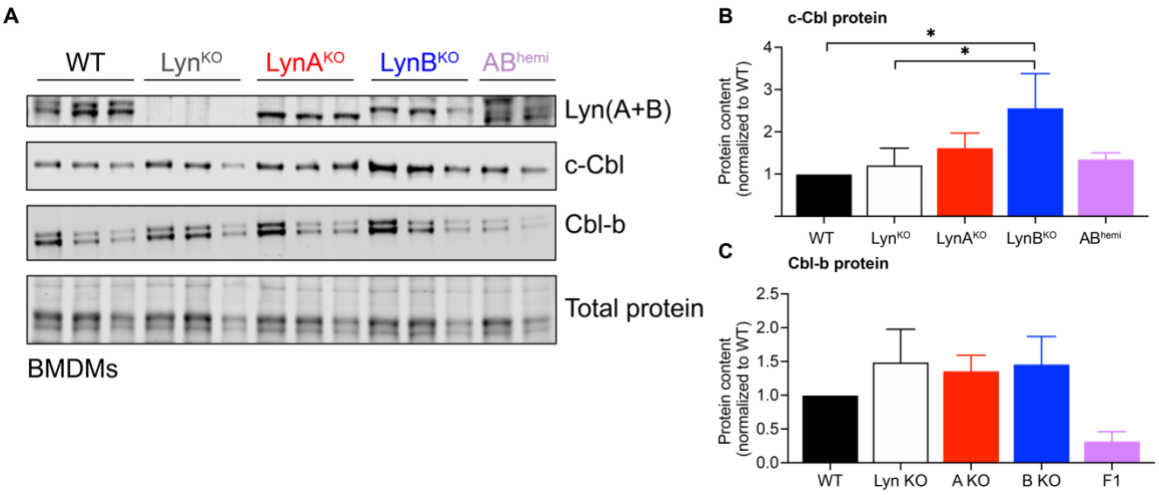

Figure 4.6. LynA and c-Cbl are co-regulated. (A) Immunoblot of LynA, LynB, c-Cbl and Cbl-b in BMDMs from WT, LynA^{KO}, LynB^{KO} and AB^{hemi} and Lyn^{KO} mice. Total protein is shown as a loading control. **(B)** Quantification of c-Cbl and **(D)** Cbl-b protein levels in BMDMs relative to WT mice.

4.2.2 LynB deletion predisposes mice to develop splenomegaly

Lyn has a prominent role in suppressing hematopoiesis and cell proliferation [151]. Lyn^{KO} mice develop a myeloproliferative syndrome characterized by an increase in spleen mass (splenomegaly) driven by increased numbers of neutrophils, eosinophils and monocytes. This phenotype is myeloid-cell-intrinsic, as depletion of B and T cells in Lyn^{KO} mice does not affect the progression of splenomegaly [151, 152]. The development of splenomegaly in Lyn^{KO} mice is age-dependent and generally occurs between 6-8 months of age [117, 118, 151]. Despite the intriguing evidence that LynA and LynB may differentially regulate cancer-cell migration [150] and FcεR-ITAM-pathway signaling [149], the contributions of LynA and LynB in driving splenomegaly is unknown.

We saw no differences in spleen mass at 3 months in any of the genotypes (**Figure 4.7A**). Although we detected a small decrease in body mass of 3-month-old male and female $LynB^{KO}$ mice (**Figure 4.7B**), there was no corresponding increase in the size of the spleens in comparison to body mass (**Figure 4.7C**). We next compared the spleen mass of 8-month-old knockout mice. We discovered that spleen mass was 2.6-fold and 2.1-fold significantly increased in Lyn^{KO} and $LynB^{KO}$ mice respectively (**Figure 4.7C, D**). Furthermore, the body mass of Lyn^{KO} and $LynB^{KO}$ mice was significantly decreased compared to WT mice (17% and 18% lower, respectively) (**Figure 4.7E**)**.** Correspondingly, the splenic mass in relation to body mass (**Figure 4.7F**) was significantly increased in Lyn^{KO} (3.1-fold) and $LynB^{KO}$ (2.6-fold). AB^{hemi} mice ($LynA^{-/-}$ $LynB^{+/+}$ x $LynA^{+/+}LynB^{-/-}$) had similar spleen and body mass to WT mice, demonstrating that the CRISPR-induced mutations preserve normal LynA and LynB function. When we characterized the incidence of mild splenomegaly (0.45%-0.75% body mass) and severe splenomegaly (>0.75% of body mass) we found that both $LynB^{KO}$ and Lyn^{KO} mice had a significant increase in the rate of splenomegaly, suggesting that LynB negatively regulates immune function by suppressing immune cell proliferation (**Figure 4.7G**).

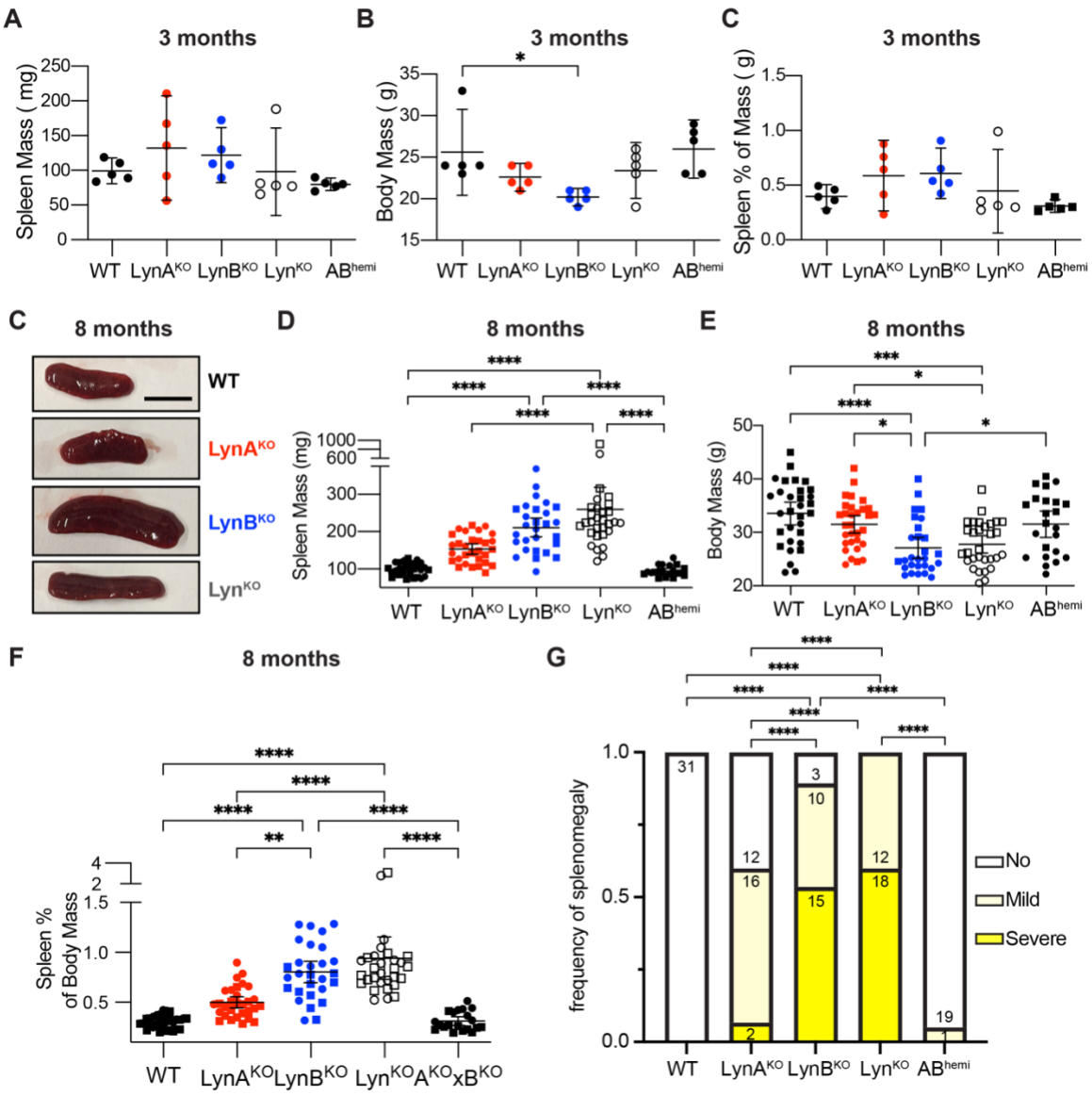

Figure 4.7. Loss of LynB predisposes aged mice to splenomegaly. (A) Total spleen mass, **(B)** Total body mass, and **(C)** Spleen mass as a percentage of body mass of 3-month-old mice. (**A**) Representative spleens based on mass quantification of 8-month-old mice. Scale bar = 1 cm. **(D)** Total spleen mass, **(E)** Total body mass, and **(F)** Spleen mass as a percentage of body mass of 8-month-old mice Squares represent male mice, circles represent female mice. The significance (Sig.) from one-way ANOVA with Tukey's multiple comparison test (-Tukey) are as follows: **** P<0.0001, *** P<0.0002, ** P<0.0021,* P<0.0332. Error bars represent mean with 95% confidence interval. **(G)** Frequency of spleens with no, mild and severe cases of splenomegaly in 8-month-old WT, LynA^{KO}, LynB^{KO}, Lyn^{KO}, and AB^{hemi} mice. Significance for raw contingency data was assessed using two-sided Fisher's exact test (GraphPad Prism) from binarized data reflecting animal numbers with no or mild vs. severe splenomegaly without correction for multiple comparisons. With Bonferroni Correction, significance is preserved for pairwise comparisons with the exception of [LynB^{KO} vs. F1] and [Lyn^{KO} vs. F1]

4.2.3 LynB^{KO} mice have selective myeloid expansion and B cell activation

We proceeded to further characterize the spleens of 8-month-old knockout mice. Lyn is known to regulate the development of monocytes and previous research has shown that Lyn^{KO} mice have increased numbers of total monocytes, and a skewing of monocytes towards Ly6C^{-} patrolling monocytes [117, 151, 255]. Accordingly, we found that 8-month-old Lyn^{KO} mice had increased numbers of spleen monocytes (**Figure 4.8A**), both classical and patrolling. LynB^{KO} mice also had an increase in patrolling monocytes compared to WT mice, although less than total Lyn^{KO} mice. Interestingly, we discovered that LynB^{KO} mice had a selective expansion of mature, CD64^{+} CD11b^{-} MerTK^{+} macrophages (**Figure 4.8B**). This population has not previously been studied in Lyn^{KO} mice, and together these results suggest that LynB normally exerts a negative role in the development of monocytes and macrophages.

Lyn has been shown to negatively regulate dendritic cell development in cultured bone-marrow cells treated with GM-CSF, and via selective deletion of Lyn using Cre-recombinase under the control of the CD11c promoter [117, 256]. We found no differences in the numbers of spleen dendritic cells in WT and global Lyn^{KO} mice, however we did discover that both LynA^{KO} and LynB^{KO} had increased numbers of conventional DC (cDC) but that this increase was heavily skewed towards cDC2s, especially for LynB^{KO} mice (**Figure 4.8C**). cDC2 are important regulators of CD4 T cell activation [257, 258]. The expansion of cDC2s in LynB^{KO} mice fits with an increase in the numbers of CD4+ T cells in LynB^{KO} and LynA^{KO} mice that we also observed (**Figure 4.10A-D**). We further discovered the LynB^{KO} mice had increased numbers of plasmacytoid DC3 (pDC) (**Figure 4.8D**). pDC are potent cytokine secretors and have been implicated in autoimmune disease development [259] and Lyn has also been shown to regulate pDC function [123].

Although LynB deletion resulted in an increase in monocytes, we did not detect any increase in the numbers of granulocytes (neutrophils and eosinophils) in the spleens of LynB^{KO} mice (**Figure 4.8E**). Thus, LynB deletion appears to have selective effects on myeloid activation and maturation.

Previous research has shown that Lyn^{KO} mice have a substantial defect in B-cell development, leading to a lack of mature splenic B cells. We examined 8-month-old spleens by hematoxylin and eosin (H&E) staining to examine cellular distribution and organization to investigate whether Lyn expression affects splenic architecture and B-cell follicle organization. We observed that LynA^{KO} mice had increased numbers and larger follicles than WT mice, whereas LynB^{KO} mice had smaller and less organized B cell follicles (**Figure 4.9A**). Lyn^{KO} mice had very few observable follicles, likely due to the defect in B-cell maturation. We further examined B-cell populations in the spleen by flow cytometry and found that LynA expression (LynB^{KO} mice) restores the number of mature B cells to WT levels, but that expression of LynB (LynA^{KO}) leads to increased numbers of B cells compared to WT mice (**Figure 4.9B**). We further probed B-cell subsets in older mice and discovered that both LynA^{KO} and LynB^{KO} had higher total numbers of cells with a GL7+ CD38- germinal center (GC) phenotype (**Figure 4.9C**). The fraction of B220+ B cells with GC phenotype was elevated in both LynA^{KO} and LynB^{KO} mice, but higher in LynB^{KO} mice (**Figure 4.9D**). Furthermore, the CD69 and MHCII mean fluorescence index (MFI) of B220+ B cells was significantly elevated in both LynB^{KO} and Lyn^{KO} (**Figure 4.9E,F)** and GC B cells had higher CD69 expression in LynB-deficient mice (**Figure 4.9G**). These data suggest that loss of LynB induces B cell activation, without a corresponding defect in B cell development and maturation, although whether these changes are B-cell intrinsic or related to changes to myeloid and dendritic cells remains to be investigated.

In summary, loss of either LynA or LynB induces unique changes in spleen immune cells. LynB^{KO} mice have increased numbers of mature macrophages, patrolling monocytes, conventional Type 2, and plasmacytoid dendritic cells. LynB^{KO} mice also have normal numbers of B cells compared to WT mice, but increased numbers of GC and activated B cells. In contrast, LynA^{KO} mice have increased numbers of B cells, and normal numbers of myeloid cells.

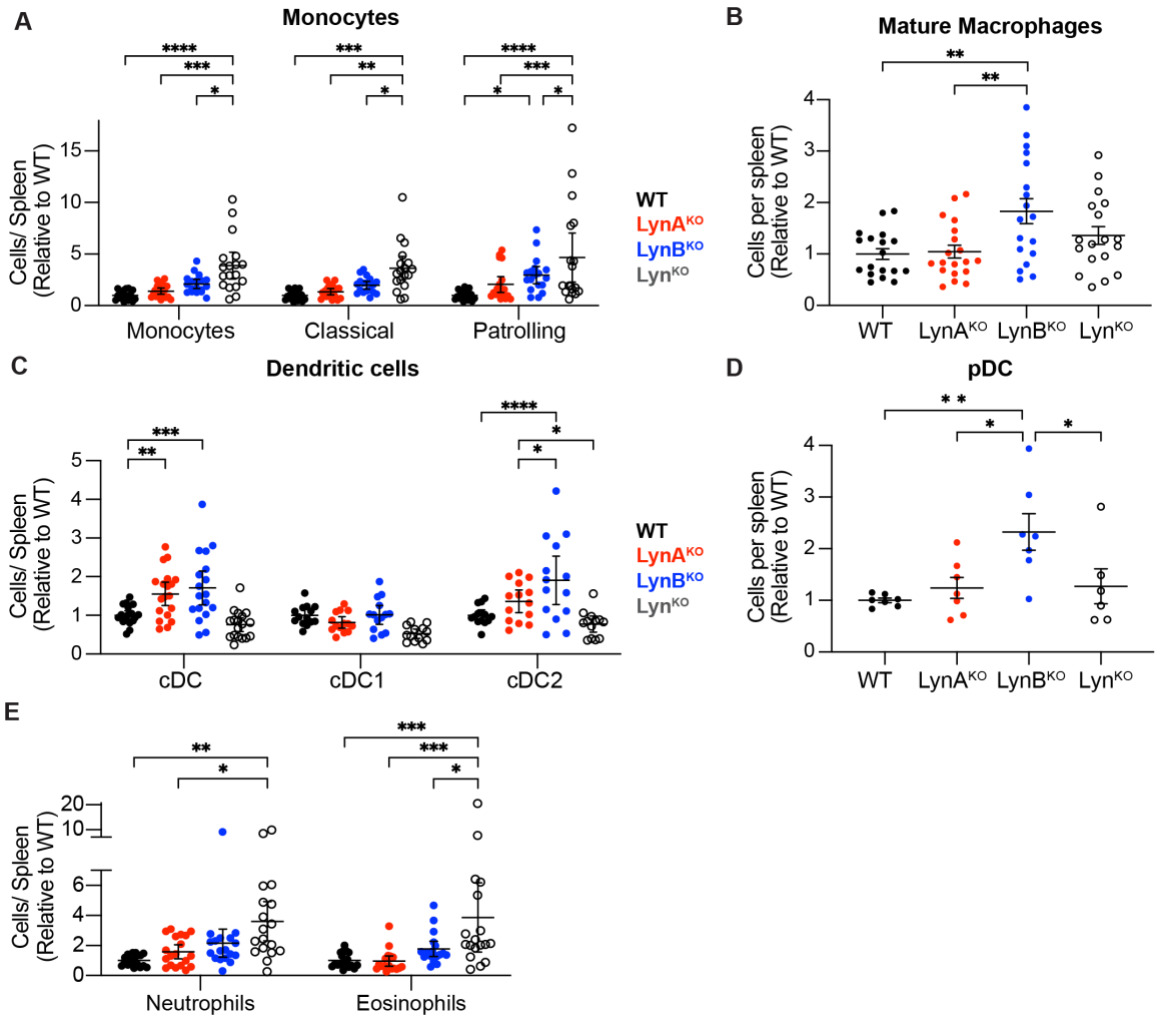

Figure 4.8. LynB^{KO} mice have selective myeloid expansion. (A) Total monocytes, classical monocytes and patrolling monocytes, **(B)** Total CD64+ MerTK+ mature macrophages, **(C)** Total conventional dendritic cells (cDC), Type 1 cDC (cDC1) and Type 2 cDC (cDC2), **(D)** total plasmacytoid dendritic cells (pDC) **(E)** and granulocytes per spleen of 8-month-old mice, relative to WT mice. The significance (Sig.) from one-way ANOVA with Tukey's multiple comparison test (-Tukey) are as follows: **** P<0.0001, *** P<0.0002, ** P<0.0021,* P<0.0332. Error bars represent mean with 95% confidence interval.

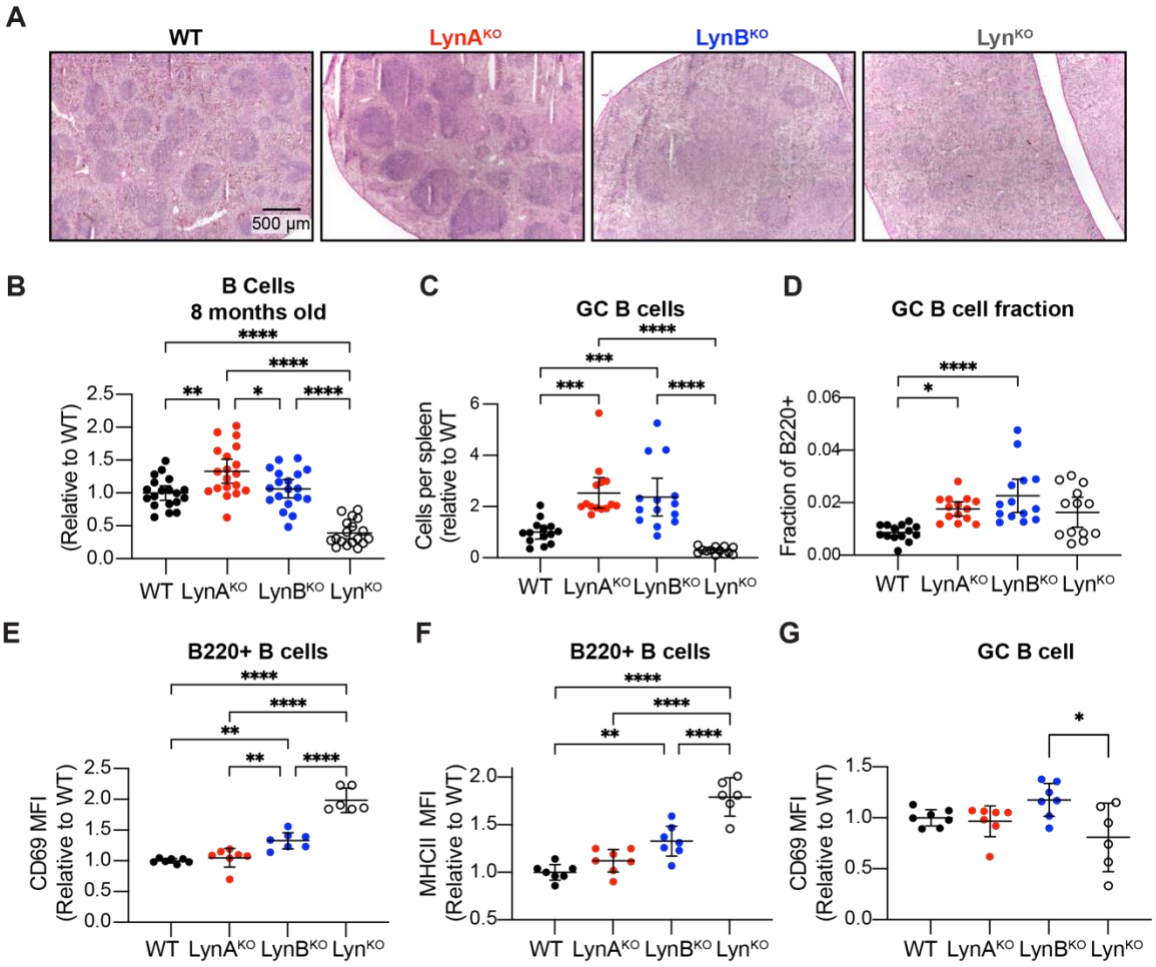

Figure 4.9. LynB^{KO} mice have activated B cells. (A) H&E-stained splenic section from 8-month-old mice. **(B)** Total B cells and **(C)** Total germinal center (GC) B cells per spleen of 8-month-old mice, relative to WT mice. **(D)** Fraction of B cells with a GC phenotypes **(E)** CD69 MFI and **(F)** MHCII MFI in B cells compared to WT mice. **(G)** CD69 MFI in GC B cells compared wot WT mice. The significance (Sig.) from one-way ANOVA with Tukey's multiple comparison test (-Tukey) are as follows: **** P<0.0001, *** P<0.0002, ** P<0.0021,* P<0.0332. Error bars represent mean with 95% confidence interval.

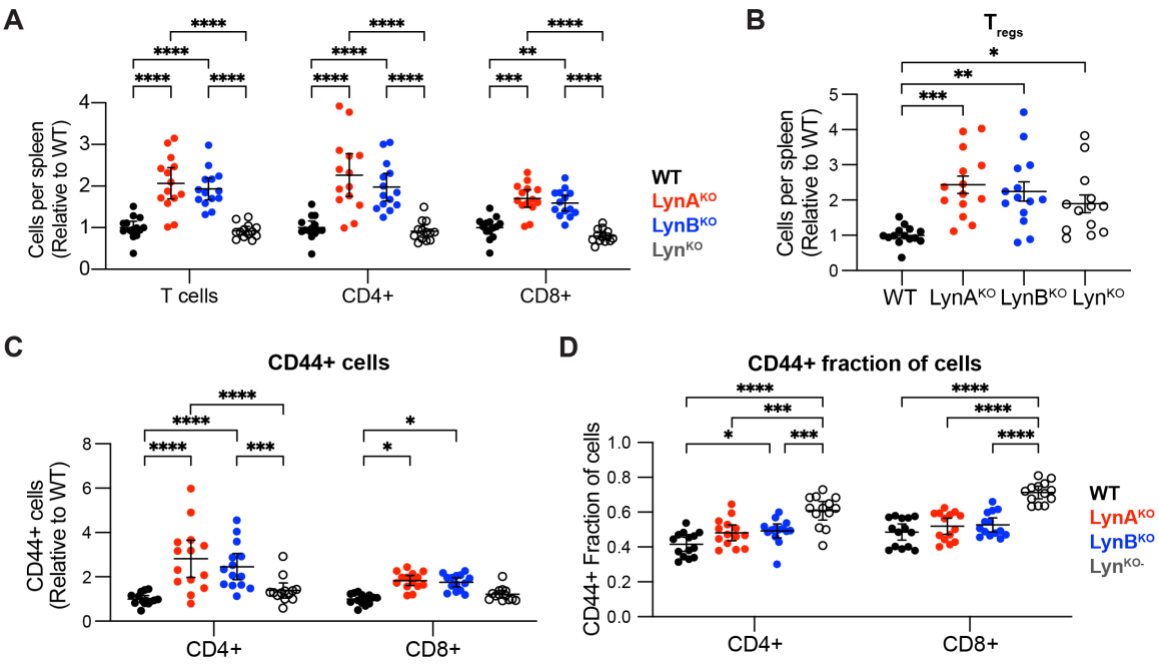

Figure 4.10. Lyn deletion affects T cell maturation and activation. **(A)** Total T cells, CD4+ and CD8+ T cells **(B)** Tregs, **(C)** and CD44+ CD4+ and CD8+ T cells per spleen of 8-month-old mice, relative to WT mice. **(D)** Fraction of T cells that are CD44+. The significance (Sig.) from one-way ANOVA with Tukey's multiple comparison test (-Tukey) are as follows: **** P<0.0001, *** P<0.0002, ** P<0.0021,* P<0.0332. Error bars represent mean with 95% confidence interval

4.2.4 Deletion of LynB predisposes mice to autoantibody production and glomerulonephritis

Lyn^{KO} mice develop an autoimmune disease similar to human SLE. Lyn^{KO} plasma cells produce anti-nuclear antibodies (ANAs) that are deposited in the kidneys, causing immune-cell infiltration, activation, and the development of glomerulonephritis [111, 112, 132].

We investigated whether they also developed symptoms of systemic autoimmunity. We tested serum from 8-month-old WT, $LynA^{KO}$, $LynB^{KO}$ and total Lyn^{KO} mice for the presence of ANAs by indirect immunofluorescence using Human Epithelial (HEp)-2 substrate slides [260], modified for the detection of mouse anti-nuclear IgG. We found that the preponderance of $LynB^{KO}$ (10/12 mice) and Lyn^{KO} (12/12) mice had high levels of ANAs (**Figure 4.11A, B)**, whereas $LynA^{KO}$ and WT mice had rare instances of nuclear IgG staining. Because ANAs can be detected in healthy human populations in the absence of any autoimmune disease [261], we examined H&E-stained kidneys from 8-month-old WT, $LynA^{KO}$, $LynB^{KO}$ and total Lyn^{KO} mice to detect immune-cell infiltration and fibrosis. A majority of kidneys from Lyn^{KO} (5/6) and $LynB^{KO}$ (6/7) mice had evidence of immune infiltration, expanded glomeruli and tubular inflammation (**Figure 4.11C, D**), suggesting that the increased levels of ANA in the $LynB^{KO}$ mice do contribute to the development of autoimmune disease.

Finally, we examined the total incidence of abnormalities (splenomegaly, ANA, and nephritis) in male and female knockout mice (**Figure 4.12A)**. A majority of male and female $LynB^{KO}$ and Lyn^{KO} mice had at least one severe finding, whereas only a small subset of WT (1/34 mice) and $LynA^{KO}$ (9/36) mice had any severe findings. These data further suggest that LynB, and not LynA, has a previously undescribed role in limiting immune cell activation and autoimmune disease.

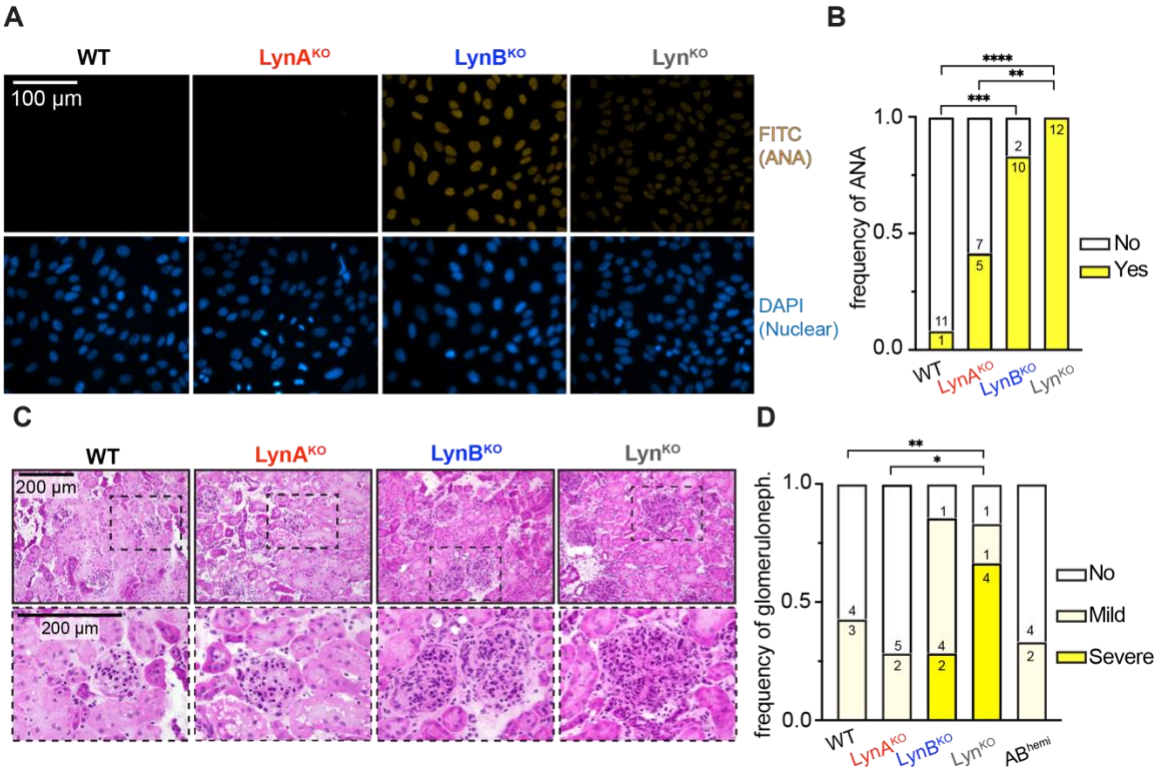

Figure 4.11. Loss of LynB induces the development of anti-nuclear antibodies and glomerulonephritis. (A) Sera from 8-month-old WT, LynA^{KO}, LynB^{KO} and Lyn^{KO} mice were used for detection of IgG ANAs on fixed Hep-2 ANA slides and imaged. Pictures are representative of 3 experiments. **(B)** Frequency of sera with ANA staining. Significance for raw contingency data was assessed using two-sided Fisher's exact test (GraphPad Prism) from binarized data reflecting animal numbers with no vs. severe ANA without correction for multiple comparisons. With Bonferroni Correction, significance is preserved in pairwise comparisons with the exception of [LynA^{KO} vs. Lyn^{KO}]. **(C)** Kidney sections from 8-month-old WT, LynA^{KO}, LynB^{KO} and Lyn^{KO} mice were analyzed for signs of nephritis (H&E staining). Dashed boxes show areas enlarged in the bottom row. **(D)** Frequency of kidneys with no, mild and severe cases of glomerulornephritis. Significance for raw contingency data was assessed using two-sided Fisher's exact test (GraphPad Prism) from binarized data reflecting animal numbers with no or mild vs. severe glomerulonephritis without correction for multiple comparisons. With Bonferroni Correction, significance is preserved in [WT vs. Lyn^{KO}] but not [LynA^{KO} vs. Lyn^{KO}].

A

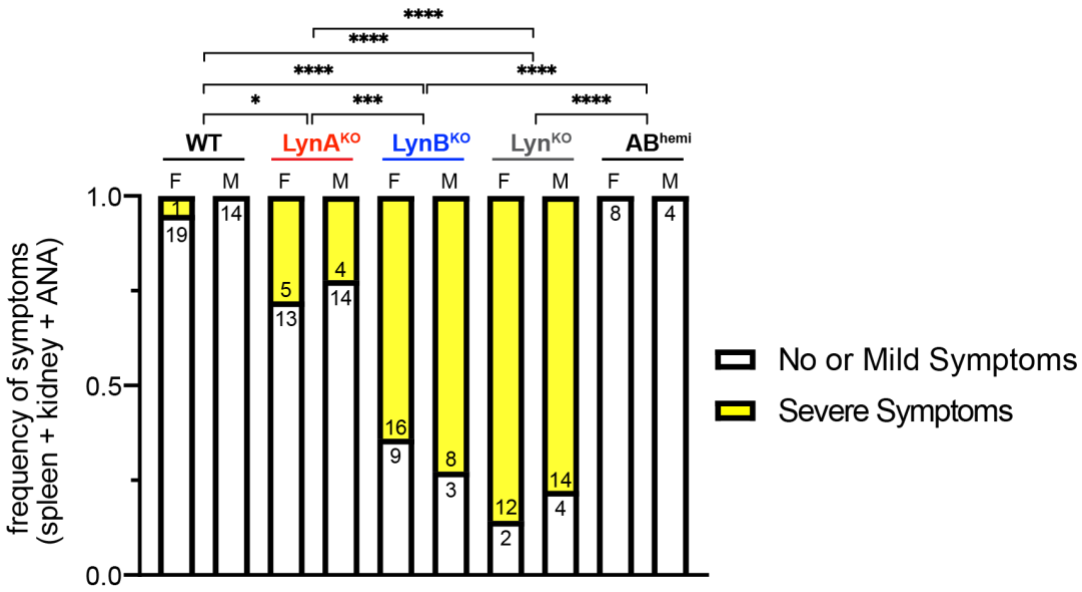

Figure 4.12. Loss of LynB induces multiple symptoms of autoimmune disease. (A) Frequency of symptoms (ANA, splenomegaly or nephritis) in 8-month old male and female mice. Significance for raw contingency data was assessed using two-sided Fisher's exact test (GraphPad Prism) from binarized data reflecting animal numbers with no or mild vs. severe symptoms without correction for multiple comparisons. With Bonferroni Correction, significance is preserved in pairwise comparisons with the exception of [WT vs. LynA^{KO}]. There were no significant differences in overall symptom frequency between males and females of each genotype

4.2.5 LynB^{KO} and Lyn^{KO} mice express higher levels of TLR4 and increased response to TLR ligation

Activation of TLR by microbial ligands and signaling through MyD88 has been shown to induce the development of autoimmune disease in Lyn^{KO} mice [117, 120, 183]. MyD88 associates with multiple TLRs upon receptor ligation and links TLRs to cellular activation by recruiting downstream kinases and ubiquitin ligases that facilitate activation of NF-κB and other transcription factors. We probed whether immune cells in single-isoform knockout mice had changes in TLR protein expression. We examined TLR expression on immune cells in the blood of 8-month-old mice. Both LynB^{KO} and Lyn^{KO} mice had elevated TLR4 expression on multiple cell types, including neutrophils and patrolling monocytes (**Figure 4.13C,D**). Lyn has been shown to negatively regulate TLR4 signaling in dendritic cells [117, 119] but Lyn's role in TLR4 signaling in monocytes and granulocytes has not been studied. Because we saw increased patrolling monocytes and dendritic cells in LynB^{KO} and Lyn^{KO} mice, dysregulated-TLR4 expression and signaling could be one driver of autoimmunity in these mice. LynA^{KO}, LynB^{KO} and Lyn^{KO} mice had also have increased protein levels of TLR2 on patrolling monocytes (**Figure 4.13A**) but only Lyn^{KO} mice have increased TLR2 expression on classical monocytes. The pattern of TLR9 expression (**Figure 4.13B**) varied depending on the cell type: TLR9 expression was decreased on LynA^{KO}, LynB^{KO} and Lyn^{KO} patrolling monocytes, but only decreased on LynA^{KO} and Lyn^{KO} B cells

To further probe whether LynB-deficient mice had increased responsiveness to TLR ligation, we treated splenocytes *ex vivo* with LPS or CpG-oligonucleotides to induce TLR4 or TLR9 signaling, respectively. We then used flow cytometry to examine the cells that produced TNFα upon stimulation. As expected, a significant number of pDC were TNFα^{+} in response to either LPS or CpG treatment (**Figure 4.13E**), whereas other cell types were more variable (**Figure 4.13F**). We discovered that a higher percentage of pDC in LynB^{KO} were TNFα^{+} in response to CpG (55% in LynB^{KO}, compared to 38% in WT mice) (**Figure 4.13G**), while a higher percentage of patrolling monocytes in LynB^{KO} were TNFα+ in response to CpG and LPS (**Figure 4.13G**). pDC are potent cytokine secretors and can drive autoimmune disease [259]. LynB^{KO} mice in particular have increased numbers of spleen pDC. Increased TLR responsiveness and numbers of pDC may be one element that drives autoimmune disease in LynB^{KO} mice. The pattern of

TNFα responsiveness was variable in other cell types (**Figure 4.14A-D**), but in general Lyn^{KO} and $LynB^{KO}$ cells were more responsive to TLR4 and TLR9 stimulation. These data further confirm that LynB, and not LynA, negatively regulates TLR signaling and may prevent TLR-driven autoimmune disease.

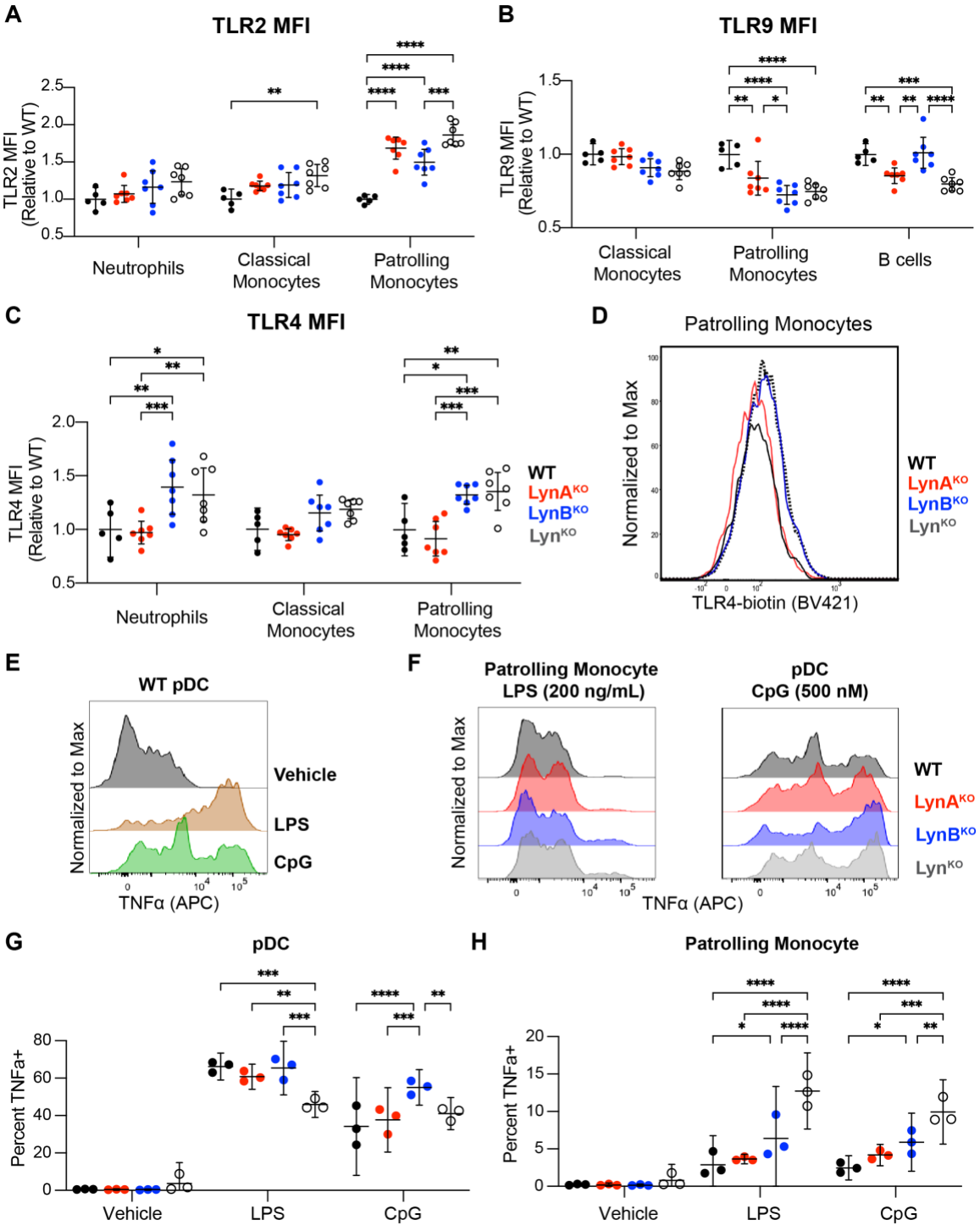

Figure 4.13. LynB^{KO} mice have higher TLR4 expression and increased response to TLR stimulation (A) Relative MFI of TLR2, **(B)** TLR9, **(C)** and TLR4 in circulating immune cells from 8-month-old WT, LynA^{KO}, LynB^{KO}, and Lyn^{KO} mice. **(D)** Representative histogram of TLR4 expression on patrolling monocytes. **(E)** Representative histogram of WT pDC treated with vehicle, LPS and CpG. **(F)**

Representative histograms of WT, LynA^{KO}, LynB^{KO}, and Lyn^{KO} mice pDC treated with CpG and patrolling monocyte treated with LPS**. (G)** Quantification of TNFα+ pDC and patrolling monocytes treated with CpG and LPS. The significance (Sig.) from two-way ANOVA with Tukey's multiple comparison test (-Tukey) are as follows: **** P<0.0001, *** P<0.0002, ** P<0.0021,* P<0.0332. Error bars represent mean with 95%

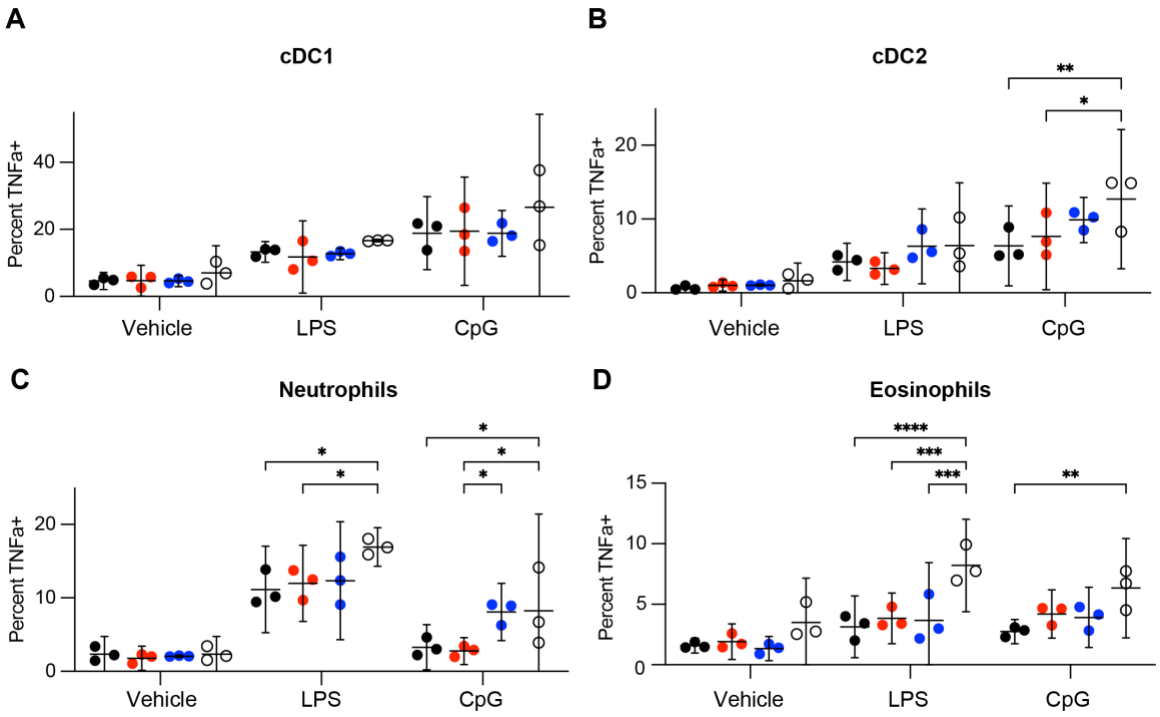

Figure 4.14. LynB^{KO} splenocytes have increased responsiveness to TLR stimulation (A) Quantification of TNFα+ cDC1, **(B)** cDC2, **(C)** neutrophils and **(D)** eosinophils treated with CpG and LPS. The significance (Sig.) from two-way ANOVA with Tukey's multiple comparison test (-Tukey) are as follows: **** P<0.0001, *** P<0.0002, ** P<0.0021,* P<0.0332. Error bars represent mean with 95%

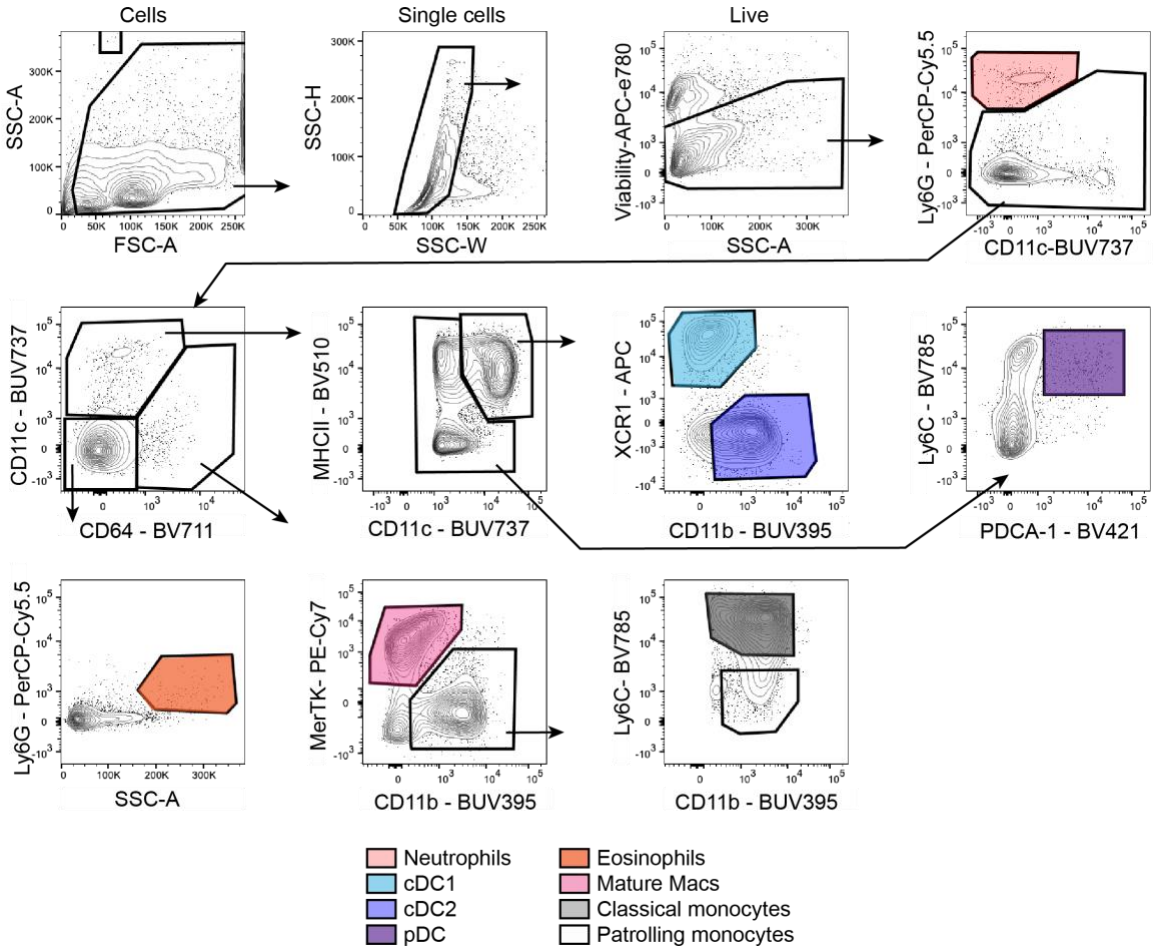

Figure 4.15. Gating scheme used to identify myeloid cell populations in WT and knockout spleens

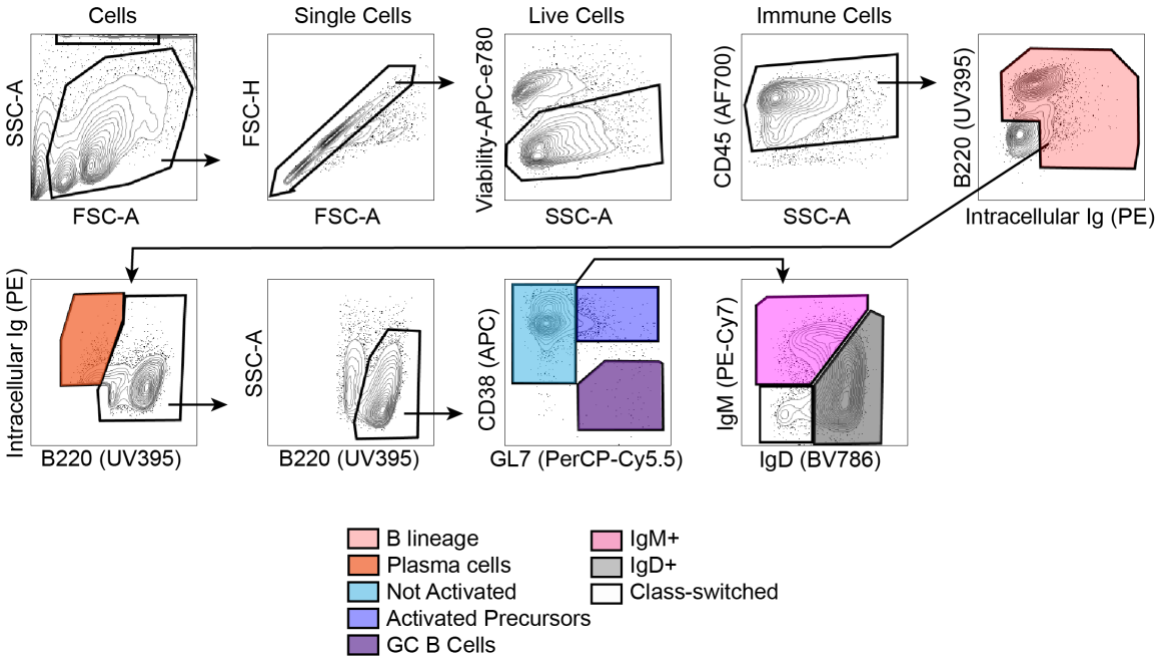

Figure 4.16. Gating scheme used to identify B cell populations in WT and knockout spleens

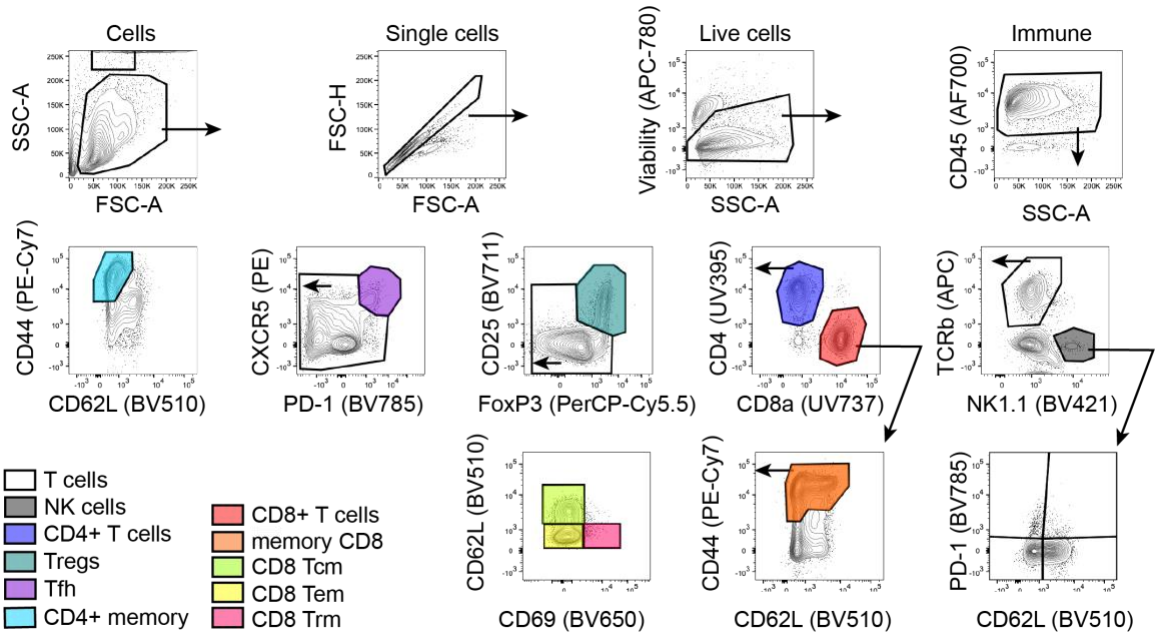

Figure 4.17. Gating scheme used to identify T cell populations in WT and knockout spleens

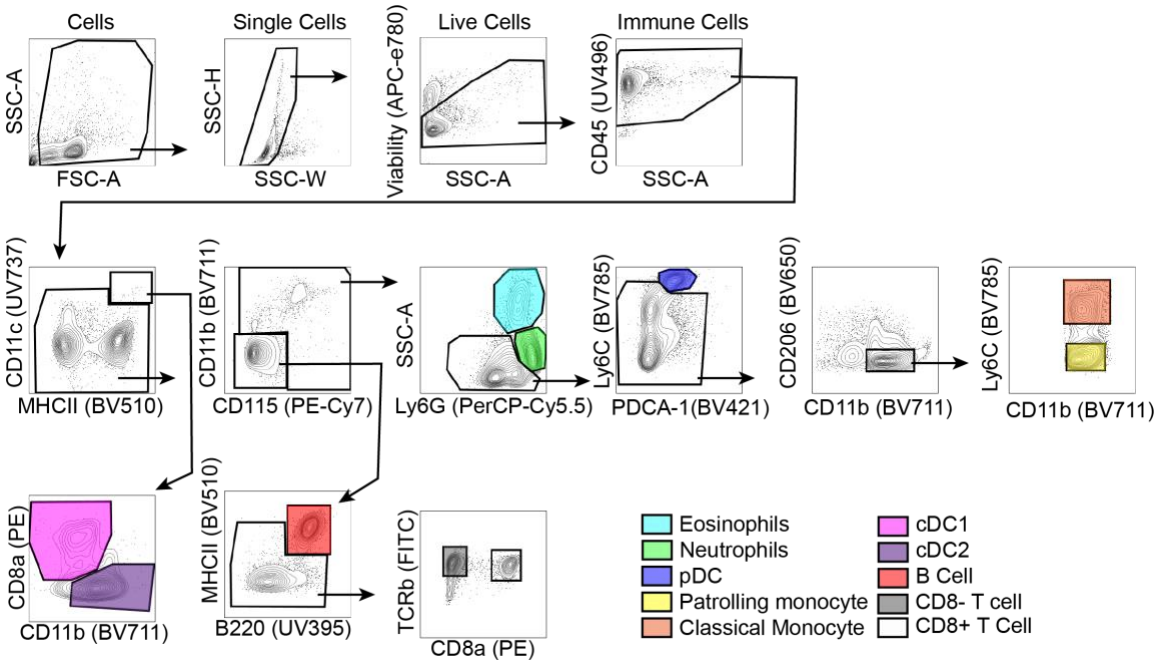

Figure 4.18. Gating scheme used to identify cell populations in *ex vivo* TLR-treated splenocytes

4.3 Discussion

In this chapter we report that the protein splice-variants of *lyn*, LynA and LynB, have different roles in preventing the development of autoimmune disease. Until now there have been no reliable *in vivo* models to independently study LynA and LynB signaling. Using CRISPR-Cas9 gene editing we created two novel knockout models, $LynA^{KO}$ and $LynB^{KO}$ mice. To our knowledge, this is the first use of CRISPR to create global knockout models to alter expression of splice-variants from the same gene. Our novel mouse strains retain the regulatory gene elements of the *lyn* gene and are expressed at wild-type levels in immune cells.

Previous research has demonstrated that Lyn has prominent roles in both activating and dampening immunoreceptor signaling. Lyn is activated following BCR and FcR signaling and can phosphorylate secondary kinases such as Syk, or second-messenger generators such as PI3K and PLCγ1/2. However, Lyn can also recruit and activate phosphatases, such as SHP-1 and SHIP-1, that dephosphorylate tyrosines and lipids, dampening immunoreceptor signaling. Lyn^{KO} mice develop an autoimmune disease with symptoms similar to human lupus, including the production of anti-nuclear antibodies which cause glomerulonephritis. Previous research from our groups and others has demonstrated that LynA and LynB are differentially regulated in macrophages [22, 27] as well as Mast and B cells [42, 148]. Other work has suggested that LynA and LynB have the propensity to activate different signaling cascades [149, 150]. These studies have suggested that LynB associates with and phosphorylates inhibitory proteins such as SHIP-1, while LynA more readily activates signaling pathways that may produce an immune response. Using these novel mice strains, we show that LynA and LynB have unique roles and that LynB is required for preventing autoimmunity.

We discovered that both Lyn^{KO} and $LynB^{KO}$ mice had increased presence of ANAs, more pronounced glomerulonephritis, and increased development of splenomegaly compared to WT and $LynA^{KO}$ mice. Knocking out either LynA or LynB resulted in pronounced changes to the immune system. While Lyn^{KO} mice have a defect in B cell development, expression of either isoform restored the numbers of B cells. However, while mature B cells in Lyn^{KO} mice were more likely to become activated plasma cells, $LynB^{KO}$ mice had both increased plasma cells, as well as GC B cells. Both $LynA^{KO}$ and $LynB^{KO}$ mice had

more CD4 and CD8 T cells in the spleen, which might be due to the fact that LynA^{KO} and LynB^{KO} mice had more cDCs than WT mice. Interestingly, while previous research has shown that Lyn negatively regulates the development of myeloid cells such as neutrophils, eosinophils and monocytes, we did not detect an increase in those cell types in either LynA^{KO} or LynB^{KO} mice, with the exception that LynB^{KO} mice had more patrolling monocytes than WT mice. We did however detect an increased population of pDCs in LynB^{KO} mice, and pDCs are known to contribute to autoimmune disease [259].

Because TLR signaling can drive splenomegaly and autoimmune disease in the absence of Lyn, we investigated TLR expression in LynA^{KO} and LynB^{KO} mice and discovered increased expression of TLR4 in multiple circulating immune cells in LynB^{KO} and Lyn^{KO} mice. Previous research has not detected different levels of TLR4 expression on immune cells in Lyn^{KO} mice [256], although these reports have focused on different immune cells than we have, and should be investigated more extensively. Lyn is known to negatively regulate TLR4 signaling [119, 124, 262]. It is possible that the increased surface expression of TLR4 is due to altered inflammatory environments in the LynB^{KO} and Lyn^{KO} mice that promote splenomegaly and autoimmune disease. We further discovered the LynB^{KO} and Lyn^{KO} mice had enhance responses to TLR4 and TLR9 stimulation, particularly in monocytes and pDCs, suggesting that increased expression of TLR4 and altered TLR signaling drive autoimmunity in LynB-deficient mice. Because we saw an increase both the numbers of spleen pDC and the pDC response to TLR stimulation in LynB^{KO} mice, this suggests LynB plays a unique role in negatively regulating pDC function and pDC role in autoimmunity.

In summary, we used CRISPR-Cas9 to constrain splicing of Lyn, developing the first models to independently study LynA and LynB signaling *in vivo.* We demonstrate that LynB restricts the development of autoimmune disease and negatively regulates TLR signaling. These mice strains will be useful tools to investigate the mechanisms by which LynB uniquely prevents autoimmunity and will deepen our understanding of the pathways and proteins involved in human autoimmune disease.

CHAPTER 5: Discussion

5.1 Future Directions

My thesis work has elucidated unique regulatory mechanisms and functions of the two proteins, LynA and LynB, formed by alternative splicing of the *lyn* transcript. I have shown that phosphorylation of Y32, in the unique region of LynA, induces interaction with a ubiquitin ligase, c-Cbl, causing LynA to be rapidly and specifically poly-ubiquitinated and degraded upon activation. I have shown that selective expression of cbl-family members in different immune cells controls the rate of LynA degradation and subsequent downstream signaling responses. In macrophages, high expression of c-Cbl causes LynA to be degraded rapidly and prevents signal cascade propagation. However, in mast cells, low c-Cbl and high Cbl-b expression causes LynA to be degraded slowly, leading to elevated signaling. I have also shown that phosphorylation of Y32 requires SFK signaling and is likely a site of trans-phosphorylation by the SFKs.

Previous research suggests that LynA and LynB have a propensity to activate different signaling cascades. In mast cells, LynA was better able to increase intracellular free calcium upon FcεR ligation, whereas LynB associated with, and phosphorylated, inhibitory proteins such as SHIP-1 [149]. However, studying the roles for LynA and LynB in immune cells had been hampered by a lack of animal models in which LynA and LynB are selectively knocked out. In this dissertation, I have described our work creating novel $LynA^{KO}$ and $LynB^{KO}$ mice using CRISPR/Cas9 gene editing to constrain alternative splicing. I discovered that loss of LynB particularly prevented mice from developing splenomegaly and symptoms of autoimmune disease, including the production of anti-nuclear antibodies and the development of glomerulonephritis. Furthermore, deletion of either LynA or LynB resulted in altered immune populations. Both $LynA^{KO}$ and $LynB^{KO}$ mice had elevated numbers of T and B cells in their spleens, while $LynB^{KO}$ mice had increased numbers of germinal center B cells, cDC2 and plasmacytoid dendritic cells. Furthermore, a higher percentage of $LynB^{KO}$ pDC and monocytes were TNFα+ when treated with TLR4 and TLR9 agonists. These results point to differential roles for LynA and LynB in regulating immune cell proliferation and activation, particularly for LynB in negatively regulating the development of autoimmune diseases.

My thesis work demonstrates unique features of LynA and LynB regulation and signaling that are important for immune function. By demonstrating that c-Cbl controls the protein levels and signaling capacity of LynA, I have demonstrated that differential expression of cbl-family members regulates immune function, which has implications for strategies that attempt to alter immunoreceptor signaling, such as chimeric-antigen receptor (CAR)-T cells. By demonstrating that mast cells express low levels of c-Cbl and high levels of LynA which result in enhanced signaling responses upon SFK activation, my work suggests that therapies that increase c-Cbl expression in mast cells or enhance SFK poly-ubiquitination and degradation may help resolve allergic diseases.

I have further demonstrated that LynB has a strong negative-regulatory role in immune-cell activation. Understanding how LynB mediates this unique function will aid our understanding of the cells and pathways involved in autoimmunity. One of the major adverse effects of current therapeutics for autoimmune-related diseases is immune suppression. $LynA^{KO}$ (LynB-expressing) mice do not develop autoimmunity but are rescued from the many immune defects present in Lyn^{KO} mice. Understanding how LynB prevents autoimmunity and rescues these defects will improve our ability to develop therapeutics that selectively modulate signaling thresholds in immune cells to prevent aberrant activation but retain pathogen-clearing abilities.

Despite these advances, our understanding of LynA and LynB function remains incomplete. In the following sections I will discuss several directions for research dissecting the roles for LynA and LynB in different aspects of immunity.

5.1.1 LynA and LynB signaling and interactome

The one previous attempt to characterize the contribution of LynA and LynB to immunoreceptor signaling relied on lentiviral expression of LynA or LynB in Lyn^{KO} cells [149]. These studies revealed novel roles for LynA and LynB in immunoreceptor regulation. However, a lack of *in vivo* models to study LynA and LynB independentaly has prevented studying signaling pathways in cells that are resistant to lentiviral-Lyn expression, including macrophages [22]. However, the novel $LynA^{KO}$ and $LynB^{KO}$ mice, described in this dissertation, are reliable tools to study the precise signaling pathways and protein-protein interactions of each isoform.

I have shown that phosphorylation of LynA at Y32 (absent in LynB) uniquely recruits the ubiquitin ligase c-Cbl to poly-ubiquitinate LynA and leads to the rapid degradation of LynA in macrophages [27]. Although these studies (and others) suggest unique protein-protein interactions that differentiate LynA and LynB, one of the major unanswered questions of this work was comprehensive understanding of those interactions and how those interactions modulate immunoreceptor signaling and cell activation. We have now bred the $LynA^{KO}$ and $LynB^{KO}$ strains to generate $Csk^{AS}LynA^{KO}$ and $Csk^{AS}LynB^{KO}$ which express an inhibitable form of Csk from a transgene. After treating macrophages from these mice with 3-IB-PP1 to induce SFK activation, two approaches could be taken to investigate LynA and LynB signaling and interaction: interactomics and phosphoproteomics. Co-immunoprecipitation of either Lyn isoform, followed by protease digestion and mass spectrometry could reveal differences in their interactomes. Such approaches have been successful with lentivirally-expressed LynA and LynB in breast cancer cells [150], revealing distinct interaction patterns for the two isoforms. Although this study revealed that LynA is more likely to interact with proteins that modulate actin dynamics, one could argue that these methods could fail to identify meaningful protein-protein interactions, because kinase-substrate phosphorylation and interaction occur on relatively short time scales and may be missed by co-immunoprecipitation. Therefore, a broad tandem mass-spectrometry-based phosphoproteomics approach [165, 167, 263] (**Figure 5.1)** could be used to reveal the specific proteins, and specific sites of phosphorylation, phosphorylated following either LynA or LynB activation.

The beauty of these two approaches is that they can be applied to multiple cell types. Treatment of Csk^{AS} cells with 3-IB-PP1 induces broad SFK signaling and the activation of multiple pathways, which is useful for identifying the extent of substrates phosphorylated downstream of LynA and LynB activation. However, targeted approaches, such as a phosphoproteomic analysis of TLR4 and TLR9 receptor ligation could reveal insights as well. There is ample evidence to suggest that Lyn signaling differentially regulates TLR signaling in macrophages vs. dendritic cells [117, 119]. While Lyn^{KO} dendritic cells had increased levels of Erk phosphorylation following treatment with LPS, TLR4 signaling did not appear to be negatively regulated by Lyn in macrophages. These approaches could elucidate the differences in LynA and LynB signaling between

these two cell types, giving us a more complete understanding of the importance of LynA and LynB in regulating cellular activation.

A third approach to understand LynA and LynB signaling would be to use RNA sequencing (RNAseq) to identify differentially regulated transcripts in $LynA^{KO}$ and $LynB^{KO}$ cells. RNAseq uses high-throughput sequencing to identify the transcriptional state of bulk cell populations [264], and can be combined with cell sorting methodologies to identify transcriptional patterns in single cell populations (scRNA-seq). In Chapter 4, we identified numerous changes in the immune system of $LynA^{KO}$ and $LynB^{KO}$ mice, including increased expression of TLR4 in circulating $LynB^{KO}$ cells, and increased pDCs in the spleens of $LynB^{KO}$ mice. Both bulk RNAseq and scRNAseq could be leveraged to identify whether TLR4 expression is increased due to transcriptional changes in $LynB^{KO}$ mice and elucidate whether the pDCs in $LynB^{KO}$ mice are functionally different from those in $LynA^{KO}$ and WT mice.

In summary, co-immunoprecipitation and phosphoproteomics approaches, along with RNAseq, will help identify the different protein-protein interactions, signaling dynamics, and transcriptional changes of immune cells in $LynA^{KO}$ and $LynB^{KO}$ mice, giving us a more complete understanding of how LynA and LynB regulate immunity.

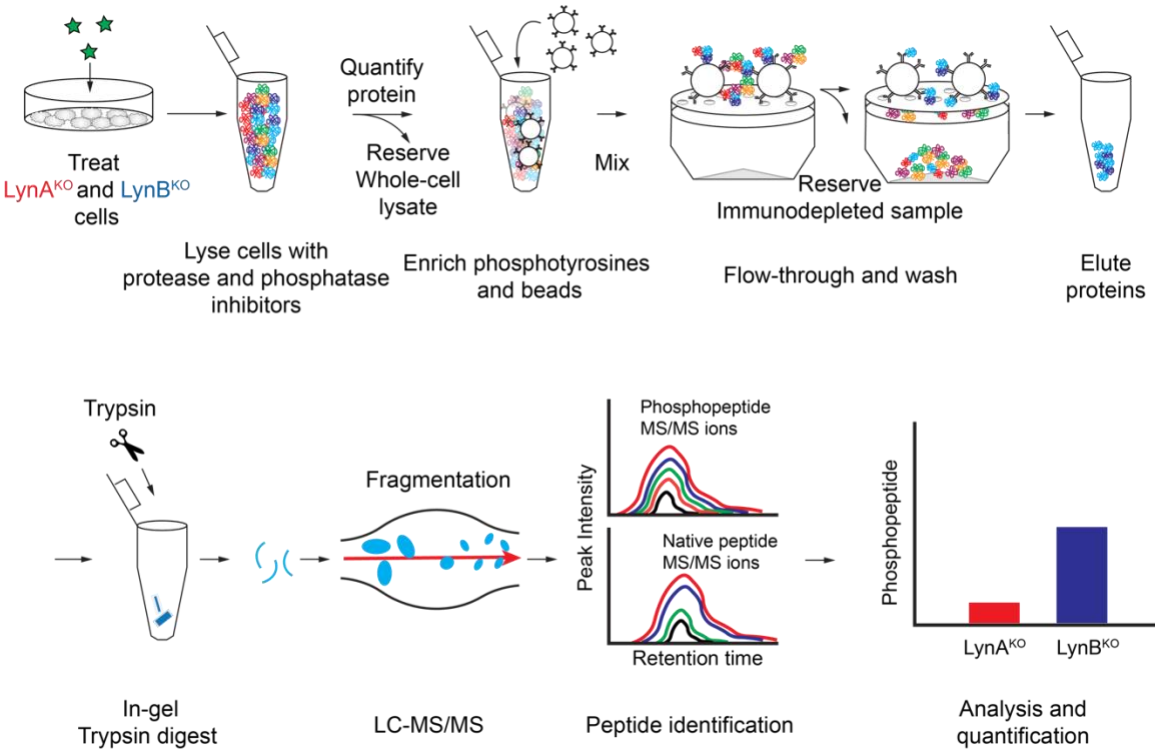

Figure 5.1. Conceptual framework for phosphoproteomic analysis of LynA and LynB signaling. Mass-spectrometry-based identification of phosphorylated peptides in cells from $LynA^{KO}$ and $LynB^{KO}$ mice could be used to identify enriched signaling pathways activated by either kinase.

5.1.2 LynA and LynB in B-cell dynamics

By acting as a regulator of both the BCR and TLRs, Lyn signaling must be tightly controlled for proper B cell maturation and activation. Lyn deficiency in mice prevents the proper maturation of Pro/Pre-B cells towards mature B cells [132], but also predisposes mature B cells to become activated plasma cells that may secrete auto-reactive antibodies [118]. Mature follicular Lyn^{KO} B cells have delayed but increased signaling responses, as measured by increases in free intracellular calcium, following BCR ligation, but there is little knowledge about how LynA and LynB impact BCR signaling, B cell maturation, B cell activation and various B cell responses. I have shown the expression of either isoform restores the defect in B cell maturation, and in the case of $LynA^{KO}$ mice, actually results in an increased number of B cells in the spleen. However, whether these findings are due to intrinsic effects of LynA or LynB signaling in the B cells themselves, or due to LynA/LynB deficiency in other cell types that create a more permissive environment for B cell proliferation in the spleen remains unknown.

The repertoire of mature B cells and autoreactive plasma cells in Lyn^{KO} mice has been relatively understudied. The developmental defect in B cell maturation in Lyn^{KO} mice suggests that mature Lyn^{KO} B cells and plasma cells might be dominated by relatively few clones and a less diverse repertoire compared to WT mice. Autoreactive plasma cells have limited clonality in other models [265] but how autoreactive Lyn-deficient B cells escape tolerance and whether there is limited clonality is unanswered. Failure to create a productive BCR that induces sufficient PI3K signaling causes B cells to die by neglect. Lyn has been shown to be critical for promoting PI3K signaling in B cells [104], suggesting that lack of Lyn may promote B cell death at this early stage. Under normal circumstances, highly autoreactive B cells undergo receptor editing in the bone marrow, mutating the antibody light chain fragment to create a less autoreactive BCR [266]. Despite this negative selection process, an estimated 10-15% of (human) B cells that exit the bone marrow possess self-reactive BCRs [267]. I have shown that $LynB^{KO}$ mice express normal levels of B Cells, but still develop nephritis from ANA deposition. Whether this is driven by a select few autoreactive clones that end up making it to the periphery and escape central tolerance mechanisms, or whether the cells that make it past negative selection in $LynB^{KO}$ have a limited repertoire, should be investigated further. Understanding the BCR arrangements that promote autoimmunity in Lyn^{KO} and

LynB^{KO} mice will aid our understanding of the antigens and signals involved in autoreactive B cell development.

Interestingly, self-reactivity/tonic signaling seems to be required for normal B cell function [268]. By using a model that drives GFP expression in response to transcription of the protein, Nur77, the Zikherman lab showed that mature follicular B cells respond to self-antigens at steady state. In B cells, Nur77 transcription is driven by BCR signaling, and importantly, not by TLR signaling. Thus, Nur77-driven GFP expression can be used to reliably measure BCR activity *in vivo*. Interestingly, this model showed that Lyn-deficient B cells express high levels of Nur77 at steady state, suggesting either high levels of tonic BCR signaling or an increased response to self-antigens. The Zikherman lab further demonstrated that IgM expression was required for ANA production and the direction of Lyn^{KO} B cells towards a short-lived plasma cell (SLPC) phenotype. Because we saw differences in the number of mature B cells in LynA^{KO} and LynB^{KO} mice, it is intriguing to suggest that each isoform may have different roles in regulating tonic signaling or may modulate signaling downstream of different BCR classes. Identifying the level of Nur77-GFP expression in mature LynA^{KO} and LynB^{KO} B cells would help clarify whether there is an increase in self-reactivity and the contribution of LynA and LynB to tonic BCR signaling. Further experiments with Nur77-GFP mice may help elucidate how BCR signaling in LynB^{KO} mice generates more GC B cells than WT and Lyn^{KO} mice.

B cell fate upon antigen exposure is highly dependent on BCR affinity. Strong BCR signaling (high affinity) predisposes B cells towards a SLPC fate, while low affinity drives B cells towards a GC fate [269, 270]. Because we saw an increase in GC B cells in the LynB^{KO} mice, this suggests LynA signaling may alter affinity sensing by the BCR in response to antigen activation. Adoptive transfer of either LynA^{KO} or LynB^{KO} B cells into WT host mice, followed by vaccination would answer many questions about the fate of LynA^{KO} and LynB^{KO} B cells in response to antigen stimulation: whether intrinsic LynA or LynB deficiency predisposes B cells to GC fates, and whether these cells produce high-affinity, edited and/or class-switched immunoglobulin upon vaccination.

In macrophages, phosphorylation of LynA Y32 recruits the ubiquitin ligase c-Cbl. This interaction offers potentially intriguing insights to the B cell germinal center response. In B cells, both c-Cbl and Cbl-b are required for ubiquitination of the BCR, which causes BCR-surface downregulation, and is required for normal GC entry and dynamics [94, 95]. Data from Immgen (**Figure 5.2**) suggests that *Cbl* and *Cblb* expression are differentially regulated in B cells and shows that *Cbl* expression peaks in GC B cells. Because of the close interaction between LynA and c-Cbl in macrophages, it is tempting to suggest that LynA may be required for proper c-Cbl activation in germinal center B cells, BCR downregulation and GC dynamics. Interestingly, $LynB^{KO}$ (LynA-expressing) spleens have more GC B cells (**Figure 4.9)** and a higher proportion of GC B cells. However, this could be caused by a multitude of cell changes in these total-$LynB^{KO}$ animals. Future studies should examine whether B cell receptor trafficking is altered in $LynA^{KO}$ and $LynB^{KO}$ mice, and whether these mice are able to form efficient germinal centers upon vaccination or pathogen challenge.

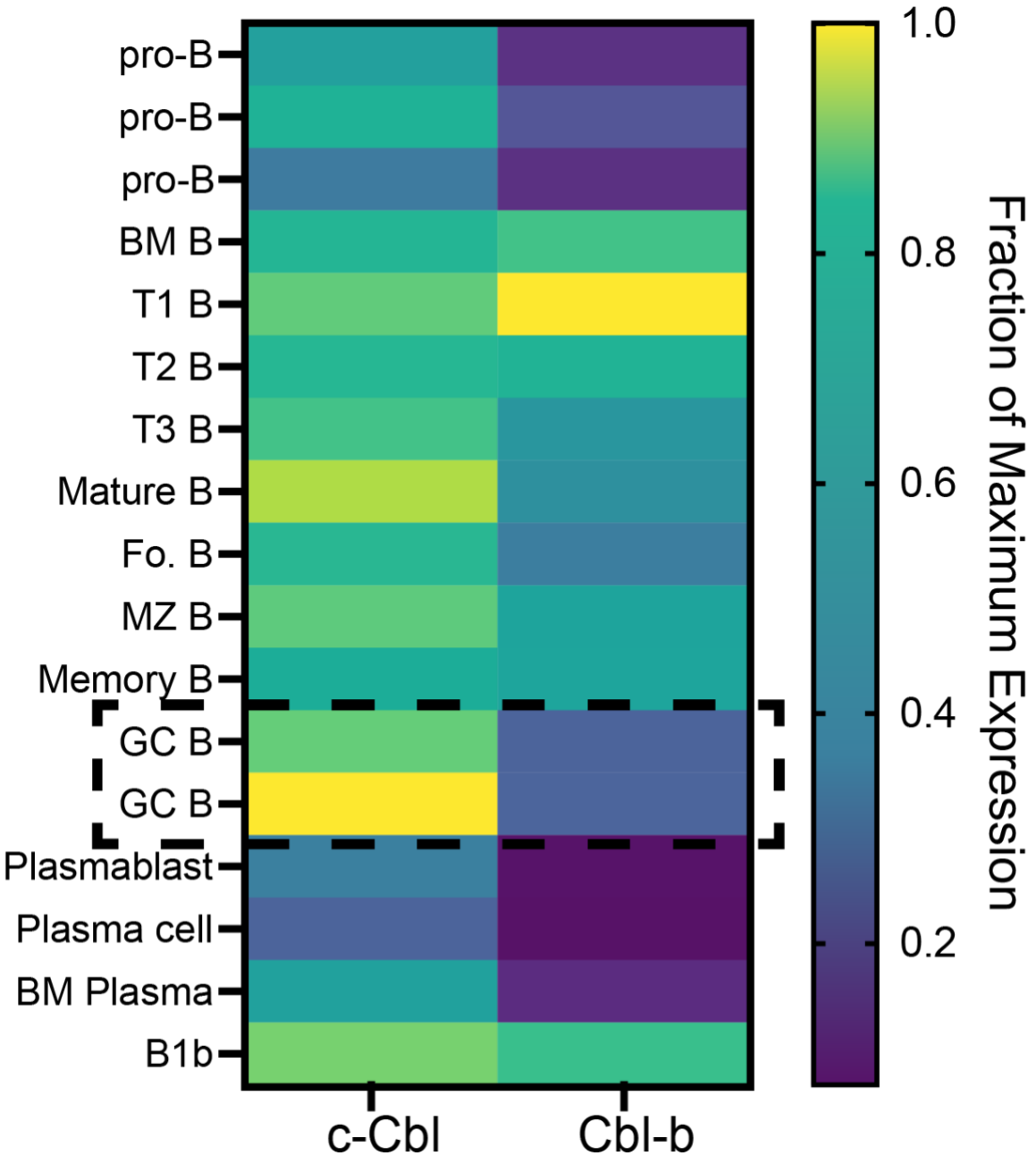

Figure 5.2. c-Cbl, and Cbl-b mRNAs are differentially regulated in B cells. Mouse RNAseq data derived from the Immunological Genome Project [ImmGen, http://rstats.immgen.org/Skyline/skyline.html, 226, 227]. RNA levels of c-Cbl, and Cbl-b are shown for B cell subsets, Germinal center (GC) B cells are boxed. RNA values are computed as a fraction of the maximum expression value, normalized by DESeq2, across the B cell subsets pictured.

5.1.3 Lyn, TLR signaling, commensals, and autoimmunity

TLR signaling is a potent driver of both human autoimmune disease [126, 252], and autoimmune disease in Lyn-deficient mice [120, 122]. TLR signaling in both B cells and dendritic cells is sufficient to drive the development of ANA and nephritis [117, 118], illustrating that Lyn regulates TLR signaling in multiple cell types. I have shown that $LynB^{KO}$ mice also develop aspects of autoimmune disease and have elevated responses to TLR4 and TLR9 stimulation, depending on the cell type. Despite these observations, the mechanisms linking LynA and LynB to TLR signaling, and TLR signaling to autoimmune disease in LynB-deficient mice, are not well understood.

The primary function of TLRs is to sense components of bacterial, viral, and fungal pathogens. The mice used in ours and other studies were housed in specific-pathogen-free (SPF) facilities, in the absence of pathogens that could potentially create an inflammatory environment. Previous research has shown that Lyn^{KO} mice given dextran sulfate sodium (DSS) in their drinking water fatally succumb to colitis, whereas wild-type mice survive [119]. DSS induces colitis by disrupting mucus function and increasing commensal-bacterial translocation across the digestive epithelium [271]. Whether specific commensal viral/fungal/bacterial species drive TLR activation and autoimmune-disease development in Lyn^{KO} mice remains unanswered, but the premise is intriguing.

Changes to the microbiome have been linked to the development and severity of autoimmunity in humans [272-274]. Specific bacterial species, such as *Prevotella copri*, have been linked closely to select diseases such as rheumatoid arthritis (RA) [273], while a large number of bacterial genii have links to SLE in particular [273]. These studies suggest that sensing of specific bacteria by TLRs could play a role in autoimmune disease. However, studies from human twins also suggest that genetic factors, as opposed to environmental (commensal bacteria), pose the greatest risk for developing autoimmune disease, particularly in human SLE [275]. Commensal bacteria could drive disease in LynB-deficient mice through two (non-mutually exclusive) main mechanisms. In one circumstance, specific commensals may trigger TLR signaling that activates immune cells in the absence of negative-regulatory signaling by LynB.

In another circumstance, B cells may make commensal-self cross-reactive antibodies that drive disease in the absence of properly functioning central tolerance mechanisms. Cross-reactive antibodies have been demonstrated for RA and Sjogren's syndrome [273, 276] but have not been identified in Lyn^{KO} mice. It would be interesting to examine whether autoantibodies in Lyn^{KO} and $LynB^{KO}$ mice also target commensal antigens by analyzing microbiota-reactive antibodies in the mouse feces via flow cytometry [277]. A failure to develop tolerance to commensals has been linked to worse disease outcome later in life [278]. It is unknown whether LynB impacts commensal tolerance, but it's tempting to suggest that a breakdown in tolerance, via altered dendritic-cell and B-cell phenotypes, contributes to T cell activation and the development of autoimmune disease upon aging in Lyn^{KO} and $LynB^{KO}$ mice. Future experiments should investigate whether T cells and B cells in Lyn^{KO} and $LynB^{KO}$ mice have TCRs and BCRs specific for commensal antigens, and whether these cells have a more activated phenotype than those in WT mice.

Interestingly, multiple epidemiological studies in humans and experiments with different infectious agents and TLR agonists in mice suggest that pathogen exposure may play a protective role in autoimmune disease [279]. The 'hygiene hypothesis' suggests that activation of the immune system by pathogens, particularly through TLRs, can drive tolerance mechanisms that limit exuberant immune responses later in life. It is unknown whether Lyn or LynB signaling affects TLR tolerance, although one study has suggested that tolerance decreases phosphorylation of Lyn following TLR4 activation [280]. Future studies should examine whether microbial exposure regulates the incidence of autoimmune disease in $LynB^{KO}$ and Lyn^{KO} mice. Treating these knockout mice with antibiotics to deplete commensal bacteria could theoretically improve autoimmune disease severity by decreasing the exposure to TLR ligands, thereby limiting activation of immune cells via TLR signaling. Conversely, treating mice with antibiotics may prevent some semblance of TLR tolerance from occurring. In contrast, normalizing the microbial exposure (NME) with so-called "dirty mice" [281] may induce tolerance mechanisms that prevent aberrant TLR signaling in LynB-deficient mice. Although it is probably more likely that LynB-deficient mice might fatally succumb more rapidly upon NME due to B cell defects and increased cytokine production in response to TLR4/9

ligation, the impact of microbial exposure on LynB-mediated autoimmunity is still an unanswered question.

5.2 Concluding remarks

facilis descensus Averno; noctes atque dies patet atri ianua Ditis; sed revocare gradum superasque evadere ad auras, hoc opus, hic labor est.

The descent from Avernus is easy; the black door of Ditis stands open night and day; but to return and to escape to heavenly skies, this is the work, this is the struggle.

Virgil*, The Aeneid*

By Book XI of Virgil's *Aeneid*, the titular, duty-bound Aeneas is a wearied traveler. And although he finds himself currently displaced, he is yet endowed by divine providence for future glory. Having escaped the fall of Troy and having been buffeted by wind, sea, and divine forces from port to port, Book XI sees Aeneas seeking divine guidance in search of a final stopping point on his long journey. He makes sacrifices to the gods, performs augury to interpret coded meanings of natural phenomena, and he even journeys through the gates of the underworld, *Averno*, to seek guidance from his deceased father, all to fulfill the duty set upon him by his divine forebears: founding the empire that would become Rome. The lives of the cells of our immune system have striking similarities to the journeys of Aeneas and his fellow Trojan refugees. Immune cells are "duty-bound" from differentiation to protect the body from pathogenic insults and respond to tissue inflammation. They circulate through their own *Mare Nostrum*, blood and lymph, in search of a home and purpose. And just like Aeneas surveys both the natural and infernal worlds, immune cells sense and respond to environmental cues, including those from dead and dying cells, which activate receptors that direct immune cell function. These receptors often trigger the activation of tyrosine kinases that propagate signaling cascades that direct an immune response. The Src-family kinases (SFKs) are a group of non-receptor tyrosine kinases important for many aspects of an immune response, including T cell recognition of antigen bound to MHC, activation of B cells by antigen binding to the B cell receptor, and phagocytosis by myeloid cells. The Src-family kinase Lyn is an important regulator of the responses initiated by many immunoreceptors and is a key regulator of immune function. Lyn is unique among the Src-family kinases due its ability to *both* activate immunoreceptor signaling, by recruiting and phosphorylating phosphoinositide kinases and phospholipases, *and* dampen immunoreceptor signaling, primarily by recruiting phosphatases that limit cascade propagation. Alternative splicing of the *lyn* transcript yields two proteins, LynA and LynB, that are well-conserved in mammals. My thesis has demonstrated unique regulatory mechanisms that selectively

control the protein levels of active LynA, in contrast to LynB and other SFKs. Furthermore, my thesis research has demonstrated unique roles for both LynA and LynB in regulating the development and maturation of immune cells, the development of autoimmune disease in mice, and TLR signaling. During the Trojan War, Aeneas is rescued from imminent harm on two separate occasions by both of the twin deities, Apollo and Artemis. As twins, Apollo and Artemis both share predilections towards archery, and supported the Trojans, as opposed to the Greeks during the famous war. However, Apollo and Artemis are also partial to their own dedicated pursuits. Similarly, LynA and LynB can play both similar and divergent roles in immune function, dependent on both the cell type and signaling pathway being studied (**Figure 5.3**). Understanding how cells balance the positive and negative signaling induced by these isoforms will help us understand the mechanisms by which the immune system preserves pathogen clearance and limit autoimmune disease.

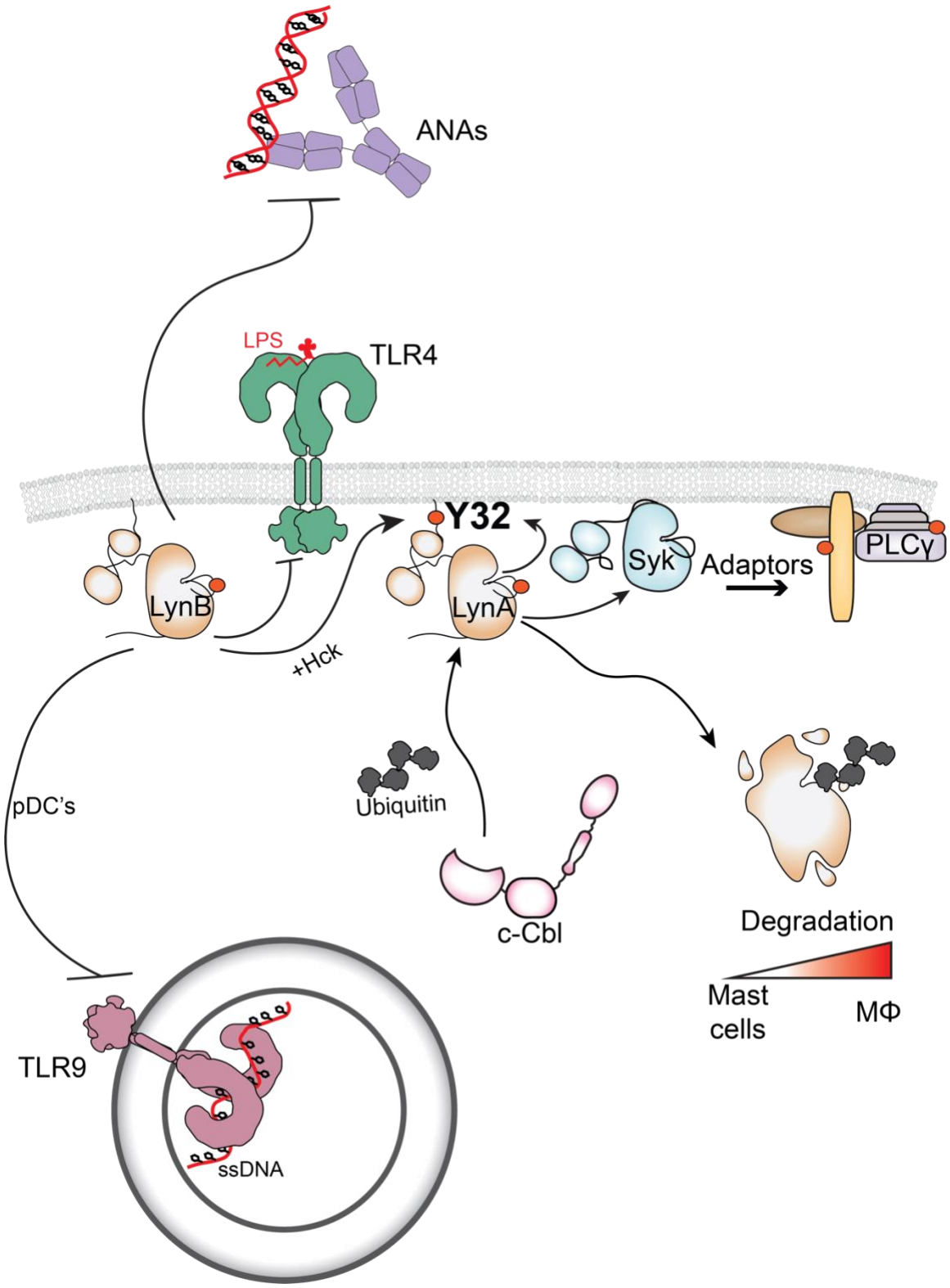

Figure 5.3. Model of LynA and LynB signaling and regulation

BIBLIOGRAPHY

1. Belkaid, Y. and O.J. Harrison, *Homeostatic Immunity and the Microbiota.* Immunity, 2017. **46**(4): p. 562-576.

2. Wang, Y., et al., *Tissue-resident macrophages promote extracellular matrix homeostasis in the mammary gland stroma of nulliparous mice.* Elife, 2020. **9**.

3. Roberts, A.W., et al., *Tissue-Resident Macrophages Are Locally Programmed for Silent Clearance of Apoptotic Cells.* Immunity, 2017. **47**(5): p. 913-927 e6.

4. Bosurgi, L., et al., *Macrophage function in tissue repair and remodeling requires IL-4 or IL-13 with apoptotic cells.* Science, 2017. **356**(6342): p. 1072-1076.

5. Proto, J.D., et al., *Regulatory T Cells Promote Macrophage Efferocytosis during Inflammation Resolution.* Immunity, 2018.

6. DeNardo, D.G., P. Andreu, and L.M. Coussens, *Interactions between lymphocytes and myeloid cells regulate pro- versus anti-tumor immunity.* Cancer Metastasis Rev, 2010. **29**(2): p. 309-16.

7. Hanahan, D. and R.A. Weinberg, *Hallmarks of cancer: the next generation.* Cell, 2011. **144**(5): p. 646-74.

8. Chao, M.P., R. Majeti, and I.L. Weissman, *Programmed cell removal: a new obstacle in the road to developing cancer.* Nat Rev Cancer, 2011. **12**(1): p. 58-67.

9. Murray, P.J. and T.A. Wynn, *Protective and pathogenic functions of macrophage subsets.* Nat Rev Immunol, 2011. **11**(11): p. 723-37.

10. Wang, J. and P. Kubes, *A Reservoir of Mature Cavity Macrophages that Can Rapidly Invade Visceral Organs to Affect Tissue Repair.* Cell, 2016. **165**(3): p. 668-78.

11. Mrdjen, D., et al., *High-Dimensional Single-Cell Mapping of Central Nervous System Immune Cells Reveals Distinct Myeloid Subsets in Health, Aging, and Disease.* Immunity, 2018. **48**(2): p. 380-395 e6.

12. Brodie, E.J., et al., *Lyn, Lupus, and (B) Lymphocytes, a Lesson on the Critical Balance of Kinase Signaling in Immunity.* Front Immunol, 2018. **9**: p. 401.

13. Solouki, S., A. August, and W. Huang, *Non-receptor tyrosine kinase signaling in autoimmunity and therapeutic implications.* Pharmacol Ther, 2019. **201**: p. 39-50.

14. Libby, P., A.H. Lichtman, and G.K. Hansson, *Immune effector mechanisms implicated in atherosclerosis: from mice to humans.* Immunity, 2013. **38**(6): p. 1092-104.

15. Bryan, M.C. and N.S. Rajapaksa, *Kinase Inhibitors for the Treatment of Immunological Disorders: Recent Advances.* J Med Chem, 2018. **61**(20): p. 9030-9058.

16. Lemmon, M.A. and J. Schlessinger, *Cell signaling by receptor tyrosine kinases.* Cell, 2010. **141**(7): p. 1117-34.

17. Wang, H., et al., *ZAP-70: an essential kinase in T-cell signaling.* Cold Spring Harb Perspect Biol, 2010. **2**: p. a002279.

18. Lowell, C.A., *Src-family and Syk kinases in activating and inhibitory pathways in innate immune cells: signaling cross talk.* Cold Spring Harb Perspect Biol, 2011. **3**(3).

19. Hwang, J.R., et al., *Recent insights of T cell receptor-mediated signaling pathways for T cell activation and development.* Exp Mol Med, 2020. **52**(5): p. 750-761.

20. Futosi, K. and A. Mocsai, *Tyrosine kinase signaling pathways in neutrophils.* Immunol Rev, 2016. **273**(1): p. 121-39.

21. Cox, D. and S. Greenberg, *Phagocytic signaling strategies: Fc(gamma)receptor-mediated phagocytosis as a model system.* Semin Immunol, 2001. **13**(6): p. 339-45.

22. Freedman, T.S., et al., *LynA regulates an inflammation-sensitive signaling checkpoint in macrophages.* Elife, 2015. **4**.

23. Bradshaw, J.M., *The Src, Syk, and Tec family kinases: distinct types of molecular switches.* Cell Signal, 2010. **22**(8): p. 1175-84.

24. Villarino, A.V., Y. Kanno, and J.J. O'Shea, *Mechanisms and consequences of Jak-STAT signaling in the immune system.* Nat Immunol, 2017. **18**(4): p. 374-384.

25. Masson, K. and L. Ronnstrand, *Oncogenic signaling from the hematopoietic growth factor receptors c-Kit and Flt3.* Cell Signal, 2009. **21**(12): p. 1717-26.

26. Rothlin, C.V., et al., *TAM receptor signaling in immune homeostasis.* Annu Rev Immunol, 2015. **33**: p. 355-91.

27. Brian, B.F., et al., *Unique-region phosphorylation targets LynA for rapid degradation, tuning its expression and signaling in myeloid cells.* Elife, 2019. **8**: p. e46043.

28. Courtney, A.H., et al., *A Phosphosite within the SH2 Domain of Lck Regulates Its Activation by CD45.* Mol Cell, 2017. **67**(3): p. 498-511 e6.

29. Salter, A.I., et al., *Phosphoproteomic analysis of chimeric antigen receptor signaling reveals kinetic and quantitative differences that affect cell function.* Sci Signal, 2018. **11**(544).

30. Roschewski, M., et al., *Inhibition of Bruton tyrosine kinase in patients with severe COVID-19.* Sci Immunol, 2020. **5**(48).

31. Brown, M.T. and J.A. Cooper, *Regulation, substrates and functions of src.* Biochim Biophys Acta, 1996. **1287**(2-3): p. 121-49.

32. Ingley, E., *Src family kinases: regulation of their activities, levels and identification of new pathways.* Biochim Biophys Acta, 2008. **1784**(1): p. 56-65.

33. Roskoski, R., Jr., *Src protein-tyrosine kinase structure and regulation.* Biochem Biophys Res Commun, 2004. **324**(4): p. 1155-64.

34. Sato, I., et al., *Differential trafficking of Src, Lyn, Yes and Fyn is specified by the state of palmitoylation in the SH4 domain.* J Cell Sci, 2009. **122**(Pt 7): p. 965-75.

35. Sigal, C.T., et al., *Amino-terminal basic residues of Src mediate membrane binding through electrostatic interaction with acidic phospholipids.* Proceedings of the National Academy of Sciences of the United States of America, 1994. **91**(25): p. 12253-12257.

36. Kim, P.W., et al., *A zinc clasp structure tethers Lck to T cell coreceptors CD4 and CD8.* Science, 2003. **301**(5640): p. 1725-8.

37. Li, L., et al., *Ionic CD3-Lck interaction regulates the initiation of T-cell receptor signaling.* Proc Natl Acad Sci U S A, 2017. **114**(29): p. E5891-E5899.

38. Johnson, T.M., et al., *Modulation of the catalytic activity of the Src family tyrosine kinase Hck by autophosphorylation at a novel site in the unique domain.* J Biol Chem, 2000. **275**(43): p. 33353-64.

39. Amata, I., M. Maffei, and M. Pons, *Phosphorylation of unique domains of Src family kinases.* Front Genet, 2014. **5**: p. 181.

40. Wu, J.L., et al., *O-GlcNAcylation is required for B cell homeostasis and antibody responses.* Nat Commun, 2017. **8**(1): p. 1854.

41. Arbesu, M., et al., *The Unique Domain Forms a Fuzzy Intramolecular Complex in Src Family Kinases.* Structure, 2017. **25**(4): p. 630-640 e4.

42. Teixeira, J., et al., *The Two Isoforms of Lyn Display Different Intramolecular Fuzzy Complexes with the SH3 Domain.* Molecules, 2018. **23**(11).

43. Shah, N.H., et al., *The Src module: an ancient scaffold in the evolution of cytoplasmic tyrosine kinases.* Critical reviews in biochemistry and molecular biology, 2018. **53**(5): p. 535-563.

44. Lim, W.A., F.M. Richards, and R.O. Fox, *Structural determinants of peptide-binding orientation and of sequence specificity in SH3 domains.* Nature, 1994. **372**(6504): p. 375-9.

45. Songyang, Z., et al., *SH2 domains recognize specific phosphopeptide sequences.* Cell, 1993. **72**(5): p. 767-78.

46. Xu, W., et al., *Crystal structures of c-Src reveal features of its autoinhibitory mechanism.* Mol Cell, 1999. **3**(5): p. 629-38.

47. Williams, J.C., et al., *The 2.35 A crystal structure of the inactivated form of chicken Src: a dynamic molecule with multiple regulatory interactions.* J Mol Biol, 1997. **274**(5): p. 757-75.

48. Sicheri, F., I. Moarefi, and J. Kuriyan, *Crystal structure of the Src family tyrosine kinase Hck.* Nature, 1997. **385**(6617): p. 602-9.

49. Young, M.A., et al., *Dynamic coupling between the SH2 and SH3 domains of c-Src and Hck underlies their inactivation by C-terminal tyrosine phosphorylation.* Cell, 2001. **105**(1): p. 115-26.

50. Banavali, N.K. and B. Roux, *Flexibility and charge asymmetry in the activation loop of Src tyrosine kinases.* Proteins, 2009. **74**(2): p. 378-389.

51. Ozkirimli, E. and C.B. Post, *Src kinase activation: A switched electrostatic network.* Protein science : a publication of the Protein Society, 2006. **15**(5): p. 1051-1062.

52. Moarefi, I., et al., *Activation of the Src-family tyrosine kinase Hck by SH3 domain displacement.* Nature, 1997. **385**(6617): p. 650-3.

53. Foda, Z.H., et al., *A dynamically coupled allosteric network underlies binding cooperativity in Src kinase.* Nat Commun, 2015. **6**: p. 5939.

54. Quintin, J., et al., *Candida albicans infection affords protection against reinfection via functional reprogramming of monocytes.* Cell Host Microbe, 2012. **12**(2): p. 223-32.

55. Mustelin, T., K.M. Coggeshall, and A. Altman, *Rapid activation of the T-cell tyrosine protein kinase pp56lck by the CD45 phosphotyrosine phosphatase.* Proc Natl Acad Sci U S A, 1989. **86**(16): p. 6302-6.

56. Zhu, J.W., et al., *Structurally distinct phosphatases CD45 and CD148 both regulate B cell and macrophage immunoreceptor signaling.* Immunity, 2008. **28**(2): p. 183-96.

57. Chang, V.T., et al., *Initiation of T cell signaling by CD45 segregation at 'close contacts'.* Nat Immunol, 2016. **17**(5): p. 574-582.

58. Okada, M., et al., *CSK: a protein-tyrosine kinase involved in regulation of src family kinases.* J Biol Chem, 1991. **266**(36): p. 24249-52.

59. Furukawa, T., et al., *Specific interaction of the CD45 protein-tyrosine phosphatase with tyrosine-phosphorylated CD3 zeta chain.* Proc Natl Acad Sci U S A, 1994. **91**(23): p. 10928-32.

60. Ostrowski, P.P., S. Grinstein, and S.A. Freeman, *Diffusion Barriers, Mechanical Forces, and the Biophysics of Phagocytosis.* Dev Cell, 2016. **38**(2): p. 135-46.

61. Freeman, S.A., et al., *Integrins Form an Expanding Diffusional Barrier that Coordinates Phagocytosis.* Cell, 2016. **164**(1-2): p. 128-140.

62. Goodridge, H.S., et al., *Activation of the innate immune receptor Dectin-1 upon formation of a 'phagocytic synapse'.* Nature, 2011. **472**(7344): p. 471-5.

63. Davis, S.J. and P.A. van der Merwe, *The kinetic-segregation model: TCR triggering and beyond.* Nat Immunol, 2006. **7**(8): p. 803-9.

64. Underhill, D.M. and H.S. Goodridge, *Information processing during phagocytosis.* Nat Rev Immunol, 2012. **12**(7): p. 492-502.

65. Taylor, M.J., et al., *A DNA-Based T Cell Receptor Reveals a Role for Receptor Clustering in Ligand Discrimination.* Cell, 2017. **169**(1): p. 108-119 e20.

66. Branzk, N., et al., *Neutrophils sense microbe size and selectively release neutrophil extracellular traps in response to large pathogens.* Nat Immunol, 2014. **15**(11): p. 1017-25.

67. Warnatsch, A., et al., *Reactive Oxygen Species Localization Programs Inflammation to Clear Microbes of Different Size.* Immunity, 2017. **46**(3): p. 421-432.

68. Hukelmann, J.L., et al., *The cytotoxic T cell proteome and its shaping by the kinase mTOR.* Nat Immunol, 2016. **17**(1): p. 104-12.

69. Nika, K., et al., *Constitutively active Lck kinase in T cells drives antigen receptor signal transduction.* Immunity, 2010. **32**(6): p. 766-77.

70. Schoenborn, J.R., et al., *Feedback circuits monitor and adjust basal Lck-dependent events in T cell receptor signaling.* Sci Signal, 2011. **4**(190): p. ra59.

71. Tan, Y.X., et al., *Inhibition of the kinase Csk in thymocytes reveals a requirement for actin remodeling in the initiation of full TCR signaling.* Nat Immunol, 2014. **15**(2): p. 186-94.

72. Freeman, S.A., et al., *Transmembrane Pickets Connect Cyto- and Pericellular Skeletons Forming Barriers to Receptor Engagement.* Cell, 2018. **172**(1-2): p. 305-317 e10.

73. Mylvaganam, S.M., S. Grinstein, and S.A. Freeman, *Picket-fences in the plasma membrane: functions in immune cells and phagocytosis.* Semin Immunopathol, 2018.

74. Jaumouille, V., et al., *Actin cytoskeleton reorganization by Syk regulates Fcgamma receptor responsiveness by increasing its lateral mobility and clustering.* Dev Cell, 2014. **29**(5): p. 534-546.

75. Ogawa, A., et al., *Structure of the carboxyl-terminal Src kinase, Csk.* J Biol Chem, 2002. **277**(17): p. 14351-4.

76. Bolland, S. and J.V. Ravetch, *Inhibitory pathways triggered by ITIM-containing receptors.* Adv Immunol, 1999. **72**: p. 149-77.

77. Daëron, M., et al., *Immunoreceptor tyrosine-based inhibition motifs: a quest in the past and future.* Immunol Rev, 2008. **224**: p. 11-43.

78. Lopes, F.B., et al., *Membrane nanoclusters of FcgammaRI segregate from inhibitory SIRPalpha upon activation of human macrophages.* J Cell Biol, 2017. **216**(4): p. 1123-1141.

79. Morrissey, M.A., N. Kern, and R.D. Vale, *CD47 Ligation Repositions the Inhibitory Receptor SIRPA to Suppress Integrin Activation and Phagocytosis.* Immunity, 2020. **53**(2): p. 290-302.e6.

80. Green, M.C. and L.D. Shultz, *Motheaten, an immunodeficient mutant of the mouse. I. Genetics and pathology.* J Hered, 1975. **66**(5): p. 250-8.

81. Deng, Z., et al., *Tyrosine phosphatase SHP-2 mediates C-type lectin receptor-induced activation of the kinase Syk and anti-fungal TH17 responses.* Nat Immunol, 2015. **16**(6): p. 642-52.

82. Tamir, I., J.M. Dal Porto, and J.C. Cambier, *Cytoplasmic protein tyrosine phosphatases SHP-1 and SHP-2: regulators of B cell signal transduction.* Curr Opin Immunol, 2000. **12**(3): p. 307-15.

83. Ben-Neriah, Y., *Regulatory functions of ubiquitination in the immune system.* Nat Immunol, 2002. **3**(1): p. 20-6.

84. Duan, L., et al., *The Cbl family and other ubiquitin ligases: destructive forces in control of antigen receptor signaling.* Immunity, 2004. **21**(1): p. 7-17.

85. Thien, C.B. and W.Y. Langdon, *c-Cbl and Cbl-b ubiquitin ligases: substrate diversity and the negative regulation of signalling responses.* Biochem J, 2005. **391**(Pt 2): p. 153-66.

86. Swaminathan, G. and A.Y. Tsygankov, *The Cbl family proteins: ring leaders in regulation of cell signaling.* J Cell Physiol, 2006. **209**(1): p. 21-43.

87. Dou, H., et al., *Structural basis for autoinhibition and phosphorylation-dependent activation of c-Cbl.* Nat Struct Mol Biol, 2012. **19**(2): p. 184-92.

88. Amacher, J.F., et al., *Phosphorylation control of the ubiquitin ligase Cbl is conserved in choanoflagellates.* Protein Sci, 2018. **27**(5): p. 923-932.

89. Belizaire, R., et al., *CBL mutations drive PI3K/AKT signaling via increased interaction with LYN and PIK3R1.* Blood, 2021.

90. Bunda, S., et al., *Juvenile myelomonocytic leukaemia-associated mutation in Cbl promotes resistance to apoptosis via the Lyn-PI3K/AKT pathway.* Oncogene, 2015. **34**(6): p. 789-97.

91. Chiang, Y.J., et al., *Cbl-b regulates the CD28 dependence of T-cell activation.* Nature, 2000. **403**(6766): p. 216-20.

92. Naramura, M., et al., *c-Cbl and Cbl-b regulate T cell responsiveness by promoting ligand-induced TCR down-modulation.* Nat Immunol, 2002. **3**(12): p. 1192-9.

93. Wang, H., et al., *Tonic ubiquitylation controls T-cell receptor:CD3 complex expression during T-cell development.* EMBO J, 2010. **29**(7): p. 1285-98.

94. Li, X., et al., *Cbl Ubiquitin Ligases Control B Cell Exit from the Germinal-Center Reaction.* Immunity, 2018. **48**(3): p. 530-541 e6.

95. Li, X., et al., *Cbl and Cbl-b control the germinal center reaction by facilitating naive B cell antigen processing.* J Exp Med, 2020. **217**(9).

96. Sanjay, A., et al., *Cbl associates with Pyk2 and Src to regulate Src kinase activity, alpha(v)beta(3) integrin-mediated signaling, cell adhesion, and osteoclast motility.* J Cell Biol, 2001. **152**(1): p. 181-95.

97. Kyo, S., et al., *Negative regulation of Lyn protein-tyrosine kinase by c-Cbl ubiquitin-protein ligase in FceRI-mediated mast cell activation.* Genes to Cells, 2003. **8**(10): p. 825-836.

98. Qu, X., et al., *Negative regulation of FcepsilonRI-mediated mast cell activation by a ubiquitin-protein ligase Cbl-b.* Blood, 2004. **103**(5): p. 1779-86.

99. Dale, B.M., et al., *Phagocytosis in macrophages lacking Cbl reveals an unsuspected role for Fc gamma receptor signaling and actin assembly in target binding.* J Immunol, 2009. **182**(9): p. 5654-62.

100. Zhu, L.L., et al., *E3 ubiquitin ligase Cbl-b negatively regulates C-type lectin receptor-mediated antifungal innate immunity.* J Exp Med, 2016. **213**(8): p. 1555-70.

101. Yamanashi, Y., et al., *The yes-related cellular gene lyn encodes a possible tyrosine kinase similar to p56lck.* Mol Cell Biol, 1987. **7**(1): p. 237-43.

102. Lindberg, R.A., D.P. Thompson, and T. Hunter, *Identification of cDNA clones that code for protein-tyrosine kinases by screening expression libraries with antibodies against phosphotyrosine.* Oncogene, 1988. **3**(6): p. 629-33.

103. Yamanashi, Y., et al., *Association of B cell antigen receptor with protein tyrosine kinase Lyn.* Science, 1991. **251**(4990): p. 192-4.

104. Yamanashi, Y., et al., *Activation of Src-like protein-tyrosine kinase Lyn and its association with phosphatidylinositol 3-kinase upon B-cell antigen receptor-mediated signaling.* Proc Natl Acad Sci U S A, 1992. **89**(3): p. 1118-22.

105. Hutchcroft, J.E., et al., *Fc epsilon RI-mediated tyrosine phosphorylation and activation of the 72-kDa protein-tyrosine kinase, PTK72, in RBL-2H3 rat tumor mast cells.* Proc Natl Acad Sci U S A, 1992. **89**(19): p. 9107-11.

106. Eiseman, E. and J.B. Bolen, *Engagement of the high-affinity IgE receptor activates src protein-related tyrosine kinases.* Nature, 1992. **355**(6355): p. 78-80.

107. Jouvin, M.H., et al., *Differential control of the tyrosine kinases Lyn and Syk by the two signaling chains of the high affinity immunoglobulin E receptor.* J Biol Chem, 1994. **269**(8): p. 5918-25.

108. Katagiri, K., et al., *Expression of src family genes during monocytic differentiation of HL-60 cells.* J Immunol, 1991. **146**(2): p. 701-7.

109. Huang, M.M., et al., *Membrane glycoprotein IV (CD36) is physically associated with the Fyn, Lyn, and Yes protein-tyrosine kinases in human platelets.* Proc Natl Acad Sci U S A, 1991. **88**(17): p. 7844-8.

110. Corey, S.J., et al., *Granulocyte colony-stimulating factor receptor signaling involves the formation of a three-component complex with Lyn and Syk protein-tyrosine kinases.* Proc Natl Acad Sci U S A, 1994. **91**(11): p. 4683-7.

111. Hibbs, M.L., et al., *Multiple defects in the immune system of Lyn-deficient mice, culminating in autoimmune disease.* Cell, 1995. **83**(2): p. 301-11.

112. Nishizumi, H., et al., *Impaired proliferation of peripheral B cells and indication of autoimmune disease in lyn-deficient mice.* Immunity, 1995. **3**(5): p. 549-60.

113. Tsantikos, E., et al., *Autoimmune disease in Lyn-deficient mice is dependent on an inflammatory environment established by IL-6.* J Immunol, 2010. **184**(3): p. 1348-60.

114. Scapini, P., et al., *Myeloid cells, BAFF, and IFN-gamma establish an inflammatory loop that exacerbates autoimmunity in Lyn-deficient mice.* J Exp Med, 2010. **207**(8): p. 1757-73.

115. Moon, B.G., et al., *Abrogation of autoimmune disease in Lyn-deficient mice by the deletion of IL-5 receptor alpha chain gene.* Cell Immunol, 2004. **228**(2): p. 110-8.

116. Pore, D., et al., *Cutting Edge: Deletion of Ezrin in B Cells of Lyn-Deficient Mice Downregulates Lupus Pathology.* J Immunol, 2018. **201**(5): p. 1353-1358.

117. Lamagna, C., et al., *Hyperactivated MyD88 signaling in dendritic cells, through specific deletion of Lyn kinase, causes severe autoimmunity and inflammation.* Proc Natl Acad Sci U S A, 2013. **110**(35): p. E3311-20.

118. Lamagna, C., et al., *B cell-specific loss of Lyn kinase leads to autoimmunity.* J Immunol, 2014. **192**(3): p. 919-28.

119. Ma, J., et al., *CARD9 mediates dendritic cell-induced development of Lyn deficiency-associated autoimmune and inflammatory diseases.* Sci Signal, 2019. **12**(602).

120. Ban, T., et al., *Lyn Kinase Suppresses the Transcriptional Activity of IRF5 in the TLR-MyD88 Pathway to Restrain the Development of Autoimmunity.* Immunity, 2016. **45**(2): p. 319-32.

121. Stefanová, I., et al., *Lipopolysaccharide induces activation of CD14-associated protein tyrosine kinase p53/56lyn.* J Biol Chem, 1993. **268**(28): p. 20725-8.

122. Silver, K.L., et al., *MyD88-dependent autoimmune disease in Lyn-deficient mice.* Eur J Immunol, 2007. **37**(10): p. 2734-43.

123. Dallari, S., et al., *Src family kinases Fyn and Lyn are constitutively activated and mediate plasmacytoid dendritic cell responses.* Nat Commun, 2017. **8**: p. 14830.

124. Keck, S., M. Freudenberg, and M. Huber, *Activation of murine macrophages via TLR2 and TLR4 is negatively regulated by a Lyn/PI3K module and promoted by SHIP1.* J Immunol, 2010. **184**(10): p. 5809-18.

125. Avila, M., et al., *Lyn kinase controls TLR4-dependent IKK and MAPK activation modulating the activity of TRAF-6/TAK-1 protein complex in mast cells.* Innate Immun, 2012. **18**(4): p. 648-60.

126. Liu, B., et al., *TLR4 up-regulation at protein or gene level is pathogenic for lupus-like autoimmune disease.* J Immunol, 2006. **177**(10): p. 6880-8.

127. Lyn-Cook, B.D., et al., *Increased expression of Toll-like receptors (TLRs) 7 and 9 and other cytokines in systemic lupus erythematosus (SLE) patients: ethnic differences and potential new targets for therapeutic drugs.* Mol Immunol, 2014. **61**(1): p. 38-43.

128. Akilesh, H.M., et al., *Chronic TLR7 and TLR9 signaling drives anemia via differentiation of specialized hemophagocytes.* Science, 2019. **363**(6423).

129. Marshak-Rothstein, A., *Toll-like receptors in systemic autoimmune disease.* Nat Rev Immunol, 2006. **6**(11): p. 823-35.

130. Christensen, S.R., et al., *Toll-like receptor 9 controls anti-DNA autoantibody production in murine lupus.* J Exp Med, 2005. **202**(2): p. 321-31.

131. Summers, S.A., et al., *TLR9 and TLR4 are required for the development of autoimmunity and lupus nephritis in pristane nephropathy.* J Autoimmun, 2010. **35**(4): p. 291-8.

132. Chan, V.W., et al., *Characterization of the B lymphocyte populations in Lyn-deficient mice and the role of Lyn in signal initiation and down-regulation.* Immunity, 1997. **7**(1): p. 69-81.

133. Smith, K.G., et al., *Inhibition of the B cell by CD22: a requirement for Lyn.* J Exp Med, 1998. **187**(5): p. 807-11.

134. Sármay, G., et al., *Cooperation between SHP-2, phosphatidyl inositol 3-kinase and phosphoinositol 5-phosphatase in the Fc gamma RIIb mediated B cell regulation.* Immunol Lett, 1999. **68**(1): p. 25-34.

135. Ding, C., et al., *Integrin CD11b negatively regulates BCR signalling to maintain autoreactive B cell tolerance.* Nat Commun, 2013. **4**: p. 2813.

136. Flores-Borja, F., et al., *Decreased Lyn expression and translocation to lipid raft signaling domains in B lymphocytes from patients with systemic lupus erythematosus.* Arthritis Rheum, 2005. **52**(12): p. 3955-65.

137. Liu, Y., et al., *MicroRNA-30a promotes B cell hyperactivity in patients with systemic lupus erythematosus by direct interaction with Lyn.* Arthritis Rheum, 2013. **65**(6): p. 1603-11.

138. Liossis, S.N., et al., *B-cell kinase lyn deficiency in patients with systemic lupus erythematosus.* J Investig Med, 2001. **49**(2): p. 157-65.

139. Lu, R., et al., *Genetic associations of LYN with systemic lupus erythematosus.* Genes Immun, 2009. **10**(5): p. 397-403.

140. Skrzypczynska, K.M., J.W. Zhu, and A. Weiss, *Positive Regulation of Lyn Kinase by CD148 Is Required for B Cell Receptor Signaling in B1 but Not B2 B Cells.* Immunity, 2016. **45**(6): p. 1232-1244.

141. Xiao, W., et al., *Positive and negative regulation of mast cell activation by Lyn via the FcepsilonRI.* J Immunol, 2005. **175**(10): p. 6885-92.

142. Fitzer-Attas, C.J., et al., *Fcgamma receptor-mediated phagocytosis in macrophages lacking the Src family tyrosine kinases Hck, Fgr, and Lyn.* J Exp Med, 2000. **191**(4): p. 669-82.

143. Roberts, M.E., et al., *Lyn deficiency leads to increased microbiota-dependent intestinal inflammation and susceptibility to enteric pathogens.* J Immunol, 2014. **193**(10): p. 5249-63.

144. Li, X., et al., *Lyn Delivers Bacteria to Lysosomes for Eradication through TLR2-Initiated Autophagy Related Phagocytosis.* PLoS Pathog, 2016. **12**(1): p. e1005363.

145. Li, X., et al., *Lyn regulates inflammatory responses in Klebsiella pneumoniae infection via the p38/NF-κB pathway.* Eur J Immunol, 2014. **44**(3): p. 763-73.

146. Yi, T.L., J.B. Bolen, and J.N. Ihle, *Hematopoietic cells express two forms of lyn kinase differing by 21 amino acids in the amino terminus.* Mol Cell Biol, 1991. **11**(5): p. 2391-8.

147. Suthers, A.N. and L.J. Young, *Molecular identification and expression of Lyn tyrosine kinase isoforms in marsupials.* Mol Immunol, 2013. **55**(3-4): p. 310-8.

148. Yamanashi, Y., et al., *Differential responses of p56lyn and p53lyn, products of alternatively spliced lyn mRNA, on stimulation of B-cell antigen receptor.* Cell Regul, 1991. **2**(12): p. 979-87.

149. Alvarez-Errico, D., et al., *Functional analysis of Lyn kinase A and B isoforms reveals redundant and distinct roles in Fc epsilon RI-dependent mast cell activation.* J Immunol, 2010. **184**(9): p. 5000-8.

150. Tornillo, G., et al., *Dual Mechanisms of LYN Kinase Dysregulation Drive Aggressive Behavior in Breast Cancer Cells.* Cell Rep, 2018. **25**(13): p. 3674-3692 e10.

151. Scapini, P., et al., *Multiple roles of Lyn kinase in myeloid cell signaling and function.* Immunol Rev, 2009. **228**(1): p. 23-40.

152. Harder, K.W., et al., *Gain- and loss-of-function Lyn mutant mice define a critical inhibitory role for Lyn in the myeloid lineage.* Immunity, 2001. **15**(4): p. 603-15.

153. El-Brolosy, M.A. and D.Y.R. Stainier, *Genetic compensation: A phenomenon in search of mechanisms.* PLoS Genet, 2017. **13**(7): p. e1006780.

154. Peng, J., *Gene redundancy and gene compensation: An updated view.* J Genet Genomics, 2019. **46**(7): p. 329-333.

155. Davies, S.P., et al., *Specificity and mechanism of action of some commonly used protein kinase inhibitors.* Biochem J, 2000. **351**(Pt 1): p. 95-105.

156. Manning, G., et al., *The protein kinase complement of the human genome.* Science, 2002. **298**(5600): p. 1912-34.

157. Fabian, M.A., et al., *A small molecule-kinase interaction map for clinical kinase inhibitors.* Nat Biotechnol, 2005. **23**(3): p. 329-36.

158. Herbrink, M., et al., *Inherent formulation issues of kinase inhibitors.* J Control Release, 2016. **239**: p. 118-27.

159. Eckstein, N., et al., *Clinical pharmacology of tyrosine kinase inhibitors becoming generic drugs: the regulatory perspective.* J Exp Clin Cancer Res, 2014. **33**: p. 15.

160. Lopez, M.S., J.I. Kliegman, and K.M. Shokat, *The logic and design of analog-sensitive kinases and their small molecule inhibitors.* Methods Enzymol, 2014. **548**: p. 189-213.

161. Bishop, A.C., et al., *A chemical switch for inhibitor-sensitive alleles of any protein kinase.* Nature, 2000. **407**(6802): p. 395-401.

162. Levin, S.E., et al., *Inhibition of ZAP-70 kinase activity via an analog-sensitive allele blocks T cell receptor and CD28 superagonist signaling.* J Biol Chem, 2008. **283**(22): p. 15419-30.

163. Kurien, B.T. and R.H. Scofield, *Western blotting: an introduction.* Methods Mol Biol, 2015. **1312**: p. 17-30.

164. Thofte, O., et al., *EF-Tu From Non-typeable Haemophilus influenzae Is an Immunogenic Surface-Exposed Protein Targeted by Bactericidal Antibodies.* Front Immunol, 2018. **9**: p. 2910.

165. Liu, Y. and M.R. Chance, *Integrating phosphoproteomics in systems biology.* Comput Struct Biotechnol J, 2014. **10**(17): p. 90-7.

166. Hu, A., W.S. Noble, and A. Wolf-Yadlin, *Technical advances in proteomics: new developments in data-independent acquisition.* F1000Res, 2016. **5**.

167. Dekker, L.J.M., et al., *Determination of Site-Specific Phosphorylation Ratios in Proteins with Targeted Mass Spectrometry.* J Proteome Res, 2018. **17**(4): p. 1654-1663.

168. Rafiq, K., et al., *c-Cbl inhibition improves cardiac function and survival in response to myocardial ischemia.* Circulation, 2014. **129**(20): p. 2031-43.

169. Myers, M.D., et al., *Src-like adaptor protein regulates TCR expression on thymocytes by linking the ubiquitin ligase c-Cbl to the TCR complex.* Nat Immunol, 2006. **7**(1): p. 57-66.

170. Weiss, A. and J.D. Stobo, *Requirement for the coexpression of T3 and the T cell antigen receptor on a malignant human T cell line.* J Exp Med, 1984. **160**(5): p. 1284-99.

171. Straus, D.B. and A. Weiss, *Genetic evidence for the involvement of the lck tyrosine kinase in signal transduction through the T cell antigen receptor.* Cell, 1992. **70**(4): p. 585-93.

172. Goldsmith, M.A. and A. Weiss, *Isolation and characterization of a T-lymphocyte somatic mutant with altered signal transduction by the antigen receptor.* Proc Natl Acad Sci U S A, 1987. **84**(19): p. 6879-83.

173. Phee, H., R.T. Abraham, and A. Weiss, *Dynamic recruitment of PAK1 to the immunological synapse is mediated by PIX independently of SLP-76 and Vav1.* Nat Immunol, 2005. **6**(6): p. 608-17.

174. Schindelin, J., et al., *Fiji: an open-source platform for biological-image analysis.* Nat Methods, 2012. **9**(7): p. 676-82.

175. Takeshita, S., K. Kaji, and A. Kudo, *Identification and characterization of the new osteoclast progenitor with macrophage phenotypes being able to differentiate into mature osteoclasts.* J Bone Miner Res, 2000. **15**(8): p. 1477-88.

176. Kalesnikoff, J. and S.J. Galli, *Antiinflammatory and immunosuppressive functions of mast cells.* Methods Mol Biol, 2011. **677**: p. 207-20.

177. Voutila, J., et al., *Gene Expression Profile Changes After Short-activating RNA-mediated Induction of Endogenous Pluripotency Factors in Human Mesenchymal Stem Cells.* Mol Ther Nucleic Acids, 2012. **1**: p. e35.

178. Thu, Y.M., et al., *Slx5/Slx8 Promotes Replication Stress Tolerance by Facilitating Mitotic Progression.* Cell Rep, 2016. **15**(6): p. 1254-65.

179. Brian, B.F.t., C.R. Guerrero, and T.S. Freedman, *Immunopharmacology and Quantitative Analysis of Tyrosine Kinase Signaling.* Curr Protoc Immunol, 2020. **130**(1): p. e104.

180. MacLean, B., et al., *Skyline: an open source document editor for creating and analyzing targeted proteomics experiments.* Bioinformatics, 2010. **26**(7): p. 966-8.

181. Concordet, J.-P. and M. Haeussler, *CRISPOR: intuitive guide selection for CRISPR/Cas9 genome editing experiments and screens.* Nucleic Acids Research, 2018. **46**(W1): p. W242-W245.

182. Miura, H., et al., *Easi-CRISPR for creating knock-in and conditional knockout mouse models using long ssDNA donors.* Nat Protoc, 2018. **13**(1): p. 195-215.

183. Hua, Z., et al., *Requirement for MyD88 signaling in B cells and dendritic cells for germinal center anti-nuclear antibody production in Lyn-deficient mice.* J Immunol, 2014. **192**(3): p. 875-85.

184. Guilliams, M., et al., *The function of Fcgamma receptors in dendritic cells and macrophages.* Nat Rev Immunol, 2014. **14**(2): p. 94-108.

185. Brown, G.D., *Dectin-1: a signalling non-TLR pattern-recognition receptor.* Nat Rev Immunol, 2006. **6**(1): p. 33-43.

186. Takai, T., *Roles of Fc receptors in autoimmunity.* Nat Rev Immunol, 2002. **2**(8): p. 580-92.

187. Sondermann, P., *The FcgammaR/IgG Interaction as Target for the Treatment of Autoimmune Diseases.* J Clin Immunol, 2016. **36 Suppl 1**: p. 95-9.

188. Chiffoleau, E., *C-Type Lectin-Like Receptors As Emerging Orchestrators of Sterile Inflammation Represent Potential Therapeutic Targets.* Front Immunol, 2018. **9**: p. 227.

189. Bakalar, M.H., et al., *Size-Dependent Segregation Controls Macrophage Phagocytosis of Antibody-Opsonized Targets.* Cell, 2018. **174**(1): p. 131-142 e13.

190. Abram, C.L. and C.A. Lowell, *The diverse functions of Src family kinases in macrophages.* Front Biosci, 2008. **13**: p. 4426-50.

191. Hamerman, J.A. and L.L. Lanier, *Inhibition of immune responses by ITAM-bearing receptors.* Sci STKE, 2006. **2006**(320): p. re1.

192. Hamerman, J.A., et al., *The expanding roles of ITAM adapters FcRgamma and DAP12 in myeloid cells.* Immunol Rev, 2009. **232**(1): p. 42-58.

193. Lutz-Nicoladoni, C., D. Wolf, and S. Sopper, *Modulation of Immune Cell Functions by the E3 Ligase Cbl-b.* Front Oncol, 2015. **5**: p. 58.

194. Liyasova, M.S., K. Ma, and S. Lipkowitz, *Molecular pathways: cbl proteins in tumorigenesis and antitumor immunity-opportunities for cancer treatment.* Clin Cancer Res, 2015. **21**(8): p. 1789-94.

195. Mkaddem, S.B., et al., *Lyn and Fyn function as molecular switches that control immunoreceptors to direct homeostasis or inflammation.* Nat Commun, 2017. **8**(1): p. 246.

196. Andrews, N.L., et al., *Small, mobile FcepsilonRI receptor aggregates are signaling competent.* Immunity, 2009. **31**(3): p. 469-79.

197. Felce, J.H., et al., *CD45 exclusion- and cross-linking-based receptor signaling together broaden FcepsilonRI reactivity.* Sci Signal, 2018. **11**(561).

198. Carroll-Portillo, A., et al., *Formation of a mast cell synapse: Fc epsilon RI membrane dynamics upon binding mobile or immobilized ligands on surfaces.* J Immunol, 2010. **184**(3): p. 1328-38.

199. Schwartz, S.L., et al., *Differential mast cell outcomes are sensitive to FcepsilonRI-Syk binding kinetics.* Mol Biol Cell, 2017. **28**(23): p. 3397-3414.

200. Okuzumi, T., et al., *Synthesis and evaluation of indazole based analog sensitive Akt inhibitors.* Mol Biosyst, 2010. **6**(8): p. 1389-402.

201. Okuzumi, T., et al., *Inhibitor hijacking of Akt activation.* Nat Chem Biol, 2009. **5**(7): p. 484-93.

202. Chow, L.M. and A. Veillette, *The Src and Csk families of tyrosine protein kinases in hemopoietic cells.* Semin Immunol, 1995. **7**(4): p. 207-26.

203. Zhu, J.W., et al., *Receptor-like tyrosine phosphatases CD45 and CD148 have distinct functions in chemoattractant-mediated neutrophil migration and response to S. aureus.* Immunity, 2011. **35**(5): p. 757-69.

204. Feshchenko, E.A., W.Y. Langdon, and A.Y. Tsygankov, *Fyn, Yes, and Syk phosphorylation sites in c-Cbl map to the same tyrosine residues that become phosphorylated in activated T cells.* J Biol Chem, 1998. **273**(14): p. 8323-31.

205. Sanjay, A., et al., *Identification and functional characterization of an Src homology domain 3 domain-binding site on Cbl.* FEBS J, 2006. **273**(23): p. 5442-56.

206. Tang, R., W.Y. Langdon, and J. Zhang, *Regulation of immune responses by E3 ubiquitin ligase Cbl-b.* Cell Immunol, 2018.

207. Yan, Q., et al., *Structural basis for activation of ZAP-70 by phosphorylation of the SH2-kinase linker.* Mol Cell Biol, 2013. **33**(11): p. 2188-201.

208. Law, C.L., et al., *Phospholipase C-gamma1 interacts with conserved phosphotyrosyl residues in the linker region of Syk and is a substrate for Syk.* Mol Cell Biol, 1996. **16**(4): p. 1305-15.

209. Purev, E., et al., *c-Cbl and Cbl-b act redundantly to protect osteoclasts from apoptosis and to displace HDAC6 from beta-tubulin, stabilizing microtubules and podosomes.* Mol Biol Cell, 2009. **20**(18): p. 4021-30.

210. Sohn, H.W., H. Gu, and S.K. Pierce, *Cbl-b negatively regulates B cell antigen receptor signaling in mature B cells through ubiquitination of the tyrosine kinase Syk.* J Exp Med, 2003. **197**(11): p. 1511-24.

211. Ueno, H., et al., *c-Cbl is tyrosine-phosphorylated by interleukin-4 and enhances mitogenic and survival signals of interleukin-4 receptor by linking with the phosphatidylinositol 3'-kinase pathway.* Blood, 1998. **91**(1): p. 46-53.

212. Hunter, S., et al., *Fyn associates with Cbl and phosphorylates tyrosine 731 in Cbl, a binding site for phosphatidylinositol 3-kinase.* J Biol Chem, 1999. **274**(4): p. 2097-106.

213. Stanley, E., et al., *Alternatively spliced murine lyn mRNAs encode distinct proteins.* Mol Cell Biol, 1991. **11**(7): p. 3399-406.

214. Huang, T.H., et al., *Epidermal growth factor receptor potentiates MCM7-mediated DNA replication through tyrosine phosphorylation of Lyn kinase in human cancers.* Cancer Cell, 2013. **23**(6): p. 796-810.

215. Blom, N., et al., *Prediction of post-translational glycosylation and phosphorylation of proteins from the amino acid sequence.* Proteomics, 2004. **4**(6): p. 1633-49.

216. Radivojac, P., et al., *Identification, analysis, and prediction of protein ubiquitination sites.* Proteins, 2010. **78**(2): p. 365-80.

217. Han, J., et al., *A critical role for Lyn kinase in strengthening endothelial integrity and barrier function.* Blood, 2013. **122**(25): p. 4140-9.

218. Yamamoto, N., et al., *The orally available spleen tyrosine kinase inhibitor 2-[7-(3,4-dimethoxyphenyl)-imidazo[1,2-c]pyrimidin-5-ylamino]nicotinamide dihydrochloride (BAY 61-3606) blocks antigen-induced airway inflammation in rodents.* J Pharmacol Exp Ther, 2003. **306**(3): p. 1174-81.

219. Buckbinder, L., et al., *Proline-rich tyrosine kinase 2 regulates osteoprogenitor cells and bone formation, and offers an anabolic treatment approach for osteoporosis.* Proc Natl Acad Sci U S A, 2007. **104**(25): p. 10619-24.

220. Hanke, J.H., et al., *Discovery of a novel, potent, and Src family-selective tyrosine kinase inhibitor. Study of Lck- and FynT-dependent T cell activation.* J Biol Chem, 1996. **271**(2): p. 695-701.

221. Yokoyama, N. and W.T. Miller, *Identification of residues involved in v-Src substrate recognition by site-directed mutagenesis.* FEBS Lett, 1999. **456**(3): p. 403-8.

222. Burgess, K.E., et al., *Biochemical identification of a direct physical interaction between the CD4:p56lck and Ti(TcR)/CD3 complexes.* Eur J Immunol, 1991. **21**(7): p. 1663-8.

223. Samelson, L.E., et al., *Association of the fyn protein-tyrosine kinase with the T-cell antigen receptor.* Proc Natl Acad Sci U S A, 1990. **87**(11): p. 4358-62.

224. Machiyama, H., et al., *SH3 domain of c-Src governs its dynamics at focal adhesions and the cell membrane.* Febs j, 2015. **282**(20): p. 4034-55.

225. Buitrago, L., et al., *Tyrosine phosphorylated c-Cbl regulates platelet functional responses mediated by outside-in signaling.* Blood, 2011. **118**(20): p. 5631-40.

226. Heng, T.S., M.W. Painter, and C. Immunological Genome Project, *The Immunological Genome Project: networks of gene expression in immune cells.* Nat Immunol, 2008. **9**(10): p. 1091-4.

227. Dwyer, D.F., et al., *Expression profiling of constitutive mast cells reveals a unique identity within the immune system.* Nat Immunol, 2016. **17**(7): p. 878-87.

228. Gustin, S.E., C.B. Thien, and W.Y. Langdon, *Cbl-b is a negative regulator of inflammatory cytokines produced by IgE-activated mast cells.* J Immunol, 2006. **177**(9): p. 5980-9.

229. Shelby, S.A., et al., *Functional nanoscale coupling of Lyn kinase with IgE-FcepsilonRI is restricted by the actin cytoskeleton in early antigen-stimulated signaling.* Mol Biol Cell, 2016. **27**(22): p. 3645-3658.

230. Portnoy, V., et al., *Small RNA and transcriptional upregulation.* Wiley Interdiscip Rev RNA, 2011. **2**(5): p. 748-60.

231. Voutila, J., et al., *Development and Mechanism of Small Activating RNA Targeting CEBPA, a Novel Therapeutic in Clinical Trials for Liver Cancer.* Mol Ther, 2017. **25**(12): p. 2705-2714.

232. Mohapatra, B., et al., *Protein tyrosine kinase regulation by ubiquitination: critical roles of Cbl-family ubiquitin ligases.* Biochim Biophys Acta, 2013. **1833**(1): p. 122-39.

233. Shao, Y., et al., *Differential regulation of the B cell receptor-mediated signaling by the E3 ubiquitin ligase Cbl.* J Biol Chem, 2004. **279**(42): p. 43646-53.

234. Palacios-Moreno, J., et al., *Neuroblastoma tyrosine kinase signaling networks involve FYN and LYN in endosomes and lipid rafts.* PLoS Comput Biol, 2015. **11**(4): p. e1004130.

235. Lock, P., et al., *Two isoforms of murine hck, generated by utilization of alternative translational initiation codons, exhibit different patterns of subcellular localization.* Mol Cell Biol, 1991. **11**(9): p. 4363-70.

236. Carreno, S., et al., *Lack of palmitoylation redirects p59Hck from the plasma membrane to p61Hck-positive lysosomes.* J Biol Chem, 2000. **275**(46): p. 36223-9.

237. Wynn, T.A., A. Chawla, and J.W. Pollard, *Macrophage biology in development, homeostasis and disease.* Nature, 2013. **496**(7446): p. 445-55.

238. Galli, S.J., N. Borregaard, and T.A. Wynn, *Phenotypic and functional plasticity of cells of innate immunity: macrophages, mast cells and neutrophils.* Nat Immunol, 2011. **12**(11): p. 1035-44.

239. Gentek, R., et al., *Hemogenic Endothelial Fate Mapping Reveals Dual Developmental Origin of Mast Cells.* Immunity, 2018. **48**(6): p. 1160-1171 e5.

240. Wucherpfennig, K.W., *Mechanisms for the induction of autoimmunity by infectious agents.* Journal of Clinical Investigation, 2001. **108**(8): p. 1097-1104.

241. Plotz, P.H., *The autoantibody repertoire: searching for order.* Nat Rev Immunol, 2003. **3**(1): p. 73-8.

242. Albert, L.J. and R.D. Inman, *Molecular mimicry and autoimmunity.* N Engl J Med, 1999. **341**(27): p. 2068-74.

243. Lipsky, P.E., *Systemic lupus erythematosus: an autoimmune disease of B cell hyperactivity.* Nat Immunol, 2001. **2**(9): p. 764-6.

244. Harley, J.B., et al., *Genome-wide association scan in women with systemic lupus erythematosus identifies susceptibility variants in ITGAM, PXK, KIAA1542 and other loci.* Nat Genet, 2008. **40**(2): p. 204-10.

245. Lowell, C.A., *Src-family kinases: rheostats of immune cell signaling.* Mol Immunol, 2004. **41**(6-7): p. 631-43.

246. Chan, V.W., C.A. Lowell, and A.L. DeFranco, *Defective negative regulation of antigen receptor signaling in Lyn-deficient B lymphocytes.* Curr Biol, 1998. **8**(10): p. 545-53.

247. Gross, A.J., et al., *Developmental acquisition of the Lyn-CD22-SHP-1 inhibitory pathway promotes B cell tolerance.* J Immunol, 2009. **182**(9): p. 5382-92.

248. Nishizumi, H., et al., *A double-edged kinase Lyn: a positive and negative regulator for antigen receptor-mediated signals.* J Exp Med, 1998. **187**(8): p. 1343-8.

249. Yu, C.C.K., et al., *Lupus-like kidney disease in mice deficient in the Src family tyrosine kinases Lyn and Fyn.* Current Biology, 2001. **11**(1): p. 34-38.

250. Pore, D., et al., *Cutting Edge: Deletion of Ezrin in B Cells of Lyn-Deficient Mice Downregulates Lupus Pathology.* Journal of immunology (Baltimore, Md. : 1950), 2018. **201**(5): p. 1353-1358.

251. Takeda, K. and S. Akira, *TLR signaling pathways.* Semin Immunol, 2004. **16**(1): p. 3-9.

252. Richez, C., et al., *Role for toll-like receptors in autoimmune disease: the example of systemic lupus erythematosus.* Joint Bone Spine, 2011. **78**(2): p. 124-30.

253. Ma, X., et al., *CRISPR/Cas9-mediated gene manipulation to create single-amino-acid-substituted and floxed mice with a cloning-free method.* Sci Rep, 2017. **7**: p. 42244.

254. Vérollet, C., et al., *Hck contributes to bone homeostasis by controlling the recruitment of osteoclast precursors.* Faseb j, 2013. **27**(9): p. 3608-18.

255. Roberts, M.E., et al., *Deep Phenotyping by Mass Cytometry and Single-Cell RNA-Sequencing Reveals LYN-Regulated Signaling Profiles Underlying Monocyte Subset Heterogeneity and Lifespan.* Circ Res, 2020. **126**(10): p. e61-e79.

256. Chu, C.L. and C.A. Lowell, *The Lyn tyrosine kinase differentially regulates dendritic cell generation and maturation.* J Immunol, 2005. **175**(5): p. 2880-9.

257. Briseño, C.G., et al., *Notch2-dependent DC2s mediate splenic germinal center responses.* Proc Natl Acad Sci U S A, 2018. **115**(42): p. 10726-10731.

258. Shin, C., et al., *CD8α(-) Dendritic Cells Induce Antigen-Specific T Follicular Helper Cells Generating Efficient Humoral Immune Responses.* Cell Rep, 2015. **11**(12): p. 1929-40.

259. Swiecki, M. and M. Colonna, *The multifaceted biology of plasmacytoid dendritic cells.* Nat Rev Immunol, 2015. **15**(8): p. 471-85.

260. Mariz, H.A., et al., *Pattern on the antinuclear antibody-HEp-2 test is a critical parameter for discriminating antinuclear antibody-positive healthy individuals and patients with autoimmune rheumatic diseases.* Arthritis Rheum, 2011. **63**(1): p. 191-200.

261. de Vlam, K., et al., *Detection and identification of antinuclear autoantibodies in the serum of normal blood donors.* Clin Exp Rheumatol, 1993. **11**(4): p. 393-7.

262. Borzecka-Solarz, K., et al., *Association of Lyn kinase with membrane rafts determines its negative influence on LPS-induced signaling.* Mol Biol Cell, 2017. **28**(8): p. 1147-1159.

263. Bian, Y., et al., *Ultra-deep tyrosine phosphoproteomics enabled by a phosphotyrosine superbinder.* Nat Chem Biol, 2016. **12**(11): p. 959-966.

264. Kukurba, K.R. and S.B. Montgomery, *RNA Sequencing and Analysis.* Cold Spring Harb Protoc, 2015. **2015**(11): p. 951-69.

265. Shlomchik, M., et al., *Anti-DNA antibodies from autoimmune mice arise by clonal expansion and somatic mutation.* J Exp Med, 1990. **171**(1): p. 265-92.

266. Nemazee, D., *Mechanisms of central tolerance for B cells.* Nat Rev Immunol, 2017. **17**(5): p. 281-294.

267. Watanabe, A., et al., *Self-tolerance curtails the B cell repertoire to microbial epitopes.* JCI Insight, 2019. **4**(10).

268. Noviski, M., et al., *IgM and IgD B cell receptors differentially respond to endogenous antigens and control B cell fate.* Elife, 2018. **7**.

269. Paus, D., et al., *Antigen recognition strength regulates the choice between extrafollicular plasma cell and germinal center B cell differentiation.* J Exp Med, 2006. **203**(4): p. 1081-91.

270. Pape, K.A., et al., *Naive B Cells with High-Avidity Germline-Encoded Antigen Receptors Produce Persistent IgM(+) and Transient IgG(+) Memory B Cells.* Immunity, 2018. **48**(6): p. 1135-1143 e4.

271. Chassaing, B., et al., *Dietary emulsifiers impact the mouse gut microbiota promoting colitis and metabolic syndrome.* Nature, 2015. **519**(7541): p. 92-6.

272. Dehner, C., R. Fine, and M.A. Kriegel, *The microbiome in systemic autoimmune disease: mechanistic insights from recent studies.* Curr Opin Rheumatol, 2019. **31**(2): p. 201-207.

273. De Luca, F. and Y. Shoenfeld, *The microbiome in autoimmune diseases.* Clin Exp Immunol, 2019. **195**(1): p. 74-85.

274. Thaiss, C.A., et al., *The microbiome and innate immunity.* Nature, 2016. **535**(7610): p. 65-74.

275. Generali, E., et al., *Lessons learned from twins in autoimmune and chronic inflammatory diseases.* J Autoimmun, 2017. **83**: p. 51-61.

276. Konig, M.F., *The microbiome in autoimmune rheumatic disease.* Best Pract Res Clin Rheumatol, 2020. **34**(1): p. 101473.

277. Koch, M.A., et al., *Maternal IgG and IgA Antibodies Dampen Mucosal T Helper Cell Responses in Early Life.* Cell, 2016. **165**(4): p. 827-41.

278. Zeissig, S. and R.S. Blumberg, *Life at the beginning: perturbation of the microbiota by antibiotics in early life and its role in health and disease.* Nat Immunol, 2014. **15**(4): p. 307-10.

279. Bach, J.F., *The hygiene hypothesis in autoimmunity: the role of pathogens and commensals.* Nat Rev Immunol, 2018. **18**(2): p. 105-120.

280. Xiong, Y., et al., *Endotoxin Tolerance Inhibits Lyn and c-Src Phosphorylation and Association with Toll-Like Receptor 4 but Increases Expression and Activity of Protein Phosphatases.* J Innate Immun, 2016. **8**(2): p. 171-84.

281. Beura, L.K., et al., *Normalizing the environment recapitulates adult human immune traits in laboratory mice.* Nature, 2016. **532**(7600): p. 512-6.